USE OF GENE EXPRESSION TO CHARACTERIZE HETEROGENEOUS LIVER CELL POPULATIONS

by

Brent M. Schreiber

B.S. Chemical Engineering
Massachusetts Institute of Technology, 2003

Submitted to the Division of Bioengineering in Partial Fulfillment
of the Requirements for the Degree of

Masters of Engineering in Biomedical Engineering
at the
Massachusetts Institute of Technology

June 2004

Signature of Author: _____

Division of Biological Engineering
May 7, 2004

Certified by: _____

Linda Griffith
Professor of Bioengineering & Mechanical Engineering
Thesis Supervisor

Accepted by: _____

Roger D. Kamm
Professor of Bioengineering & Mechanical Engineering
MEBE Graduate Program Director

USE OF GENE EXPRESSION TO CHARACTERIZE HETEROGENEOUS LIVER CELL POPULATIONS

by

Brent Schreiber

Submitted to the Division of Bioengineering on May 7, 2004
in Partial Fulfillment of the Requirements for the Degree of
Masters of Engineering in Biomedical Engineering

Abstract

Non-parenchymal cells (NPC's) are integral to recreate the native hepatic microenvironment and necessary to maintain *in vivo* liver function. A variety of *in vitro* culture systems have been developed to address different aspects of liver physiology and architecture in order to recreate the microenvironment. These *in vitro* co-culture strategies have been limited by their inability to systematically characterize the addition of non-parenchymal cells.

In this dissertation, I use gene expression levels quantified by real-time RT-PCR to determine tissue composition. The identified genes demonstrate significant cell-type specificity, magnitude, and stability of expression *in vivo* and throughout each step of cell isolation process. In the course of this development, we establish protocols to accurately isolate and count an enriched fraction of primary NPC's.

Experiments on the perfusion and isolation process prove that there exists an inverse correlation between perfusion flow rate and NPC yield and viability. Further, we have characterized the tissue composition of each step in the cell isolation process and the resulting NPC population to confirm that a significant number of each NPC type is delivered to *in vitro* co-culture. System output analysis of spheroids co-cultured at physiological ratios and seeded into the milliF bioreactor shows the presence of stellate cells, but the absence of endothelial (EC) and kupffer cells (KC). The same analysis of 2D collagen gel sandwiches shows the presence of all NPC cell types. This indicates that our process is currently limited by the ability of EC's and KC's to incorporate into spheroid aggregates.

Future work that validates the temporal expression stability of the identified genes in different *in vitro* culture systems and environments will enable determination of relative levels of NPC incorporation and will allow correlations to be made between operational features of *in vitro* systems, the resulting culture microenvironment, and observed tissue function.

Thesis Supervisor: Linda G. Griffith

Title: Professor of Biological Engineering

Acknowledgements:

I would like to thank Prof. Linda Griffith for the opportunity to work with her on such an exciting project. Her leadership, understanding, and support were instrumental in carving a niche in the vast abyss that is non-parenchymal cell research.

I would also like to acknowledge E.I. DuPont and NIEHS who provided the funding for this research.

This project could not have been completed without the coordinated support of many members of the Griffith lab. I would like to acknowledge the following people for their contributions to this work:

Anand Sivaraman for first proposing the idea to use PCR to quantify composition, and for his seemingly endless advice and guidance in the RT-PCR and data analysis process.

Corey Moore & Nate Tedford for their advice on how to maximize the utility of each experiment and developing a plan to sift through the broad experimental possibilities to find those few that were necessary to prove my thesis, and for their assistance in writing and revising my thesis.

Megan Whittemore for performing the immunostaining for my research.

Katy Wack & Albert Hwa for their guidance with immunostaining & sectioning protocols, and for explaining the nuances of NPC separation and culture.

Brad Hogan & Rebecca Fry for their help setting up and interpreting RT-PCR experiments.

Emily Larson for performing the rat perfusions to get my cells.

Alexandria Samms for her help in writing and revising my thesis.

Joe Moritz for his constant support and laughter during what would have been a very arduous process.

Last but not least, I would like to thank especially my family and friends for their tremendous love and support throughout my school years. Without you, none of this would have been possible. Thank you for being a part of my life.

~ The lion and the calf shall lie down together but the calf won't get much sleep.~
Woody Allen, Without Feathers (1976)

Table of Contents:

List of Figures

List of Tables

CHAPTER 1: INTRODUCTION AND BACKGROUND

This work contributes to the aim of co-culturing non-parenchymal cells with hepatocytes in a 3D microfabricated liver bioreactor to create a robust *in-vivo* analog culture system for more complete and meaningful *in vitro* study of liver tissue. Defining the role of non-parenchymal cells in maintaining the liver phenotype in 3D liver cultures requires methods to quantify the tissue composition of each step in the culture process and NPC incorporation as a function of time. This chapter reviews the basics of liver structure and function, analyzes current liver tissue co-culture techniques and their major limitations, provides an analysis of the key operating challenges associated with culture non-parenchymal cells, and outlines the merits of several methods used to evaluate cell culture systems.

1.0 Objectives

The primary focus of this project was to develop and validate a protocol to quantitatively determine the composition of co-cultured hepatocytes, stellate, endothelial, and kupffer cells. This protocol enables input/output analysis to be performed on relative cellular composition of heterogeneous tissue in a variety of cell culture systems. The secondary objective of the project was to identify and validate specific gene expression markers for each of the four cellular phenotypes of the liver

1.1 Structure and Function of the Liver

The liver possesses an extremely sophisticated engineering design. It houses a large, highly structured reactor bed, an intricate flow manifold, and a separation system that efficiently delivers metabolic products to the blood stream, while shunting bile salts into the retrograde bile duct. This system's main functions are to remove toxins and provide metabolic activity such as cytochrome P450 activity, glycogen storage, urea production, and release of proteins, carbohydrates, lipids and cholesterol, and metabolic wastes. In addition the liver serves as a storage vessel for iron (processed from hemoglobin) and copper, fat-soluble vitamins (A, E, D, and K), and blood, which can be released during hemorrhage. Total, over 500 functions have been identified in the liver many of which are vital to sustain life. These disparate functions arise from the highly intricate cellular arrangement and structure.

There are two main competing views of structural organization of the liver: the lobule and the acinus (Arias, 2001). Both models posses a hexagonal tissue structure with the portal triads at the vertices and the central vein at the centroid. In Kiernan's proposed lobule model (Kiernan, 1883) the blood passes into the periphery from the digestive tract via the portal triad, traverses the sinusoid, and then exits via the central vein (hepatic vein) (Figure 1.1A) (Jauregui 2000). The portal triad is comprised of three vessels: the hepatic artery bringing oxygenated blood from the heart, the portal vein carrying enriched blood from the intestine, and the bile duct which drains bile from individual bile ducts (Figure 1.1B). These inputs and outputs branch into complex tree structures, which supply and drain the entire liver.

Rappaport proposed the acinar model in 1954 based on the observation that as blood passes through the sinusoids, oxygen content, and dissolved solutes are altered at different positions in the sinusoid by the hepatocytes which have contacted it. Consequently, the cell types in the liver represent a heterogeneous population of cells whose function differs relative to the composition of contacted blood. Therefore, the acinus is subdivided into three zones graded by the depletion of oxygen and other metabolites in adjacent RBC's as they travel the length of the sinusoid toward the central vein (Figure 1.1C) (Ochoa et al 2002). Isolating a single sinusoid shows the fundamental unit of liver structure: a set of thin hepatocyte plates, called the acinus, strung between the portal triad and the hepatic veinule (Figure 1.1D) (McCuskey 1994, Junguiera et al. 1999, Klassen 2001).

These two models of the liver, though seemingly disparate, provide the foundation for current models. As research techniques are developed the definitive architecture of the liver will be unveiled, but for the purposes of this research the liver will be viewed as a heterogeneous hexagonal tissue, which is a simplification and an incorporation of both theories.

A.

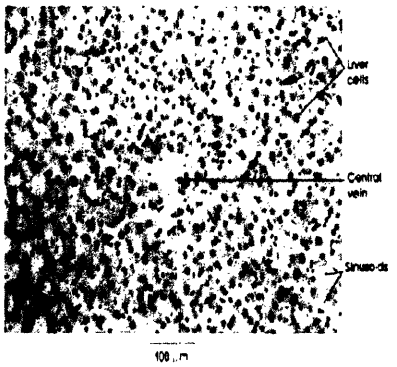

B.

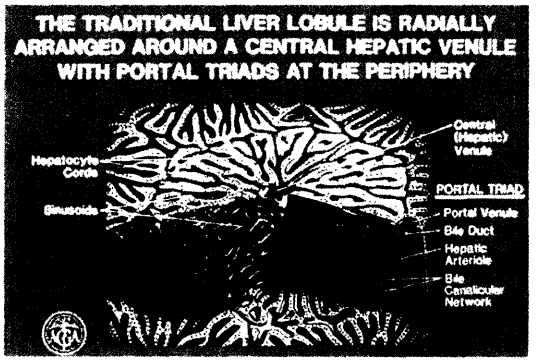

C.

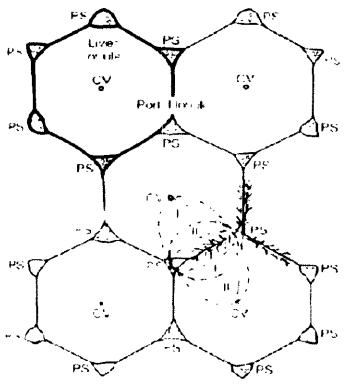

D.

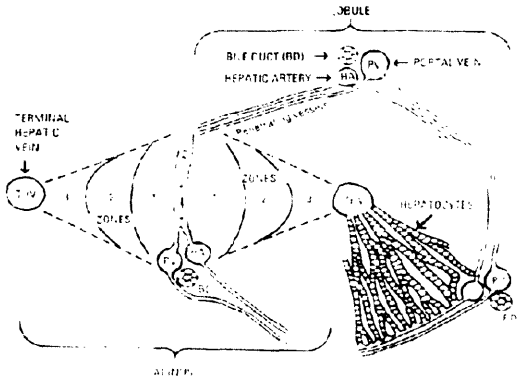

Figure 1.1: The multiple models of liver architecture

(A) Liver microarchitecture features hepatocytes around the central vein **(B)** Liver lobule showing the portal triad, hepatic sinusoids and blood flow regions **(C)** Regions of the classical lobule and acinus. **(D)** Schematic of liver operational units: Combination of the classical lobule and the acinus
(Image A is from Jauregui et al. 2000, B and C from Klassen et al. 2001, and D from Junguiera et al. 1999)

Additionally the liver has an equally intricate organization on the cellular level that may be required to be replicated to achieve proper function. The acinus is organized in a perfused, spongelike, capillary bed structure, composed primarily of mature hepatocyte plates of a single cell thickness, known as the parenchyma (Arias et al. 1994). These plates of an apical domain which forms bile canalicular networks involved in the secretion of bile components and metabolites of xenobiotics, and a basal domain which interacts with ECM and participates in cell signaling. These hepatic plates are lined by fenestrated endothelial cells, which create a physical and chemical shield between the sinusoid and the hepatic plate. The region between the endothelium and the hepatic plate, known as the Space of Disse, is traversed by Stellate cells, the resident liver fibroblasts. Interspersed in the sinusoid are kupffer cells, a specialized form of macrophage (Figure 1.2A). Fluid flows through two paths: the bulk travels "down" the acinus from the portal region to the central vein; hepatocytes also form ducts known as bile canaliculi that transport bile retrograde or "up" to the bile duct in the portal triad (Figure 1.2B). These ducts are separated from the rest of the tissue by tight junctions between neighboring hepatocytes in a similar fashion to that of the digestive system (McCuckey 1994, Junguira et al. 1999).

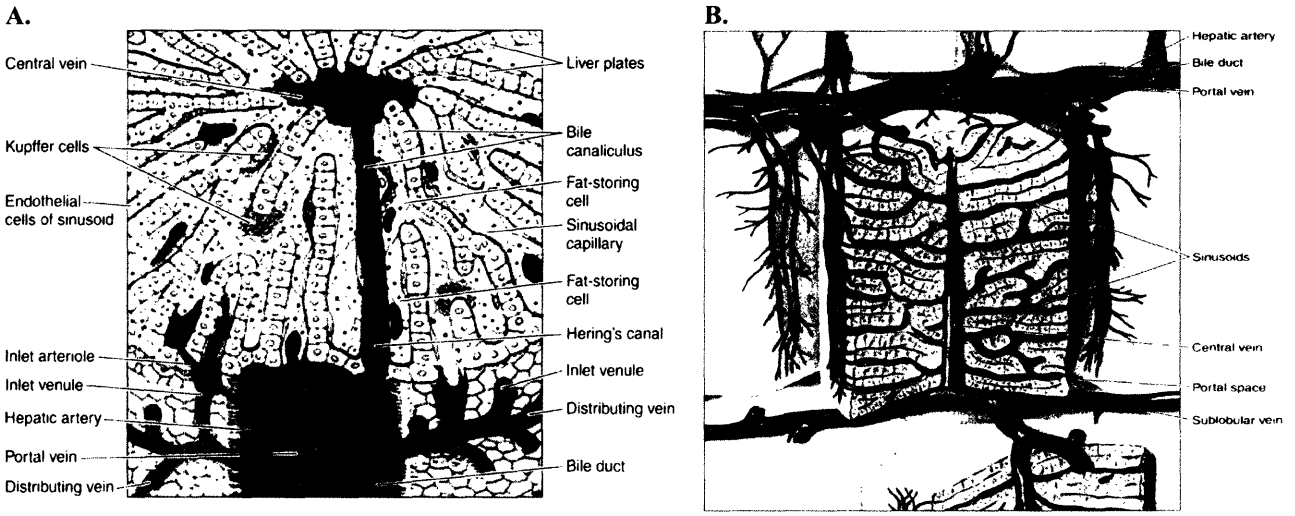

Figure 1.2: Schematic drawing of the structure of the normal liver.
(A) Sinusoidal flow conduits and cellular positioning
(B) Vascularization of one portal triad unit
Images Taken from Junqueira and Carneiro, Basic Histology, a text and atlas, p. 333, Figure 16-11.

1.2 Sinusoidal cells functions, isolation, and investigation

The normal hepatic sinusoid is formed or lined by four cell types, each with its specific phenotypic characteristics, functions, and topography (Figure 1.3). These cells may be

considered to represent a functional unit at the border between the hepatic plates and the blood. They participate in various liver functions and liver pathologies and our knowledge about this contribution is growing (emerging as a new focus in liver research). The heterogeneity of these cell-types and possible cooperation between NPC's and the hepatocytes may add to the overall understanding of liver function (Bouwens et al. 1992). This section briefly reviews the main function and phenotypic characteristics of hepatic sinusoidal cells.

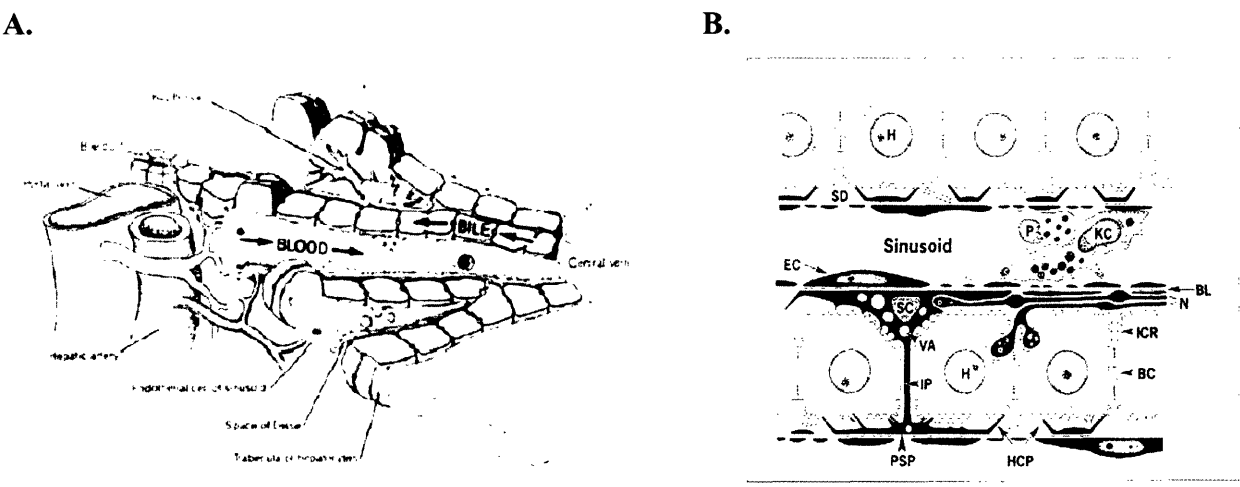

Figure 1.3: Schematic of the Liver Sinusoid
(A) Location of NPC's in reference to a capillary of the sinusoid
(B) Detailed architecture of sinusoidal microarchitecture
*(Image **(A)** is from the these of Tomo Iida, 2003, **(B)** from Wake et al. 1997)*

Hepatocytes

Hepatocytes are highly differentiated epithelial cells that form the cell plates of the liver lobule and perform the majority of the previously described functions attributed to the liver. *In vivo* liver is composed primarily of hepatocytes (~60-65%) (Arias, 2001), who function in detoxification of systemic and portal blood; secretion of plasma proteins, growth factors, and bile; metabolism of proteins, steroids, and fat; and storage of vitamins, iron, and glycogen (LeCluyse et al. 1996).

Endothelial Cells

Endothelial cells (EC's) constitute the closed lining or wall of the capillary (Figure 1.3) and make up 18-23% of all hepatic cells. EC's posses small fenestrations to allow the free diffusion of substances, like O_2, but not of particles like chylomicrons, between the blood and the hepatocyte surface. This filtering effect regulates the fat uptake by the liver. These cells also have a pronounced endocytotic capacity, which makes them an important part of the reticuloendothelial system (Wisse et al. 1996). They are also active in the secretion of bioactive factors and extracellular matrix components of the liver. Zonal heterogeneity of the endothelial lining has recently been reported with regard to its filtering capacity (fenstration) and binding capacity for lectins and cells (Braet et al. 2003).

Kupffer Cells

Kupffer cells (KC's) line the sinusoids of the liver and are attached to the endothelial cells (Figure 1.3) and represent 8-12% of hepatic cells. They are derived from blood monocytes and are the largest group of fixed cells macrophages in the body (Arias, 2001). They are potent mediators of the inflammatory response by the secretion of a variety of bioactive factors and play an important role in the immune defense. KC's are have a high endocytotic capacity and are capable of removing particulate matter from the bloodstream. They phagocytose old cells, foreign particles, tumor cells, bacteria, yeast, viruses, and parasites (Valatas et al. 2003). The large size of the liver and tremendous numbers of kupffer cells make the sinusoids a very important location for clearance of particulate matter from the plasma. About one-third of the hearts cardiac output flows through the liver and makes it a key source of plasma filtration. Kupffer cells are known to be numerically more prominent in the periportal region (Malik et al. 2002).

Stellate Cells

The stellate cells (also called Ito cells or lipocytes) lie in the space of Disse, encircling the sinusoidal endothelium and represent 5-8% of hepatic cells (Geerts et al. 2003). These cells are the main hepatic source of extracellular matrix components and are thought to be the body's main site of Vitamin-A storage (Arias, 2001). These cells are the only sinusoidal phenotype capable of forming junctions with hepatocytes (Friedman et al. 1987). Stellate cells display two phenotypes in normal *in vivo* tissue. In the resting 'quiescent' state, they resemble fibroblasts but their cytoplasm contains numerous droplets in which Vitamin-A is stored. Upon transdifferentiation to the 'activated' state stellate cells elongate to resemble myocytes (Figure 1.4) and exhibit contractile function that plays a role in regulation of sinusoidal tone and resistance (). In chronic liver disease the stellate cells synthesize and secrete collagen into the Space of Disse, leading to "capillarization" (fibrosis) of the sinusoids (Figure 1.4). Stellate cells are more numerous in the periportal region than in the pericentral region of the hepatic acinus. Periportal cells also store higher amounts of Vitamin-A.

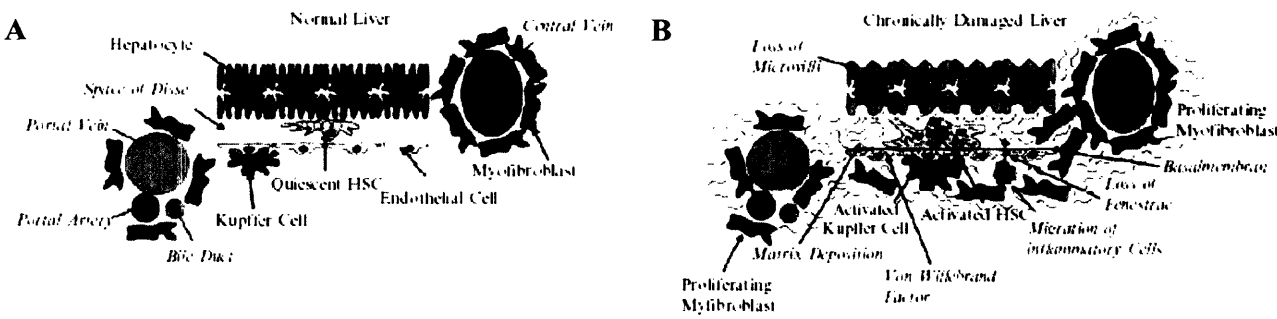

Figure 1.4: Comparative state of liver non-parenchymal cells in normal vs damaged states

Pit Cells

Known to represent a liver-associated population of large granular lymphocytes. They have the capacity to kill tumor cells and probably also play a role in the antiviral defense of the liver. The have been suggested to have a growth-regulatory function in the liver

(Arias, 2001). Like the kupffer cells, they are known to be more abundant in the periportal region of the sinusoid (Gebhardt, 1992).

1.3 NPC co-culture: Rationale and Operating Strategies & Concerns

The major challenge in toxicology and pharmacology research has been to create an *in vivo* primary cell culture analog that maintains liver-specific function and replicates biological tissue features such as polarity, architecture, and normal bile canaliculi formation (LeCluyse et al. 1996). A variety of culture systems have demonstrated the retention of original morphological characteristics and the maintenance of some hepatic function (LeCluyse et al. 1996, Dunn et al. 1992), however, none of these systems have succeeded in replicating the liver associated environmental cures and fully stabilizing the hepatic phenotype (Otsu et al. 2001, Bader et al. 1996, Bhatia et al. 1999, Powers et al 2002a). Hepatocyte viability and liver specific function have been shown to be stabilized for several weeks *in vitro* upon cocultivation with a variety of other cell types. Co-culture strategies have begun to be widely used in studies of various physiological and patho-physiological processes and are considered essential to a viable bioartifical liver device (Allen et al. 2002). This section briefly describes the major functional and operating concerns associated with NPC co-culture.

1.3.1 Purity and Isolation

One of the most fundamental challenges to co-culture is the isolation and purification of the desired non-parenchymal cell phenotype (Smedsrod et al. 1985). Purification techniques have been developed to attain high purity fractions of specific NPC's, but often have low yields and require alterations to the diet, age, or perfusion of a rat (Friedman et al. 1987). Additionally, attaining purified fractions of particular NPC's is labor and time intensive, reagents are costly, and may have undesirable effects on morphology and function of a cell phenotype (Malik et al. 2002). For these reasons many researcher have utilized immortalized cell lines for study of non-parenchymal cell interactions (Vogel et al. 2002, Bhatia et al. 1998).

1.3.2 Extracellular Microenvironment

The focus of new *in vitro* culture systems is to improve the phenotypic stability of the entire sinusoidal component. Sinusoidal cells change phenotype drastically depending on their environment. This 'transdifferentiation' is pronounced enough that it is not clear whether the gene expression differences between cell types or differences between phenotypic states of one of the cell types have a greater dynamic range (Bhadriraju et al. 2002). Thus, even though a particular sinusoidal cell type has a restricted set of expressible genes, the specific proteins that are expressed within that subset can change drastically in response to a given environment. Therefore, it is important to understand and look for replication of sinusoid microenvironmental cues within different *in vitro* culture systems.

1. Cell-Matrix Interactions

Hepatic stability and polarity have been shown to be influenced by variations in composition and topology of extracellular matrix (ECM) (LeCluyse et al. 1996). ECM interacts with cells via binding of intergrins, cell adhesion

molecules (CAM's) and other cell surface adhesion receptors and activate a number of intercellular signaling mechanisms, which enhance homeostasis of cell phenotype (Lodish et al. 2000). Culture of cells with collagen type I or Matrigel® (biologically derived, basal lamina like compound) have induced cells to maintain phenotype specific morphology and express liver-specific function longer than previous hepatocyte monolayer cell culture (LeCluyse et al. 1996, Koide et al. 1990). *In vivo*, changes in the microenviroment of the Space of Disse result in activation of stellate cells, deposition of fibronectin and production of cytokine activating agents by endothelial cells, and increased cytokine secretion and proliferation of Kupffer cells (Li et al. 1999). These results demonstrate the presence of cell-matrix interactions is essential to the homeostasis of an *in vitro* liver analog.

2. Soluble Signals

Hepatic cells communicate via soluble signaling mechanisms following injury to induce the activation and termination of tissue regeneration (Malik et al. 2002). Thus it is apparent that any in vitro system that aims for spontaneous regeneration or reconfiguration of sinusoidal structure must contain the necessary soluble signals. Though the exact mechanisms of these interactions has not been established, strong evidence exists that non-parenchymal cells play a critical role in the release and regulation of these soluble signals (Knittel et al. 1999). Because the composition and time dependence of cell signaling proteins during liver regeneration are unknown, supplementing media with the proteins seems more like a fishing expedition than an science, and a more natural approach is simply addition of physiological ratios of NPC's to *in vitro* co-cultures.

3. Cell-Cell Interactions

Cell-cell interactions, both homotypic and heterotypic have been shown to improve viability and function of in vitro hepatic cultures (Gebhardt et al. 1992, Allen et al. 2002). These cell-cell interactions consist of gap junctions, desmones, E-cadherins and tight junctions, who trigger a number of intercellular signaling mechanisms, which enhance homeostasis of cell phenotype (Lodish, 2001). Heterotypic interactions in hepatocyte-nonparenchymal cell co-cultures are thought to present a highly conserved signal that greatly augments liver specific functions (Powers et al. 1998). Specific mechanisms that stabilize hepatocyte function have not yet been elucidated, but homotypic and heterotypic interactions are thought to be imperative to the function and stabilization of the 'normal' liver phenotype (Allen et al. 2002a).

1.3.3 Bioreactor Designs

The primary concern in the development of an *in vitro* hepatic bioreactor is ensuring that the biological component performs optimally (Allen et al. 2002b). This requires insurance of a homogeneous inertial flow distribution and adequate mass transfer of O_2 and nutrient to the cells and elimination of CO_2 and toxins to meet the metabolic demands of the cells (Powers et al. 2002b, Gerlach, 1997). Additionally cells must have an anchorage substrate that is adequate to allow adhesion of all pertinent hepatic cell

types (Tzanakakis et al. 2000). Various scaffold configurations and seeding methodologies have allowed the adhesion of hepatocytes, stellate cells, and some endothelial cells (Powers et al. 2002, Bader et al. 2002, Tzanakakis et al. 2000), but have not demonstrated the adhesion and retention of all sinusoidal cell types. Future designs will optimally possess a bi-directional flow manifold (or some manner of excretory system incorporation) and consistent incorporation of physiological ratios of each hepatic cell type.

1.3.4 Fundamental Limitation of Primary NPC Co-culture Strategy

The liver sinusoid is a complex system, whose homeostasis is governed by a plethora of intercellular communication mechanisms. Presently, there are many co-culture approaches that focus on the addition of 'non-parenchymal' cells without quantifying relative composition of these cells. Therefore, comparisons between different hepatocyte-NPC co-culture systems may be reporting artifacts of the tissue composition and not actually value added by the system itself (Allen et al. 2002).

1.4 Overview of NPC-hepatocyte Co-culture Systems

The major challenge in toxicology and pharmacology research has been to create an *in vivo* primary cell culture analog that maintains liver-specific function and replicates biological tissue features such as polarity, architecture, and normal bile canaliculi formation (LeCluyse et al. 1996). Prior research strategies using primary hepatocytes has given way to a new focus on co-culturing primary hepatocytes with various types of non-parenchymal cells. These efforts aim to establish *in vivo* like cell-cell contact, cell-matrix interaction, and intercellular soluble signaling. A variety of systems have been used to this end, each with their own merits and limitations (Bhatia et al. 2001). This section describes and briefly analyzes some prominent co-culture systems, which maintain greater liver specific function by establishing conditions that mimic sinusoid architecture, microenvironment and heterogeneous liver tissue composition.

1.4.1 Collagen Gel Sandwich Culture

It has been demonstrated that overlaying primary hepatocytes with a layer of gelled collagen prolongs viability, preserves liver-specific protein synthesis, allows formation of normal bile canalicular networks (indicative of cell polarity), and shows improved maintenance of drug uptake and enzyme production potential (Dunn et al. 1989, 1991; LeCluyse et al. 1994). Co-cultures have been established by adding purified non-parenchymal cells on top of the overlay in an effort to replicate sinusoidal architecture. These co-cultures have demonstrated increased albumin secretion, urea synthesis, and enzyme induction compared to hepatocyte only cultures, and were vastly superior in long-term culture studies (Yagi et al. 1995, Bader et al. 1996, Slaus et al. 2001). This system enables polarization of hepatocytes and quasi-recreation of the sinusoid, facilitating cell signaling and cell-matrix interaction. However, this system lacks the inertial flow profile, subsequent shear stress, and does not place stellate cells in their proper niche. Further, these co-culture systems only show only a temporary stability of function on a temporal scale (Yamada et al. 2001).

1.4.2 Extracellular Matrix Substrata Culture

The complex extracellular substrata (rat liver biomatrix, or Matrigel^{TM}) was used as both an overlay and a substratum, and showed prolonged usable lifetime of hepatocytes (Rojkind et al. 1980 and Bissle et al. 1987, 1990). Cells aggregate on matrix substrata, reestablish themselves as a 3D "spheroid" with increased cell-cell contacts, and maintain liver-specific function (Powers et al. 1997). Co-cultures using Matrigel^{TM} have shown an initial increase in liver-specific gene expression as well as a temporary increase in the stability of this expression in long term cultures (Karam et al. 1997, Liu et al. 1996, Michalopoulos et al. 1999). Comparative studies of Matrigel^{TM} co-cultures and hollow fiber bioreactors reported no statistically significant difference in albumin secretion, urea synthesis or ammonia removal (Yagi et al. 1995, Yamada et al. 2001). However, these studies simply added 'non-parenchymal cells' and did not quantify the incorporation or composition of this cell fraction.

1.4.3 Spheroids

Freshly harvested primary hepatocytes cultivated in spinning cultures with non-adherent plastic substratum have been shown to form multicellular aggregates, or spheroids (Wu et al. 1996). Spheroids have been observed to exhibit enhanced liver-specific function and differentiated morphology compared to 2D cultures (Yuasa et al. 1993, Landary et al. 1985, Hansen et al. 1998, Abu-Absi et al. 2002). The ability of non-parenchymal cells to incorporate into spheroids has been demonstated on a small scale within our lab, more as an artifact than an experimental focus. A more rigorous study using stellate cells and hepatocytes showed that co-cultures spheroids were smaller in size and encapsulated by collagen matrix (Kulig et al. 2004). These co-cultures have not been exhaustively researched and will hold great potential for implantation in bioreactor scaffold systems.

1.4.4 Hollow Fiber Reactors

In an attempt to improve the hepatic microenvironment, investigators have used microcarriers; multicompartment interwoven fibers and multicoaxial configurations of hollow fiber bioreactors (Jasmund et al. 2002). These cultures, which are an adaptation of well-documented kidney reactor, allow constant bio-directional inertial flow and elimination of CO_2 and toxins. Reactor of this type have not thoroughly demonstrated the existence of proper environmental cues, sufficient O_2 and nutrient mass transfer, or the recreation of 'normal' hepatic tissue (Tzanakakis et al. 2000, Allen et al. 2002). Further, the configuration of these reactors does not allow for easy access to the tissue for immuno-imaging or for simple scale up of the reactor.

1.4.5 Roller Bottle Reactors

Primary hepatocytes co-cultured with non-parenchymal cells in collagen-coated roller bottles with a pleated surface have shown increased cellular attachment, reorganization, matrix formation and proliferation (Michalopoulos et al. 1999, 2001). These cultures have revealed the impact of media formulation and mitogens on hepatic tissue reorganization, proliferation, and stability of long-term culture (Mitaka et al. 1999). Roller bottle cultures have demonstrated significant induced proliferative ability and the identity of cell phenotypes elucidated via immunostaining (Michalopoulos et al. 2001).

This system has not demonstrated the natural existence of proper environmental cues, sufficient O_2 and nutrient mass transfer, or control of the recreation of 'normal' hepatic tissue. Thus, roller bottles are useful tools for *in vitro* investigation of embryology, but are seem insufficient as an *in vitro* liver analog.

1.4.6 Micro-fabricated Co-culture on Patterned Channels

Primary hepatocytes are selectively distributed in co-cultures with murine 3T3 – J2 (cell line) fibroblasts using microfabrication techniques to localize desired cell population in patterned configurations on rigid substrates in perfused culture (Bhatia et al. 1997). This culture strategy allows precise determination of fibroblast cell number as an independent variable (Bhatia et al. 1998). Extent of predetermined homotypic and heterotypic cell interactions were investigated at various cellular ratios and interface distances, and were shown to increase albumin secretion and urea synthesis compared to cultures of hepatocytes alone (Bhatia et al.1999). This system is novel in that it enables precise control of cellular composition, tissue architecture, however it may be considered over engineering. In these cultures sinusoidal architecture is predetermined and cells are do not spontaneously reorganize. Additionally, the adhesion and survival of primary NPC's in the fabrication process has not been demonstrated. Therefore, there may still be significant design modifications remaining before this system can be used as a bioartifical liver device.

1.4.7 3-D Micro-fabricated Liver Bioreactor

The Griffith lab has developed and characterized a perfused "capillary bed"-like liver culture system, known internally as the "MilliF bioreactor" (Figure 1.4). (Powers et al. 2002a, 2002b). Hepatocytes are seeded in spheroid aggregates into a microfabricated silicon scaffold containing 40 uniform collagen coated channels. These channels' dimensions (300μm x300μm x230μm) were designed to mimic length scales of cell sorting and self-reorganization (Griffith et al. 1997). The key feature of this system is a split flow pattern between overhead flow parallel to the scaffold and perfusion flow (cross flow) through the capillary bed. This flow manifold was designed and validated as delivering uniform perfusion flow at physiological shear stresses to tissue with minimal or no O_2 or nutrient mass transfer limitations (Powers et al. 2002a).

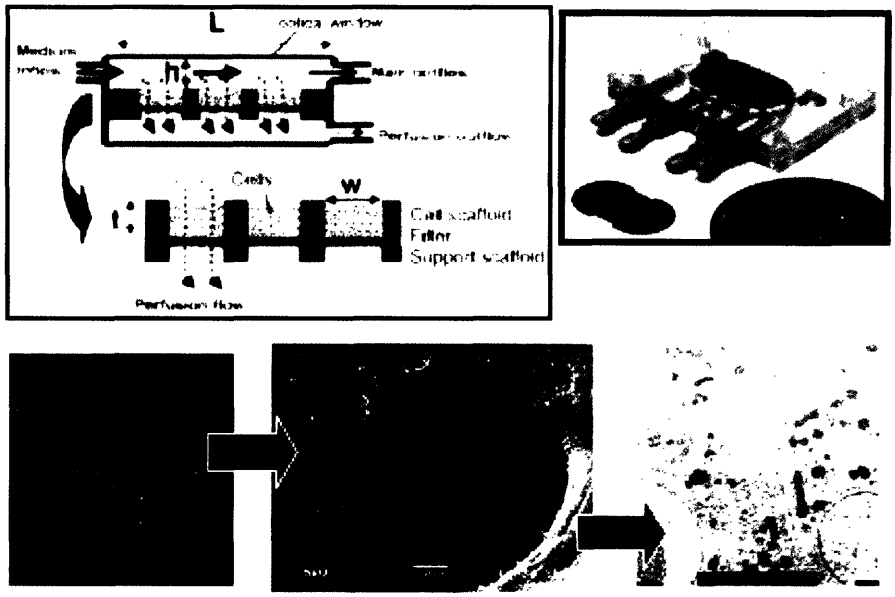

Figure 1.5: 3D microfrabricated liver bioreactor (Powers, 2002).
This figure shows a schematic of the liver bioreactor in operation, a picture of the liver bioreactor polycarbonate housing and silicon chip, and images of the tissue structures formed within the silicon channels.
(Take from the thesis proposal of Corey Moore)

Hepatic tissue cultured in this system has been shown to maintain their tissue-like structures, viability, as well as hepatocyte-specific functions such as albumin and urea synthesis for up to three weeks in culture (Powers et al. 2002b). Transcription and protein secretion of many important drug/toxin-metabolizing enzymes which are normally vastly down-regulated in *in vitro* cultures are better maintained at *in vivo*-like levels in the liver bioreactor (Iida, 2003).

Presently, co-cultures have been established in the bioreactor with hepatocytes and Lig8 stem cells, and are being attempted with endothelial cells. Development of both co-culture systems has been hindered by a lack of quantitative methods to determine presence and efficacy of incorporation of non-parenchymal cell phenotypes. Current quantitation methods focus on immuno-staining and have been hindered by limitations in optical instrumentation and navigating around the confines of the reactor scaffold. These endpoint assays cannot be coupled with functional data and therefore can only be considered semi-quantitative at best. A methodology that would allow both determination of tissue composition and function would be instrumental to further the capabilities of this system for co-culture.

1.5 Methodology for Evaluating Different Culture Systems

In order to evaluate culture systems such as the 3D microfabricated bioreactor as viable systems for NPC co-culture, where hepatic tissue maintains its enzymatic function, a new experimental technique needed to be introduced. Current culture evaluations have centered on maintenance of hepatocyte specific function and do not allow determination of tissue composition. The true impact of NPC co-culture cannot be appreciated without

first elucidating the composition of cell types comprising the tissue. Therefore, we introduce cell type incorporation as a new metric of NPC co-culture. This section briefly describes existing evaluation techniques implemented in our lab for evaluation of hepatocyte culture and their limitations in co-culture; and then introduces our new metric: NPC incorporation.

1.5.1 Existing Evaluation Methods

1. Optical Viability

Cell viability quantification have been developed for validation of the MilliF bioreactor using a solution containing ethidium homodimer for staining non-viable cells red and celcein AM for staining viable cells green (Molecular Probes, Sunnyvale, CA) (Powers et al. 2002b). The dyes are co-visualized with a 450 to 500 nm excitation filter and 520 nm long-pass emission filter (Powers et al. 2002b). A second optical viability assay has been developed that can decipher liver from dead cells using only the DAPI filter and is outlined in Chapter 3 section 1. These assays demonstrated a very general sense of health of the overall tissue.

2. Morphological/ Functional Analysis

Using phase-contrast, electron microscopy, SEM, and TEM the cellular structures of the sinusoids have been observed for stability, polarity, reorganization, cell-cell contacts, and formation of bile canaliculi (Lecluyse et al. 2001). These methods have been developed in-house by Albert Hwa (endothelial cells), Katy Wack (stellate cells), and Joseph Moritz (potential hepatic stem cells) and represent a qualitative biological approach to assess sinusoidal structure and characteristics as a metric of function.

3. Albumin Secretion, Urea Genesis, Drug Metabolism & Health Markers

Serum albumin concentrations of media samples were determined by a sandwich enzyme-linked immunosorbent assay (ELISA) and urea concentration was assessed by Bertherlot determination methods (Powers et al. 2002b). Both of these methods are very general markers of hepatic tissue function and effects by NPC's could be and have been misinterpreted (Yamada et al. 2001, Allen et al. 2002). CYP_{450} and phase II enzyme gene expression has been evaluated via the use of cDNA microarrays and quantitative real time RT-PCR (Sivaraman unpublished work). Analysis of drug metabolism associated enzymes may lack the sensitivity to appreciate value added by NPC co-culture. More meaningful results could be gauged by the determination of more fundamental biochemical tissue health markers. Presently a library of health markers has not been established or validated and thus would represent a highly beneficial, but time intensive methodology with the potential of large variations as a function of tissue composition.

4. Oligonucleotide Arrays

Oligonucleotide arrays (Hedge et al. 2000) allow the global assessment of mRNA expression of a library (hundreds, even thousands) of genes in one experiment. The most common use of these techniques is to determine patterns of differential gene expression

or to compare differences in mRNA expression levels between identical cells subjected to differing culture systems or developmental stages. Furthermore, one of the most significant applications of this technique is gene expression profiling on the whole genomic scale (Schena et al. 1998, Redig et al. 2002, Barrett et al. 2003). Protocols for the use of arrays were developed and validated in our lab by Tomo Iida to compare global gene expression of different culture systems. Such robust comparisons of culture systems will be a useful downstream tool, but the present phase in research does not warrant such a broad analysis. Additionally, these experiments are extremely time, labor, and cost intensive, thus should only be conducted after validation of system efficacy with other more high-throughput diagSnostic methods.

5. Protein Expression Levels by Western Blotting

Western blotting is an endpoint assay for identifying a specific protein in a complex mixture and simultaneously determining its molecular weight. Protein expression levels can also be estimated by comparison with total protein standards. In short, protein is collected from media samples or purified from tissue and is separated by molecular weight via gel electrophoresis. This protein is then semi-quantified by using a high-quality antibody directed against the desired protein. This method demonstrates that genes are being successfully translated following mRNA transcription, and is extremely useful The success of this approach is dependent on the quality and availability of reagents and may lack the specificity for determining protein subtype (i.e. VEGF-R_1 vs.VEGF-R_2.) In addition this method is labor and time intensive and cannot be readily implemented when new proteins or enzymes are identified (Morris et al. 1996). Protocols for western blotting already exist in our lab and antibodies are available for a variety of CYP_{450}'s. Quantification of tissue composition using this method requires knowledge of the mechanisms and kinetics of both transcription and translation, which are presently unknown, and as such is insufficient for our purposes.

6. Enzyme Activity

The enzymatic profiles of microsomal protein fractions are measured using enzyme selective substrates. The method compliments studies that quantify mRNA (transcription) or protein (translation) levels because it shows that function of post-translationally regulated of genes. These techniques require additional cofactors and can show non-selectivity for, or inhibition by certain chemical substrates, potentially resulting in misleading or inaccurate assessments of enzyme expression (Morris et al. 1996). Presently, our lab only has substrates available for measurement of CYP_{450} enzymes. NPC's function more in protein secretion and expression, so it would be prudent as a final validation step to develop assays, which could demonstrate activity of soluble signaling proteins, ECM molecules, and endocytosis. However, enzyme activity adds additional post-translational variables and can only be considered qualitative at best for function of NPC's.

1.5.2 New Metric: NPC Incorporation

The liver community is becoming increasing aware of the importance of non-parenchymal cells in the recreation of the hepatic microenvironment and overall tissue homeostasis. Presently a wide variety of *in vitro* systems are being adapted and new systems developed that support co-culture with non-parenchymal cells. These *in vitro* systems each address different physiological aspects of tissue function, however; few research groups have systematically built culture systems that allow control or determination of tissue composition. Novelty and efficacy of these systems has been evaluated based on their ability to stabilize key features of hepatocyte function. However, each NPC phenotype communicates with hepatocytes to preserve different aspects of normal liver function. Thus, evaluating a co-culture system on the basis of hepatocyte function does not delineate contributions made by the presence of different types of NPC or actual value added by a superior culture system design. Therefore, functional results reported from different in vitro culture systems cannot be meaningfully compared.

From an engineering perspective, determining the composition of NPC's enables completion of a mass balance on the culture system. Such calculation enables the tracking of cell populations to determine presence, proliferation, or death. This type of information offers insight into the phenotypic state of NPC's and the presence of their associated protein expression in the microenvironment. Thus, more focused studies can be undertaken to elucidate mechanistic relationships between NPC's and hepatocytes. From a statistics perspective, knowledge of tissue composition will allow more meaningful correlation between operational system design parameters and their influence on the replication of *in vivo* tissue function (increase the R^2 of *in vitro* analog). Therefore it is certainly prudent to develop methods to quantitatively and reproducibly ascertain the composition of cultured *in vitro* tissues.

CHAPTER 2: ANALYSIS OF METHODS TO QUANTIFY RELATIVE TISSUE COMPOSITION

As mentioned in the introduction, characterization of tissue composition is essential to interpret empirical results and to compare the utility of different co-culture systems. In order to determine tissue composition we evaluate the merits of four existing techniques. These methods are evaluated on their ability to be reliable, quantitative, high throughput, easily developed and economical. This section describes the principles of each technique, compares advantages of each, and steps through the mathematical and experimental design necessary to determine tissue composition.

2.1 Dissociation and Cell Sorting via FACS

The simplest method to quantify tissue composition would be to dissociate the tissue and then mechanically sort (or count) cell types using Fluorescence-Activated Cell Sorting (FACS). This endpoint assay entails first disrupting extracellular matrix and surface-protein associations between cells using a protease, like dispase. Cells in suspension are then reacted with a fluorescent dye that covalently binds only to the monoclonal antibodies of the particular cell of interest (Lodish et al. 2000). These cells are then forced one at a time to flow rapidly through the FACS machine where antibodies are excited by light from a focused laser beam (Shankey et al. 1993). Each cell scatters some light and label cells generate fluorescent signal from the dye. The instrument uses a complex algorithm to convert side/forward scatter of light and fluorescence intensity into electrostatic charge, which should be characteristic of a user defined (gate) unique cell type (Kuckuck et al. 2001). Cells are then separated into collection tubes of purified cell populations.

This method has the advantage that it is very reliable. Additionally, depending on dye selection, FACS can yield cell purities of $> 99\%$. This methodology is commonly used to sort stem cells in different stages of the cell cycle, and has been used effectively to sort $K^+ L^- T^+ S^+$ stem cells.

However, FACS is a terminal endpoint assay that requires the disruption of tissue culture construct and as such can only be coupled to protein secretion data. Such tissue dissociation could destroy surface proteins used to adhere monoclonal antibodies for separate. Additionally, substantial validation of the separated cell populations is still needed to confirm identity of the cell and determine purity achieved by the gates. Furthermore, this methodology requires that a sample contain minimal cell debris and contain as few dead cells as possible (Kuckuck et al. 2001). My initial studies both showed significant debris and substantial hepatocyte auto-fluorescence. Therefore, side and forward scatter data was meaningless and cells had to be separated by fluorescence alone. Monoclonal antibodies for each NPC cell type have only recently been validated in our lab (circa March 2004) and thus further work with FACS was futile. Moreover, FACS equipment is very expensive and operational software is not user friendly. Thus, FACS is not a suitable method for our purposes.

2.2 Immunostain and Section

Another method to quantify tissue composition would be to immuno-stain the tissue and manually count cell types using light microscopy. Tissue is treated *in situ* with paraformaldehyde ('fixed'), which cross-links surface proteins. Next, monoclonal antibodies are bound to targets on the cell surface. These antibodies can either be labeled with a fluorophor or have a second fluorescently conjugated antibody added which is specific for the first antibody. Additionally, functional antibodies that are taken up by the cell *in situ*, like LDL, can be used before fixing. Stained 3D tissue is then dehydrated with serial ethanol and then imbedded in a rigid 'holding material' like agarose. The holding material is then sectioned using a microtome (Leica or Cryostat) into slices of the desired thickness. Sections are then analyzed using light, deconvolution, or confocal microscopy that allow high-quality, low background imaging. These images are then manually counted to garner quantitative estimation of tissue composition. Monolayer cultures require no sectioning and can be counted simply, by microscopy.

Immuno-staining and sectioning allows first hand deterministic quantitation of tissue composition. This is a particularly attractive option since there are few operational challenges that will alter the accuracy of results once the methodology is developed. Thus, we can be certain that the observed results represent the true tissue composition. Additionally, immuno-histo-chemistry is a commonly used technique, already available in our laboratory for many tissue culture systems that allows the coupling of tissue composition with imaging of biological tissue structures.

Implementation of immunostaining techniques on bioreactor samples has proven to have many obstacles. Traditional sectioning protocols have been successfully applied to spheroid aggregates, but were ineffective when employed on the bioreactor scaffold due to the compliance mismatch between the soft tissue and the stiff scaffold. In addition, antibodies for each hepatic cell type needed to be optimized, and were not until recently (circa March 2004) available for reliable use in tissue. Present limitations in fluorescence microscopy only allow three colors of antibody; consequently, one image cannot represent all four hepatic cell types without complicated and unreliable co-localization of multiple antibodies. Furthermore, immunostaining using a fluorophor conjugated to a primary antibody has proven to generate low signal under the microscope and images with such antibodies were poor quality and difficult to quantify. Use of secondary antibodies generates much better fluorescence intensity, but necessitates that each be derived from a different species (ie rat, mouse, goat). This requires diversity of primary antibodies that does not presently exist. Moreover, antibodies can be very expensive and this technique is extremely time and labor intensive. Thus, techniques for immunostaining and sectioning of 3D cultures are not preferred for quantification of relative cell number.

2.3 Oligonucleotide Array

Oligonucleotide chips are produced using semiconductor photolithography to synthesize oligonucleotide probes on glass substrate. These chips are designed and produced on the basis of sequence information alone, without the need for any clones or

PCR products. High-density arrays of defined oligonucleotide probes are constructed using a series of photolithography and chemical syntheses steps. Multiple probe arrays are synthesized simultaneously on a large glass wafer in a method that enhances reproducibility and economies of scale (Gabig et al. 2001, Shackel et al. 2002). Each gene on a Gene Chip is represented by 16 to 21 separate oligonucleotides, with each of these targets having a partner oligonucleotide that has a single base mismatch to determine the degree of nonspecific binding (Iida, 2003). Individual gene expression is based on algorithms that determine the probability of expression based on the signal from each oligonucleotide on the array (Gabig et al. 2001, Shackel et al. 2002). The utility of microarrays was previously discussed in Chapter 1 section 5.

Oligonucleotide arrays (Hedge et al. 2000) allow the global assessment of mRNA expression of a library (hundreds, even thousands) of genes in one experiment. The most common use of these techniques is to determine patterns of differential gene expression or to compare differences in mRNA expression levels between identical cells subjected or developmental stages. Furthermore, one of the most significant applications of this technique is gene expression profiling on the whole genomic scale (Schena et al. 1998, Redig et al. 2002, Barrett et al. 2003). However, the gene expression levels can be used to determine cell number if the proper genes are selected. This analysis will be performed thoroughly in the next section.

Development of a specific 'Griffith Lab' array could lead to high-throughput quantification of desired phenotypic, health, and functional markers. The potential for such a robust data set is very attractive and could garner information on mRNA expression levels of all hepatic cell phenotypes at one time. Thus, an array can be used as a "one shot" diagnostic' to quantify relative cell number.

However, there are substantial limitations in this methodology because a large number of tested gene probes per experiment do not pass statistical filters, hindering its reproducibility and the gene libraries have not be validated for NPC specific genes (Barrett et al. 2003). Therefore, this method cannot ensure reproducibility if used to quantify transcription of specific genes in a culture sample. Further, the sample preparation process is very delicate, where small errors could compromise an entire sample. Moreover, arrays are presently very expensive and not economically feasible. Affymetrix array kits (rat-UG34T) run ~ $500 a piece All things considered, it is not feasible or advantageous to use microarray technology for quantification of hepatic tissue composition.

2.4 Selected Approach: Real Time RT-PCR

Real-time RT-PCR is the most sensitive method for quantitation of gene expression levels (Liu et al. 2002). This two-step assay measures the accumulation of fluorescent DNA product during amplification in the polymerase chain reaction (PCR) and correlates this to the initial amount of target RNA. First, template RNA is reverse transcribed to cDNA using specific primers, hexamers, or oligo-dT primers. cDNA is then copied and amplified in PCR to generate double stranded DNA products (Figure

2.4). In PCR reactions there are three regions: (1) 'baseline' phase -- where primer is in excess and cDNA is limiting; (2) 'exponential growth' phase – where primer and cDNA concentration are on the same order of magnitude; and (3) the 'plateau phase' – where cDNA is in excess and primer is limiting. There are currently four competing techniques available that detect amplified products with about the same sensitivity: (1) Molecular beacons; (2) Hybridization probes; (3) Hydrolysis probes – like TaqMan 5'-exonuclease assay; and (4) DNA binding dyes (Burton et al. 2000). Each technique has its own unique merits, but we shall focus DNA binding dyes because they are the most economic and administratively feasible in the context of this work.

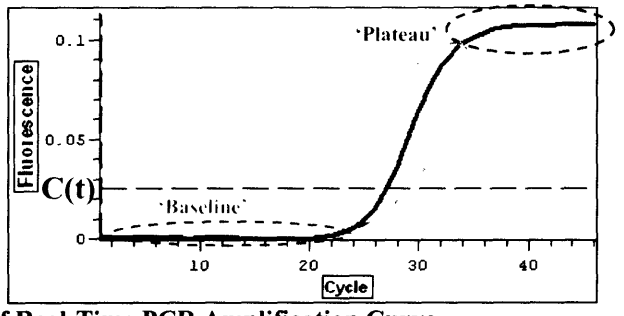

Figure 2.4.1: Example of Real-Time PCR Amplification Curve

DNA-binding dye detection involves the direct binding of a fluorescent dye (SYBR Green I) into DNA during PCR. SYBR Green I has an undetectable level of fluorescence when it is in its free form, but each time the cDNA is copied (cycle) the SYBR Green I is bound to a dsDNA (Figure 2.4.2) and begins emitting fluorescence (Giulietti et al. 2001).

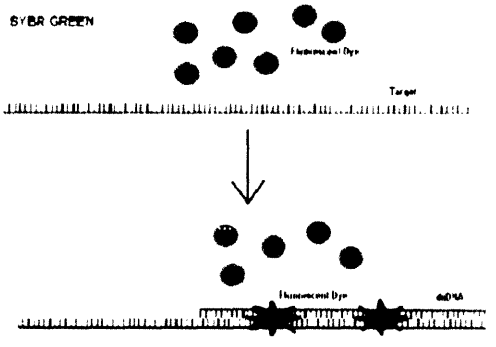

Figure 2.4.2: Schematic Diagram of SYBR Green dye incorporation into dsDNA (Image is from www.qiagen.com)

When monitored in real-time, this results in an increase in the fluorescence signal that can be observed during the 'exponential growth' phase. During the beginning of the 'exponential growth' phase a fluorescence signal threshold (Figure 2.4) is defined at which point all samples can be compared. This threshold is calculated after normalizing for the global minimum background fluorescence. Therefore, the fractional number of PCR cycles required to generate enough fluorescent signal is defined as the cycle

threshold, C(t). The value of C(t) is then directly proportional to the amount of starting template and are the basis for calculating rRNA or mRNA expression levels as follows:

$$\alpha_o = \frac{\alpha(t)}{\varepsilon_{PCR,i} * 2^{C(t)}}$$

where 'α' is fluorescence intensity, and 'ε' is the efficiency of PCR amplification of target primer '*i*' (should be unity).

These gene expression levels can be quantified to a resolution of ~ 5 x 10^4 initial templates (~ 1 cell) (Halford et al. 1999). Two different methods are commonly used to quantify results of real-time RT-PCR: the standard curve method (absolute quantitation) and the comparative threshold method (relative quantitation). Use of absolute quantification can yield cell number if a cell-specific, stable gene is defined. Relative composition can then be determined via the ratio of a particular target cell type to the total cells.

This technique is a highly sensitive, fast, accurate and quantitative means of measuring gene expression compared to other end point assays (Ginzinger et al. 2002). Further, the technique high throughput, allowing 96 samples to be run simultaneously in two hours. Additionally, there exist tremendous returns to scale. Each RNA isolation can yield up to 40 RT reactions, which can yield up to 100 PCR samples. Thus, many different genes can be analyzed in parallel, allowing the coupling of tissue composition data with tissue function data.

Quantification using gene expression is prone to culture system and temporal variability. Therefore, substantial controlled validation experiments must be performed to confirm gene expression levels in different cell culture systems, microenvironments, and time points. On a more technical level, there exists the possibility of coamplification of genomic DNA and primary dimers (Walker et al. 2002). These unwanted products can be controlled, but require careful primer design and experimental control. Additionally, small pipetting errors propagate into large differences in gene expression levels, so extreme care must be taken to ensure the technical consistency of plate loading for PCR. Furthermore, variations in amplification efficiency have been observed in different primers (Burton et al. 2000). Thus, each primer must be validated to ensure a linear trend with a slope of –1.7 on a natural log scale (-3.32 on $\log_{10}$ scale). These limitations are all manageable by carefully planned and executed experiments; hence, this is a very attractive technique for use of quantification of tissue composition.

2.5 Selection of Real Time RT-PCR

A successful analytical technique to determine tissue composition will be highly quantitative, high throughput, easy to implement, and be able to couple incorporation data with functional data. Each of the four diagnostic techniques has been previously described and their pros and cons are compared in Table 2.5

Table 2.5: Pros and Cons to Relative Cell Number Quantitation Methods

FACS	Immuno-staining
Pros	*Pros*
- Simple procedure	- Couple w/ biological imaging
- Can yield high purity separation	- Direct count of cell number
Cons	*Cons*
- Terminal assay	- Terminal assay
- Time intensive	- Need to optimize antibodies
- Need to optimize antibodies	- Time & labor intensive
- Need to purify tissue debris	- $$$
- Need significant validation	- Considerable operating limitation
Microarray	**Real-time RT-PCR**
Pros	*Pros*
- Many genes at once	- Quantitative
- Couple w/ functional data	- High throughput
Cons	- Sensitive
- Semi-quantitative	- Couple w/ functional data
- $$$	- Many genes from same sample
- Time & labor intensive	- Economies of scale
- Filter out many genes	*Cons*
- Need significant validation	- Significant system constraints
- Results prone to variations in culture system	- Need significant validation
- Tedious data analysis	- Results prone to variations in culture system
- Only one sample at once	- Error can propagate exponentially

This comparison shows that Real-time RT-PCR is the only diagnostic technique that meets the defined system criteria. It is also the most time, labor, and economically feasible choice. Additionally, techniques have already been established in our lab that reduces the barriers to implementation. However, it will have to be coupled with immunostaining assays in order to validate the quality and accuracy of standard calibrations curves before its efficacy can be shown.

2.6 Data Analysis

There are two primary methods used for the quantitiation of gene expression levels: absolute and relative quantification. We have used absolute quantitation to calculate relative tissue compositions. Relative quantitation has been used to gauge the stability of genes in different culture systems. This section steps through the mathematics used to determine our results. Herein, we briefly described the mathematics needed to make such calculations.

Absolute Quantification

In this quantitation method a sample of known concentration is used to construct a standard curve. Logarithmic regression is used to fit slope, m, and intercept, b, into the form:

$$C(t)_{standard} = m_i * \ln(C_{j,standard}) + b_i$$

where the underscript, '*standard*', refers to the sample of known (cell counted or UV spec'd) concentration, underscript, *i*, refers to any target cell-type specific gene, and underscript, *j*, refers to the representative standard curve concentration (i.e. C_{cDNA}, C_{RNA}, C_{cell}) .

Next, real-time PCR is run on tissue samples to yield sample C(t) values, $C(t)_{i,j,sample}$. Sample C(t) values are then correlated to concentration using the standard curve. Target cell-type genes should yield the same concentration. To minimize errors caused by variations in these genes' expression levels, concentrations are pooled to yield the average concentration contribution of each cell-type as follows:

$$C_{j,k,sample} = \frac{\sum_{i=1}^{n_k} e^{\left(\frac{C(t)_{sample}-b_i}{m_i}\right)}}{n_k}$$

where '*k*' refers to the cell type of the target gene (i.e. hepatocyte, stellate, KC, or EC), '*sample*' refers the nature of the tested sample (i.e. *in vivo*, standard, 2D collagen gel, etc...), and '*n*' refers to the number of pooled genes for a specific cell-type.

Relative composition can then be determined by taking the ratio of the mean concentration contribution of a particular target cell type to the total representative concentration as follows:

$$f_k = \frac{C_{j,k}}{\sum_{k=1}^{4} C_{j,k}}$$

where '*f*' refers to fraction of total concentration.

If cDNA concentration is used as the basis (*x*-axis) of the standard curves, it can be correlated to RNA concentration as follows:

$$C_{RNA} = \frac{C_{cDNA}}{\varepsilon_i}$$

where, 'ε' is the efficiency of reverse transcription, and '*i*' refers to the target RNA transcript. This RNA concentration can be further correlated to cell number of a particular cell type as follows:

$$N_{cell,i} = \frac{C_{RNA}}{C_{RNA/cell,i}}$$

where $C_{RNA/cell}$ is the concentration of RNA in a given cell of type, *i*,.

Relative Quantification

Relative quantification is a comparative C(t) method that determines the changes in RNA levels from a control state across multiple sample states and expresses it relative to the expression levels of an internal control ('housekeeping gene'). First, the relative

expression levels of a transcript is normalized to the expression levels of a stable, highly expressed reference gene as follows:

$$\Delta C(t)_j = C(t)_{i,j} - C(t)_{Ref,j}$$

where '*j*' is the origin of the sample, '*Ref*' is the selected 'housekeeping' gene, and '*i*' is the target gene. This normalization eliminates the need to for standard curves with known concentrations, and is indicative of the relative expression level of a gene in a cell. Such relative expression levels can be used to compare genes within the same sample. Next, gene expression levels in different samples are evaluated by comparing relative expressions levels of a target gene in a sample relative to those in a 'control' sample (such as *in vivo* tissue) as follows:

$$\log_2(FC_i) = \Delta\Delta C(t)_i = \Delta C(t)_{i,control} - \Delta C(t)_{i,j}$$

This type of analysis allows one to determine fluctuations in gene expression based on different permutations to cell culture environment.

2.7 Experimental Real-time PCR Design Concerns

Due to the exponential nature of PCR amplification, small technical or design errors committed prior to the PCR can yield substantial error in results. Thus, it becomes necessary to define a set of criteria that must be validated and appreciated in the experimental design in order to attain reliable results.

Experiments should be designed to possess the:

- Standardization of RNA isolation protocol.
- Validation of presence of sufficient high-quality RNA.
- Calculation and standardization of the efficiency of the reverse transcription reaction.
- Validation of 100% efficiency of primers during PCR amplification.
- Validation of the absence of multiple PCR product, primer dimer, and genomic DNA coamplification
- Standardization of PCR plate loading technique to minimize pipetting error.
- Validation of purity of standards used for development of calibration curves.

2.7.1 Importance of Replicates and Controls

Replication is essential in experimental design because it allows the averaging of expression levels of different samples. Statistically this is important because averages are less variable than their component terms, and the degree of variation can be used to assign significance to observed trends. The ability to assess such variability allows identification of biologically reproducible changes in gene expression levels (Yang et al. 2002, Slonim et al. 2002, Shackel et al. 2002).

Sources of variation in real-time RT-PCR can be partitioned into three layers: biological variation, sample variation, and technical error. In general, biological variation between different inbred rats is 30%, sample variation is 20-40%, and technical error is 5-15% (Lee et al. 2000, Churchill et al. 2002).

Biological Replicates

Biological variation is inherent to all organisms and can arise from genetic or environmental factors. The term 'biological replicate' refers to RNA collected from different rat perfusions, or passages of a cell line. The incorporation of biological replicates into experimental design will represent as close to the actual gene expression level as possible present in a given species. Therefore, biological replicates are the most important type of replication.

Sample Replicates

Sample variation is introduced by heterogeneity of samples taken from the same biological replicate or variations in the efficiency of reverse transcription to cDNA. Heterogeneity is addressed by pooling multiple samples taken from the cultures or perfusion during the RNA isolation process. This creates a more homogeneous and more representative sample of cell culture gene expression.

To curb variance in reverse transcription, multiple RT reactions should be performed on the same RNA samples and UV spec readings taken to determine the actual sample cDNA concentration. These results will allow RT reaction efficiency to be calculated and statistical analysis to be incorporated into standard curve development. This type of replicate is crucial to the validity and use of standard curves for absolute quantification.

Technical Replicates

Technical error is primarily associated with pipetting error in the loading of cDNA into PCR plates arising from 1μL cDNA samples, which fall below the pipettors' volume threshold for accuracy, 4 μL. Error at this level also arises in the reading the fluorescent signals by the detection machine, which may be affected by factors such as misalignment of PCR plate caps or the presence of dust and oil on the PCR plate caps.

2.7.2 Validation of Real-Time RT-PCR

In order to validate our PCR experiments, two methods were performed. Monolayer cultures were stained with fluorescent NPC specific antibodies and manually counted via light microscopy using the previously described methodology (Section 2.2). *In vivo* tissue composition data was pooled and averaged from reports in literature (Gebhardt et al. 1992, Malik et al. 2002, Geerts et al. 2003, Smedsrod et al. 1994).

2.7.3 Statistical Analysis

Statistical analyses were performed using the Student's two-tailed t-test for samples with unequal variances in Excel (Microsoft Excel, Redmond, Washington). Significance was assigned for $p < 0.025$. Statistical analysis was not performed if the sample population size, n, was less than three.

CHAPTER 3: STANDARD PROTOCOL DEVELOPMENT

In order to establish non-parenchymal cell co-culture in our lab, several standard protocols were necessary to develop and validate. This chapter describes the development and optimization of each procedure and generates the best current protocol for each process in the appendices.

3.1 Nuclear Stain Cell Count Protocol

The first step in the co-culture of non-parenchymal cells is the accurate estimation of cell number for input into the desired culture systems. NPC's are acquired via centrifugation of the supernatant of the hepatocyte isolation spins (Smedsrod et al. 1985). The resulting cell pellets have a red/pink hue characteristic of the presence of erythrocyte contaminants. Trypan blue nuclear exclusion has been used to characterize the cell yield and viability by cell counting on a hemacytometer (Block et al. 1996). This procedure is very difficult to consistently and accurately apply to NPC cell counts. The use of trypan blue exclusion overestimates cell count because erythrocytes have no nucleus and therefore all appear to be small live NPC's. Further error is propagated by the large incidence of cell debris, parenchymal cell blebs (necrotic and apoptotic bodies), and variation of size in NPC's (between 10-20 μm). The combination of these factors leads to the recognition that NPC counting has a large inherent technical error.

Presently, there is a scarcity of researchers that have acknowledged or aimed to circumvent this inherent error. Some groups have turned to cell lines in their co-cultures, while others don't report cell-counting protocol in their methodology (Bhatia et al. 1997). To circumvent this problem we aimed to use fluorescent nuclear staining to distinguish live cells from dead cells. Hoechst 33342 (Molecular Probes) nucleic acid stain is a popular cell-permeant nuclear counter-stain that emits blue fluorescence when bound to dsDNA, and has been used to count total cell number. SYTOX® Orange dye (Molecular Probes) stains nucleic acids in cells with compromised membranes. This stain is useful as an indicator of cell death and is much brighter than propidium iodide (Pierce et al. 2003). The combination of these two nuclear stains allows the determination of cell count and viability just as trypan blue, but will selectively exclude erythrocytes and cell debris. Therefore, the use of a fluorescent nuclear stain cell count protocol has been evaluated

3.1.1 Nuclear Stain Cell Count Protocol: Optimal Dye Concentration

Molecular Probe's researchers used calf thymus DNA to optimize each stains concentration. These concentrations were reported to be 20 μL/mL and 2 μL/mL for Hoechst 33342 and SYTOX® Orange respectively. Since calf thymus DNA is free in suspension we felt it was necessary to re-evaluate these optimal concentrations since cellular DNA is condensed rather than free floating and cellular membranes present additional diffusive resistance. To perform this optimization the concentration of stain was varied and the resulting fluorescence intensity measured using a Spectramax Gemini XPS (Molecular Devices). These measurements were done using calf thymus DNA, human 293 cells, hepatocytes, and the non-parenchymal cell supernatant at a constant incubation time of 15 minutes. Figure 3.1.1 shows that optimal concentrations of <1 μL/mL and 2 μL/mL for Hoechst 33342 and SYTOX® Orange respectively.

A.

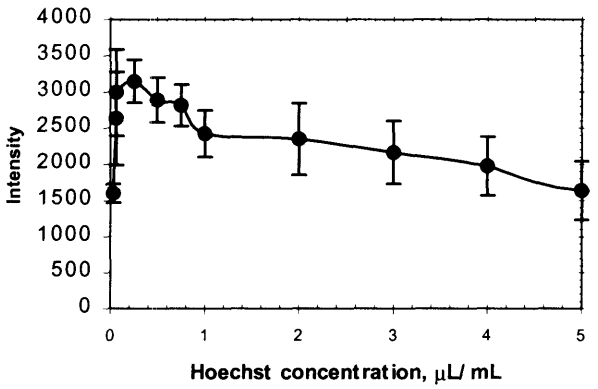

B.

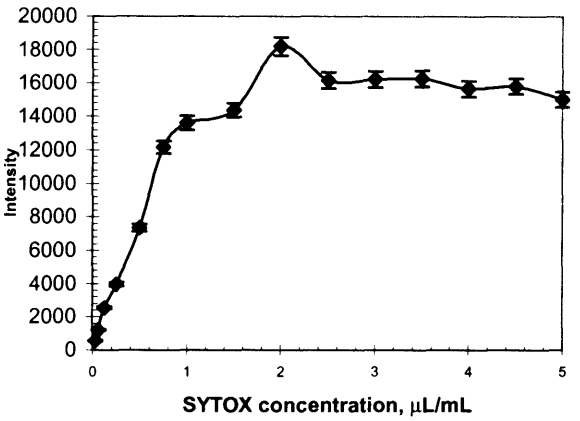

Figure 3.1.1: Determination of optimal dye concentration

Next, we examined the effect of incubation time on fluorescence. We found that after 5 minutes the shapes of concentration curves could be reproduced and maintained for up to the last time point, 30 minutes (Data not shown). This data assumes that samples were not exposed to light, which will photo-bleach the fluorophores.

3.1.2 Nuclear Stain Cell Count Protocol Evaluation

These optimized stain concentrations were then applied to cell counting. The staining protocol described in Appendix 2 is virtually identical to the Trypan Blue exclusion protocol. Use of the hemacytometer allows all of the cell-yield calculations to remain the same. Figure 3.1.2 shows the resulting hemacytometer display for the trypan blue exclusion protocol and for the nuclear stain protocol. Three features that stand out are the exclusion effective exclusion of erythrocytes, the limited background fluorescence intensity from dead cell free-floating DNA, and the exclusion of parenchymal cell blebs. Therefore, this protocol is an effective technical means to count non-parenchymal cells. However, this protocol has dual caveats of stains being extremely sensitive to light and taking approximately ten minutes more than the trypan blue exclusion protocol. A further inefficiency is that endocytosed cells give a false positive, but the number of such cells is low compared to the total yield and thus is considered negligible.

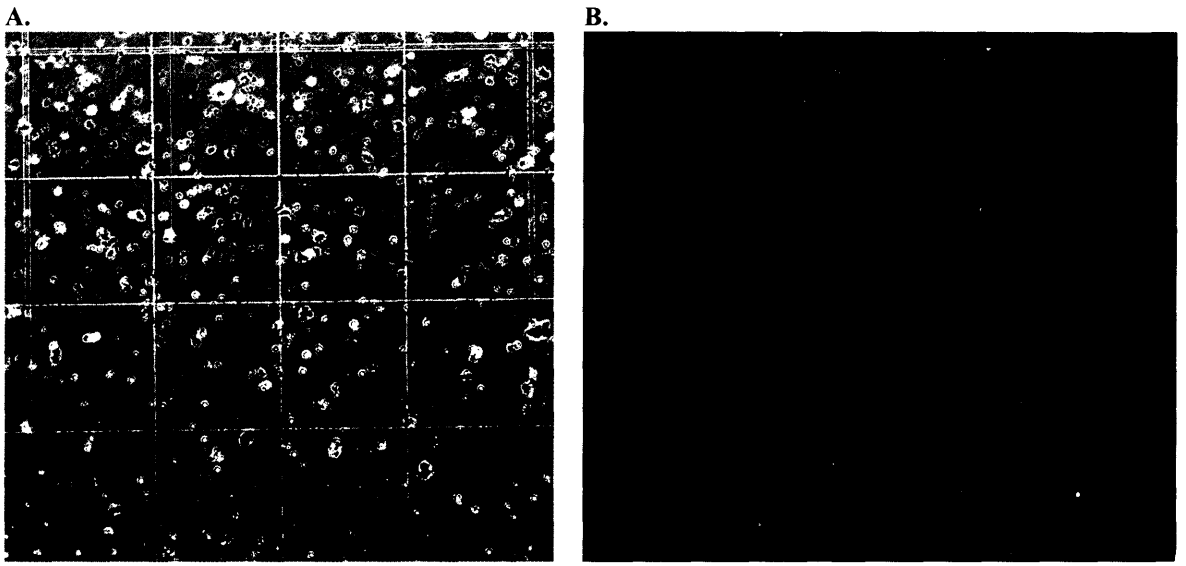

Figure 3.1.2: Comparison of Hemacytometer Display using Trypan Blue Exclusion & Nuclear Staining

Further, nuclear staining and trypan blue exclusion protocols have been compared quantitatively using cell count and viability as a metric. Figure 3.1.3 shows yield and viability as derived by each counting protocol for perfusion flow rates of 15 mL/min (n = 4) and 25 mL/min (n = 5). Three different researchers performed cell counts of each protocol to incorporate variations caused by human error. Cell counting performed using the trypan blue exclusion protocol resulted in much higher cell yields and viability for both flow rates. Statistical analysis using a Student's t-test showed that differences in both cell yield and viability from each protocol are significant ($p < 0.001$). Additionally, the cell yields ($p_{Trypan} = 0.01$, $p_{Nuc} = 0.02$) and viability ($p_{Trypan} = 0.02$, $p_{Nuc} = 0.06$) were inversely correlated to flow rates.

It is interesting to note that the cell yield determined by the trypan blue exclusion protocol is approximately the same as that of the isolated hepatocytes and of similar viability. This is surprising considering the fact that non-parenchymal cells comprise only ~ 40% of the total cells of the liver sinusoid. Further, the isolation protocol efficiency for NPC's is only ~ 50% and sinusoidal cells experience more extreme trauma from the perfusion due to greater local shear and exposure to collagenase (Smedsrod et al. 1985). Combining these factors it seems evident that trypan blue exclusion greatly overestimates both yield and viability, whereas the nuclear staining protocol garners results concomitant to theoretical yield calculations. Therefore, the nuclear staining protocol adds tremendous value in accuracy to NPC cell counting. Considering that NPC's that survive the perfusion are considered to be more phenotypically stable than hepatocytes (Valatas et al. 2003), the cost of ten additional minutes required for this staining protocol pales in comparison to the reward.

A.

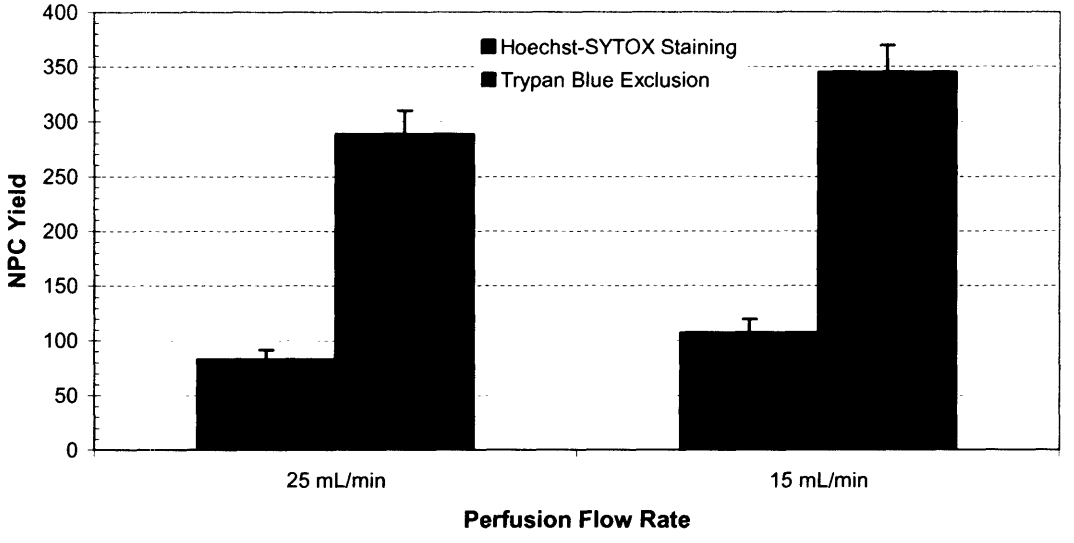

B.

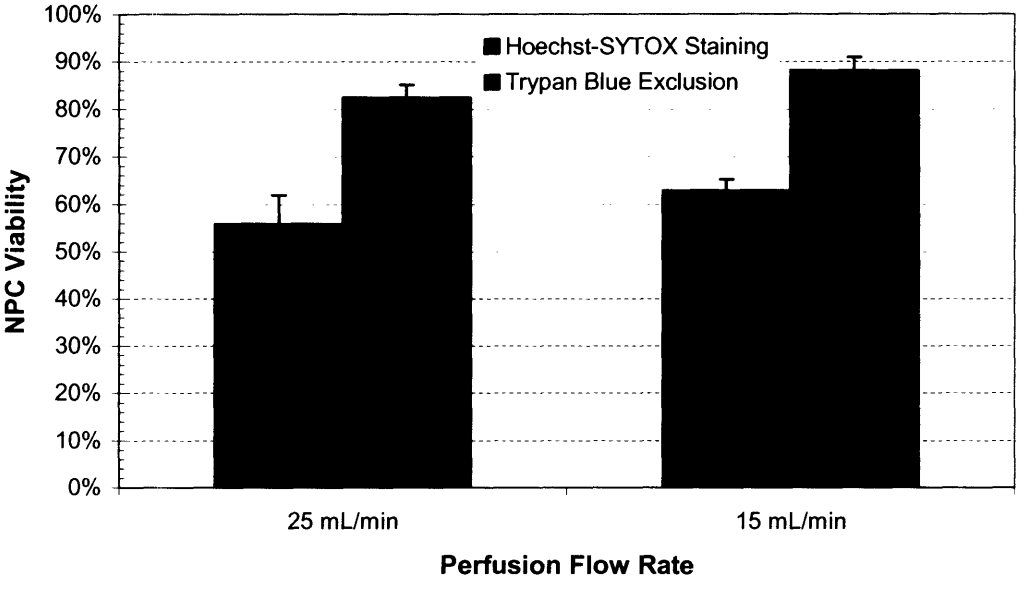

Figure 3.1.3: Variation in NPC cell count and viability using traditional Trypan blue exclusion & Hoechst/SYTOX® protocol
Perfusions performed at high (25 mL/min) and low (15 mL/min) perfusion flow rate with constant blendzyme concentration are compared by their ability to yield NPC's using traditional nuclear trypan blue exclusion (100 uL/mL) and a new Hoechst 33342 (1 uL/mL) and SYTOX® Orange (2 uL/mL) staining protocol. The fluorescence protocol yields a lower total cell due to its exclusion of contaminate erythrocytes from the overall cell count.

3.2 NPC Isolation Methodology

High-quality standards are absolutely critical in order to use real time RT-PCR to quantify cellular composition. Therefore, standards would optimally be derived from

isolated cell fractions with purity as close to 100% as possible. This section details the validation of specific NPC isolation protocols that were used to acquire 'purified' cell populations for real time RT-PCR standards.

3.2.1 Isolation and Strategies for Purified Hepatocytes

Purified hepatocytes were isolated following blendzyme perfusion by centrifugation using an isotonic Percoll gradient (LeCluyse et al. 1996) and this protocol is detailed in Appendix 3. The Percoll density gradient (1.08 g/mL) allows the penetration of the more dense hepatocytes while selectively removing smaller (less dense) non-parenchymal cells, small hepatocytes, dead or dying hepatocytes, and erythrocytes. Immunostaining of the isolated hepatocytes on collagen-gel sandwiches were negative for kupffer and stellate markers (data not shown). Endothelial cells are much less dense and have been previously shown to be unable to penetrate 45% Percoll gradient (Smedsrod et al. 1985). Following isolation cell count and viability is determined by trypan blue exclusion using a hemacytometer. It is important to note that hepatocytes rapidly loss expression of many functional genes following isolations and as such limiting the amount of time between isolation and seeding in culture or homogenization is extremely important for good results.

3.2.2 Isolation and Strategies for Purified Endothelial & Kupffer Cells

Endothelial and kupffer cells are commonly purified using either magnetic bead cell sorting or centrifugal elutriation procedures. Cationic magnetic bead sorting protocols using SE-1 antibody have been developed by the lab of Donna Stoltz (unpublished, UPitt) and show potential for >95% purity of sinusoidal endothelial cells. This protocol is time consuming was designed for much more focused approaches to endothelial cells specific research and as such was viewed as a transition to be made in the long term. Centrifugal counter-flow elutriation has been performed by researchers in the Griffith lab in collaboration with the Sherley Lab and shown to enrich kupffer cell purity to >90%, but is a time consuming process that demonstrated very low yields of Kupffer cells. An alternate approach to separate endothelial and Kupffer cells using a two-step Percoll® (Sigma-Aldrich) gradient (Smedsrod et al. 1985) followed by selective adhesion to a substrate (Appendix 3) were used. These isolation procedures were optimized for choice of substrate and adhesion time.

Two-step Percoll® Gradient

We have used a modified version of the two-step Percoll® density gradient defined by Smedsrod et al. (1985). In brief, cells are forced by centrifugation through two different density layers (ρ_{high} of 1.066 g/mL , osmolality=310mOsm and ρ_{low} = 1.037 g/mL, osmolality =300mOsm)of isotonic Percoll solution and separated based on density. In our system, stellate and endothelial cells penetrate the low-density layer, but are unable to do so to the high-density layer and are thus captured at the interface. Kupffer cells experience similar separation. They are trapped at the interface unless they have endocytosed significant debris, at which point they become denser and travel into or through the bottom layer. Both small and normal hepatocytes pellet at the bottom, while dead, dying, and compromised cells are segregated to top of the low density layer. The resulting suspension is divided into two distinct fractions (Figure 3.2.1).

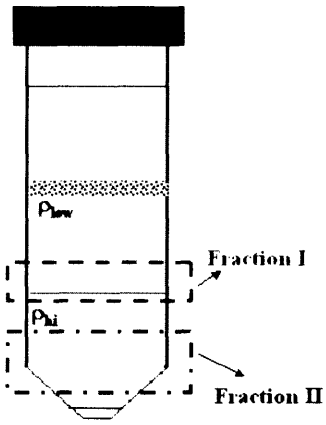

Figure 3.2.1: Two-Step Percoll® Gradient

Fraction I contains purified NPC's, enriched in endothelial cells (EC's) and free of debris, erythrocytes and most paranchymal cells (PC) and PC blebs. Fraction II contains NPC's, enriched in Kupffer cells (KC's), but with some PC, PC bleb, and erythrocyte contaminant.

Interaction of Percoll with Isolated Liver Cells

Transmission electron microscopy following a period of cultivation of EC's and KC's show that Percoll® is rarely internalized following separation. Further, culture with Percoll® in the media shows appreciable endocytosis of Percoll® particles in cytoplasmic vacuoles, but no association with the cytoplasmic membrane in both KC's and EC's (Smedsrod et al. 1985).

Methods for EC & KC Purification Optimization

Different cell phenotypes demonstrate preferential adhesion to substrate based on their surface receptor profile (Allen et al. 2002). Kupffer cells initially adhere rather quickly to almost any substrate but will eventually release and apoptose (Sun et al. 2003). While endothelial cells require more time to adhere and spread but do so with greater adhesion strength than KC's, particularly on collagen and fibronectin (Vidal-Vanaclocha, 1997). These observations make sense biologically, because endothelial cells interact directly with extracellular matrix in the sinusoid, whereas macrophages generally adhere to foreign cells preceding endocytosis. Studies done comparing glass and tissue culture treated plastic showed glass to have ~10% greater purity at the cost of significant yield (Malik et al. 2002). Additionally, initial experiments conducted by Albert Hwa showed that endothelial cells adhered weakly and spread poorly on non-tissue culture treated plastic. We chose to explore temporal differences in yield and purity of KC's and EC's on non-tissue culture treated plastic (happy medium between glass and TC-plastic), collagen and fibronectin as substrate.

Substrate adhesion and time course experiments were performed using 30 μg/mL collagen, 30 μg/mL fibronectin laid on non-tissue culture treated (nTC) plastic or

just nTC plastic. Concentrations were not optimized in this study, but selected based on previous experiments conducted by students in the Griffith group. Kupffer cell phenotype was observed via light microscopy imaging (Open Lab 2.0; Improvision, Lexington, MA) to have a high cytoplasm to nucleus ratio (looks like a fried egg) and to commonly have necrotic bodies engulfed in cytoplasmic vacuoles within its plasma membrane (Figure 3.2.1A). KC phenotype was further validated using ED-2 immuno-staining performed by Megan Whitmore (Figure 3.2.1B). Massive parenchymal cell bleb contamination was noticed in KC isolations. KC isolate contaminants stained weakly but positively with Hoechst 33342 nuclear stain which confirmed that they were in fact necrotic or apoptotic parenchymal cell bodies instead of erythrocytes (data not shown). Endothelial cell phenotype was determined by visual assessment of cell morphology using light microscopy. These cells posses a dark nucleus and their plasma membrane is visibly spread (Figure 3.2.1C). Stellate cell phenotype was determined by staining with GFAP and was rare in these cell isolates; no images of this staining are shown due to poor quality of images.

A.

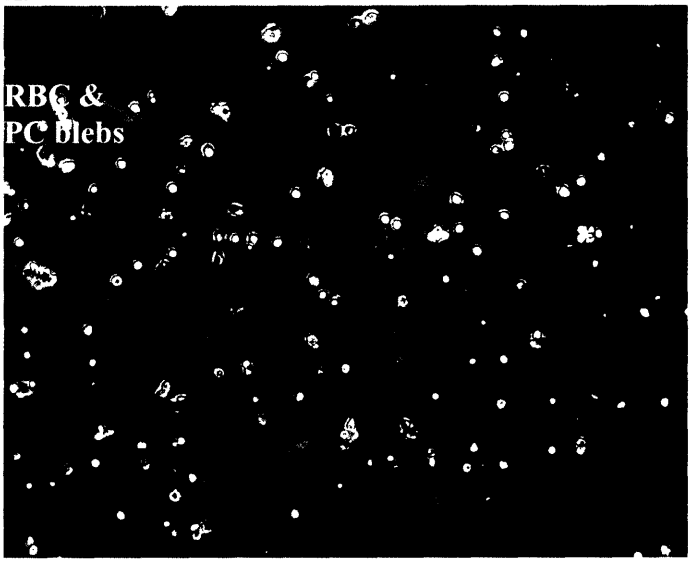

B.

C.

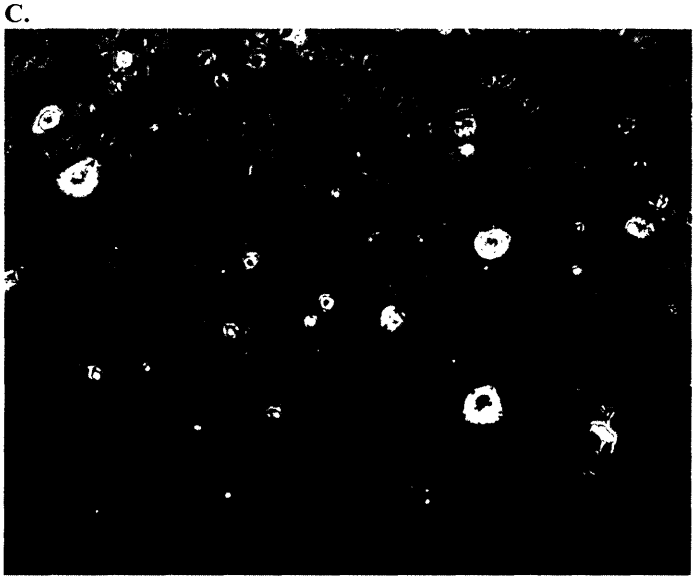

Figure 3.2.2: Images of KC and EC phenotype using light microscopy
(A) Kupffer cells isolated by selective adhesion on non-tissue culture treated plastic shows massive contamination with parenchymal cell blebs, and low overall target yield
(B) ED-2 staining of Kupffer cells on nTC-plastic gives the ability to quantify cell number of KC's
(C) EC cell fraction cultured on 30μg/μl collagen monolayer.

Cell purity calculations were made by manual counting of cells, as per the phenotype detection protocols previously described. Cell yield was determined by averaging counts of eight small sample populations in four different defined regions of a well and scaling to yield to the area of a well (similar to the counting strategy employed by hemacytometer methods).

$$N_{well} = A_{well} * \frac{\frac{\sum_{i=1}^{n} N_{field,i}}{n}}{A_{field}} \quad ; \quad n \geq 8$$

Results of EC & KC Purification Optimization

Time course experiments showed that as $t \rightarrow 0$, kupffer cells reach their maximum purity (data not known), but at the same time as $t \rightarrow 0$ cell yield $\rightarrow 0$. Therefore, purity was sacrificed for yield such that enough cells were present to reach the minimum total RNA content requirements for isolation and PCR procedures yielding a final KC adhesion time of 0.5 hr. Collagen substrate demonstrated both a higher magnitude of purity and a faster separation of endothelial cells than fibronectin and nTC plastic (Figure 3.2.3). The velocity of separation, dP_{EC}/dt, appeared to reach a maximum at ~2.5 hr and thus this maximum has been selected as the adhesion time for EC culture. This phenomenon seemingly occurred due to both increased EC adhesion to collagen and dissociation of KC's. KC impurity occurred predominantly via cell-cell contacts directly to EC's (data not shown).

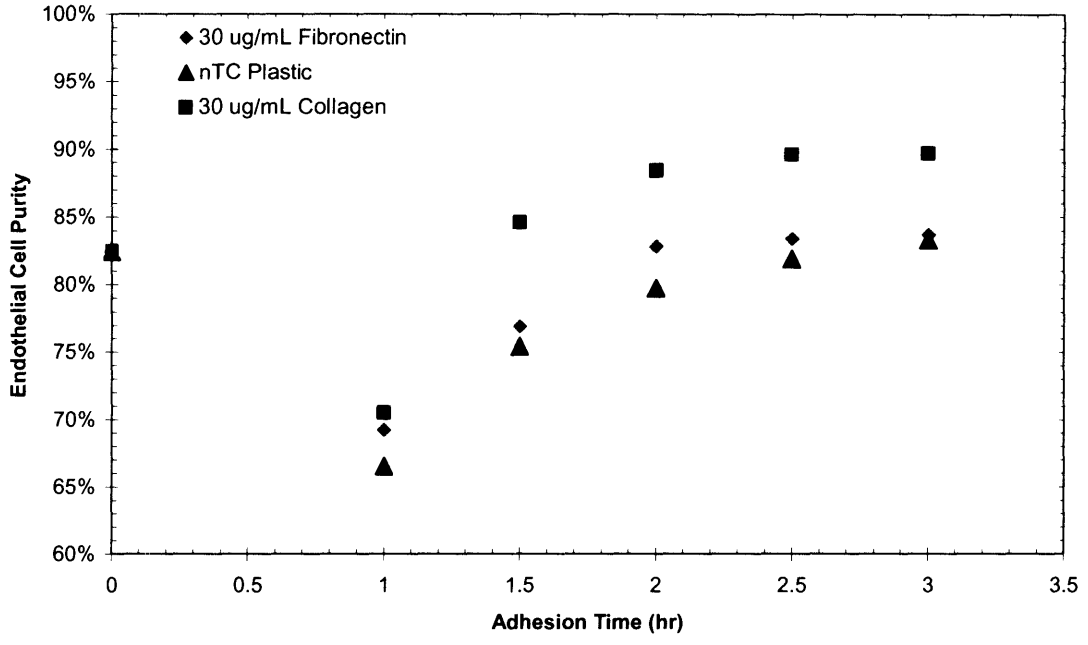

Figure 3.2.3: Effect of adhesion time on Endothelial cell culture purity
Experiments conducted (n=1) using 30 μg/mL of collagen (□), 30 μg/mL of fibronectin (♦), and Non-tissue culture treated plastic (Δ) show that there exists diminishing improvement of purity to time at ~ 2.5 hrs, and that collagen > fibronectin > non-tissue culture treated plastic across all experimental times. The goal in this separation is to maximize the purity while minimizing the culture time and thereby the ability for significant changes in mRNA expression.

Figure 3.2.4 shows that endothelial cell yield on collagen and fibronectin monolayers were high in magnitude (Y~1.5×10^6 EC's), but not statistically different from one another (n=3, p =0.82). Comparatively, EC's adhered poorly and with greater experimental variance to nTC plastic (n=3, $p < 0.001$). Additionally, Figure 3.2.5 shows that collagen substrate was superior to both fibronectin and nTC plastic at enriching the EC population ($p < 0.01$), while fibronectin was not statistically different from nTC plastic ($p = 0.71$). It appears that KC's have the ability to bind directly to fibronectin leading to greater contamination of the EC population, while the limitation for enrichment using nTC plastic is the inability of EC's to efficiently adhere to the plastic. Therefore collagen was chosen as the substrate for EC enrichment.

KC recovery was markedly lower than EC's for all tested substrates ($n = 3$, $p < 0.0001$). Fibronectin substrate enabled the greatest yield of KC's while showing with worst overall purity. KC yield using collagen was statistically lower than fibronectin ($p < 0.02$), but not appreciably different in magnitude, while the ability of these substrates to purify KC's were not statistically different ($p = 0.53$). Non-tissue culture treated plastic demonstrated statistically lower KC recovery ($p < 0.05$), while allowing significantly better enrichment ($p < 0.01$). Unfortunately, we were unable to identify a high yield, high purity KC separation strategy. However, considering that KC recovery on all

substrates was on the same order of magnitude, we chose to use non-tissue culture treated plastic because it allowed the greatest enrichment.

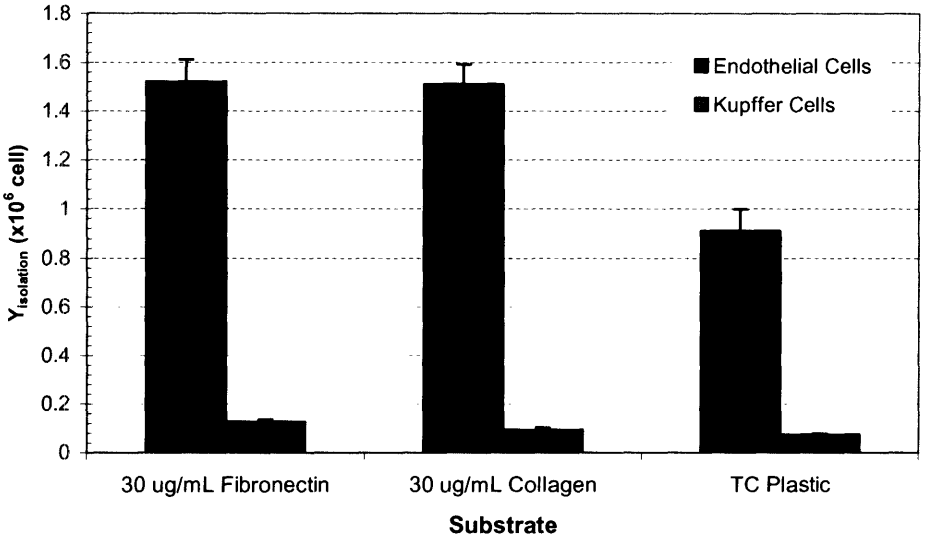

Figure 3.2.4: Differences in total cell recovery when cultured on various substrate
Substrate selective adhesion experiments conducted with endothelial (n =3; $t_{adhesion}$ = 2.5 hr) and kupffer (n =3; $t_{adhesion}$ = 0.5 hr) show that overall cell yield from culturing EC's on collagen & fibronectin monolayers are not statistically different (p = 0.82), and non-tissue culture treated plastic yields statistically fewer cells with a greater experimental variability (p < 0.001). Overall cell recovery for kupffer cells showed that FN > Col (p <0.02) > nTC-plastic (p <0.01) and that KC yield is markedly less than EC's on all substrates (p < 0.0001).

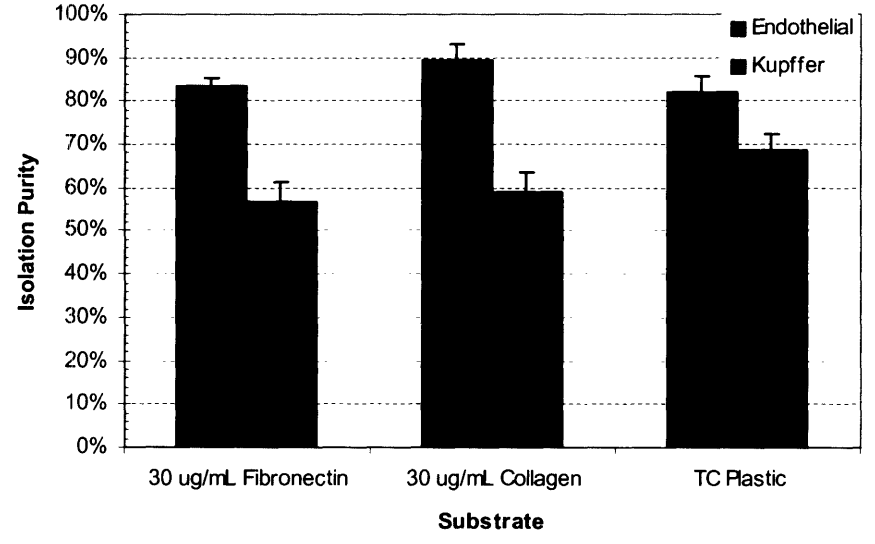

Figure 3.2.5: Differences in isolation purity when cultured on various substrate
Substrate selective adhesion experiments conducted with endothelial (n =3; $t_{adhesion}$ = 2.5 hr) and kupffer (n =3; $t_{adhesion}$ = 0.5 hr) show that culturing EC's on a collagen monolayer enables a greater purity (p < 0.01), whereas non-tissue culture treated plastic and fibronectin are not significantly different from one another (p=0.71). Purification of kupffer cells demonstrated that FN ~ Col (p =0.53) < non TC-plastic (p < 0.02) and that KC purity is significantly less than EC's on all substrates (p < 0.01).

Figure 3.2.6 shows the average (n = 6) composition of resulting KC and EC populations attained using these separation protocols. There is significant cross-contamination of both isolated cell fractions and neither population meet the original criteria for real time RT-PCR standard curve development, and as such do not allow correlation of cDNA concentration to cell number.

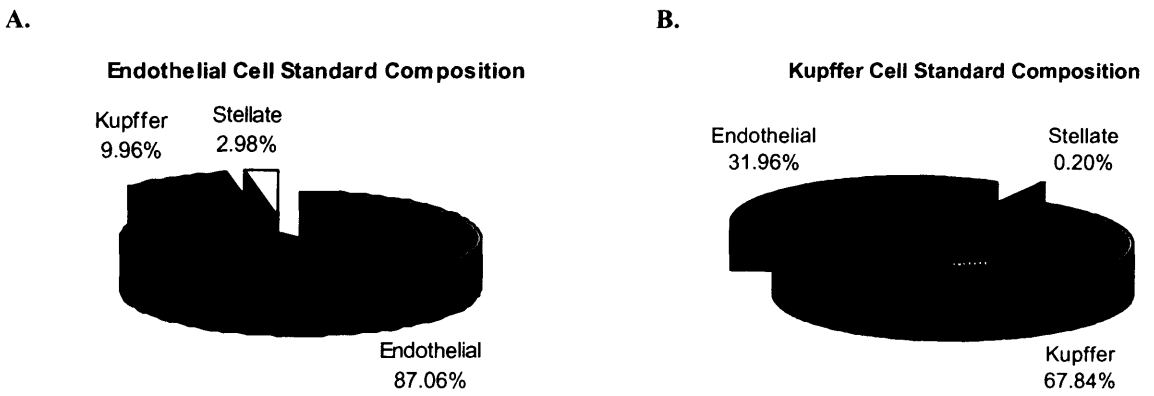

Figure 3.2.6: Average Compositions of Purified KC and EC's used for Real Time PCR standards

KC's were enriched to a mean purity of ~68% and also showed the presence of necrotic parenchymal cell bodies and erythrocytes, whose absence of significant RNA must be assessed. The EC fraction has an average purity of ~87% and showed the presence of all NPC cell types. This EC fraction appears to be the best candidate to evaluate and add to culture as the 'NPC' fraction.

These enriched cell fractions can still be used to determine specificity against stellate and hepatocyte genes. Known compositions of these purified cell fractions can be used to calculate expected gene expression. The calculations then be used to show the statistical confidence levels of whether sufficient evidence exists to prove that specificity does not exist in target cell-type markers.

3.2.4 Choice of HSC-T6 cell line for Purified Stellate Cells

Traditional primary stellate cells are traditionally isolated, with varying degrees of enrichment, from post-digested liver through a density gradient of metrizamide, stractan, nycodenz or Percoll (Geerts et al. 2003). Successful isolation requires cells to contain sufficient levels of lipid droplets so that they possess a significantly different density than other sinusoidal cells. These requirements are generally fulfilled by use of "old" rats (500+ g) or animals that received a supplementary diet of vitamin A (Friedman et al. 1987). These dietary and age requirements are very disparate from our current rat storage and isolation protocols (rat weight ~180-200 g) and therefore would require a separate perfusion and introduce additional variables into the equation and as such are not desirable. Further, isolations are extremely time consuming, yields are modest, and there is considerable preparation-to-preparation variability (Vogel et al. 2000).

A second option is to use an immortalized cell line. We received one such cell line, HSC-T6, as a gift from the Friedman lab. This cell line has been shown to demonstrate characteristics of both 'activated' and 'quiescent' stellate cell phenotype (Vogel et al. 2000) and has been shown to contain intracellular filaments typical of primary HSCs, express desmin, α-SMA, vimentin, and glial fibrillary acidic protein, take up and esterify retinol and retinol-binding protein, and are otherwise similar to primary stellate cells (Kim et al. 1998). A detailed analysis of the immuno-staining capabilities, and behavior of this cell line in our MilliF bioreactor has been discussed by Katy Wack in her thesis.

3.3 RNA isolation

RNA sample isolation is the most crucial step in real-time PCR. The quality of RNA and the method in which it is prepared can greatly influence the subsequent expression data obtained. There exist several different procedures to isolate RNA, but the effectiveness of each procedure varies depending on the culture system and tissue composition. We use a combination of two commonly used RNA isolation reagents: TRIzol® reagent (Invitrogen Life Science) and RNeasy kit (Qiagen). TRIzol® reagent is a one-step RNA isolation method, whereas RNeasy kit represents glass-binding methods. Tomo Iida validated this protocol in our lab by modifying the protocol "RNA extraction from bacterial cells" by Standford University (Standford Genomic Research, Palo Alto, CA). In brief, the cell pellet, silicon scaffold and filter, or collagen sandwich is homogenized with TRIzol® reagent using a syringe and needle. The RNeasy kit is then used to extract RNA separated from the homogenized TRIzol® reagent. This protocol (shown in Appendix 4) is time consuming, but consistently allows high quality/high yield of RNA and thus necessary.

In order to quantify RNA in a sample, UV spec readings are taken at 260nm. The absorbance coefficient of RNA at 260nm has been determined to be 40μg RNA/mL (Wang et al. 2001). Therefore, the RNA concentration of sample can be calculated as follows:

$$A_{260} * \alpha_{RNA}[\tfrac{\mu g}{mL}] * D_{factor} = C_{RNA}[\tfrac{\mu g}{mL}]$$

where A_{260} is the absorbance at 260nm, α_{RNA} is the absorbance coefficient of RNA, and D_{factor} is the dilution factor. The sample is also read at 280nm on the UV spec, purity of the sample is calculated as follows to check the quality:

$$P_{sample} = \frac{A_{260}}{A_{280}}$$

This ratio should be close to 2.0 (purity) and be in the range of $1.8 \le P_{sample} \le 2.1$. Ratios below 1.9 indicate likely protein contamination, whereas ratios above 2.1 indicate presence of degraded RNA (Affymetrix 2001). It should be noted that when dealing with samples that likely have small RNA yield that smaller dilutions factors should be used. This is because the UV spec is optimized for absorbencies in the range from 3.00-0.05.

Above this range the sample intensity can become saturated and below this range the sample cannot be considered to be different from the blank (Qiagen 2003).

3.4 Reverse Transcription Reaction

cDNA formation is considered to be a low risk, but important step in the real-time PCR process. The protocol used was adapted from the Qiagen Omniscript Reverse Transcription protocol (Qiagen) and is detailed in Appendix 5. It is optimized for reverse transcription of 50 ng to 2 μg of RNA, where the concentration cDNA varies linearly with concentration of RNA (Chapter 2 Section 7) added at a constant transcriptional efficiency. Our experiments determined that the reverse transcription reaction efficiency, contrary to the Qiagen Handbook, is inversely correlated to the amount of RNA present in the reaction ($\varepsilon = \varepsilon(C_{RNA})$) . UV spec of the resulting single stranded cDNA (α_{ssDNA} = 33 μg/mL) showed that transcriptional efficiency decrease as you reach the upper limit for the protocol. The cause of this inconsistency was never experimentally elucidated, but is possibly due to errors in the RNA UV spec readings, or in the reformulation of the T7 oligo dT Primer (Affymetrix). Based on these observations all subsequent reverse transcription reactions were performed at RNA concentrations of 10 μg/mL, UV spec readings taken on the product cDNA, and cDNA concentration normalized to a 20 ng/μL. Deviations in RT efficiency was reported in the *x*-axis error bars of standard curves

3.5 Real Time PCR

Real-time RT-PCR has been used as the metric to complete the input analysis as mentioned in Chapter 2 section 5. This was validated and optimized in our lab by Tomo Iida and Brad Hogan in collaboration with Dr. Rebecca Fry and staff at the MIT Biomicro Center (Cambridge, MA). DNA Engine Opticon Moniter 2 (MJ Research) was used to quantify the PCR reactions. Opticon Monitor 2 uses the nonspecific dye SYBR-Green I, which undergoes excitation-induced fluorescence following intercalation into double stranded PCR products during amplification (Wittwer et al. 1997).

The levels of expressed genes have been measured using absolute quantification for calculation of tissue composition. Relative quantification was used to compare the relative expression levels of different genes and culture systems. These quantification methods have been described previously in Chapter 2 section 6.

3.5.1 Primer Design

Primers for genes were designed in collaboration with Brad Hogan and Dr. Rebecca Fry. First the mRNA Rattus norvegicus sequence was attained on NCBI (PubMed) for the genes of interest. Gene sequences were input into web based Primer 3 (Whitehead Institute, Cambridge, MA) primer design software and the primers for each gene were designed following the appropriate guidelines outlined by Qiagen (6ppendix 6 6). These primers were then input into NCBI Blast online software to ensure that the designed primer was specific for only the gene of interest.

Melting curve analysis was performed using the temperature gradient feature of Opticon 2 software for each gene on purified samples of their respective target cell type. These melting curves were analyzed to assess the purity of the product. Figure 3.5.2

shows examples of a good curve which has one narrow spike, characteristic of one product, and an undesirable curve that possess' multiple peaks, characteristic of multiple products or primer dimers.

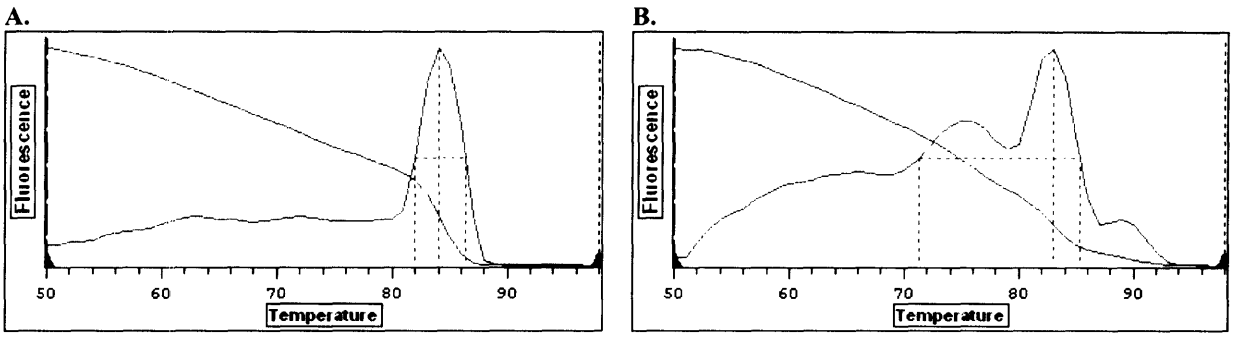

Figure 3.5.1: Example of Optimal and Undesirable Melting Curves
(A) Typical melting curve of a successful primer (HARE pictured) show the presence of one distinct peak
(B) Melting curves of bad primers (GFAP pictured) shows the presence of multiple PCR products

Optimal annealing temperature was then defined as the temperature that yields the lowest C(t) value while maintaining a "good" melting curve. Next, product-melting temperature was defined as the temperature at the maximum fluorescence intensity. The primers were then redesigned in Primer3 using the product melting temperature as a design specification. The newly designed primers were then compared to the original designs and primers with significant differences or multiple melting curves were redesigned and validated. The list of designed primers, their sequence, annealing temperature and melting temperature is summarized in Table 3.5.1.

Table 3.5.1: List of Designed Real Time RT-PCR Primers

Gene	Primer Sequence (Forward)	Primer Sequence (Reverse)	T_{anneal} °C	T_{melt} °C
18s rRNA	GCT ACT ACC GAT TGG ATG GTT TAG	GTT CAC CTA CGG AAA CCT TGT TAC	57	87
Albumin	GGT GCA GGA AGT AAC AGA CTT TG	TAA CTT GTC TCC GAA GAG AGT GTG	55	78
Transferrin	AGA TGG AGG TGG AGA TGT GG	GAG CCA CAA CAG CAT GAG AA	55	81
Vimentin	ACG AAT ACC GGA GAC AGG TG	TCC AGC AGC TTC CTG TAG GT	55	82
Desmin	CTC ACA GCC TCT GAA CCC TC	CTG GTA CCC CCT TCT AAG CC	61	82
GFAP	GGT GGA GAG GGA CAA TCT CA	TGG GAA TCT GAT CCC TGA AG	61	79
Flk-1	CTG GCA TGG TCT TCT GTG AAG CA	AAT ACC AGT CGA TGT GAT GCG GT	50	78
Flt-1	CTT TCT CAA GTG CAG AGG GG	GCC ATG TTC AAG GTC AAG GT	54	79
VE-Cadherin	GAA CTG CTG GGG TCA TGA AT	ATC GCC ACC AGA TGT GTG TA	55	82
HARE	AAG AAG CCT GTG CCA AAG AA	CAC CAC ACT TCT GAG AGG CA	57	84
CD68	GAC CAA TCT CTC TTG CTG CC	AGA GGG GCT GGT AGG TTG AT	57	82
IL-10Rα	GTA ACG TTC CAG GGC TAC CA	ACA CCC AGG AGT GAC GAT TC	57	77
CD80	TTA CAG TTG CCA GCT GAT GC	TGC CTT TTC TCT CAC CGA CT	52	82

3.5.2 Real Time PCR Protocol Description

The exponential amplification of cDNA products in PCR makes it the most prone to large propagation of small technical errors. Thus, it is necessary standardize operational techniques and validate experimental results.

Technical error is primarily associated with pipetting error in the loading of cDNA into PCR plates arising from 1μL cDNA samples, which fall below the pipettors' volume threshold for accuracy, 4 μL. Therefore a standard pipetting technique was defined and care taken to ensure its replication in each sample loading. The actual technique used is a matter of personal preference, but it is imperative that it is standardized in all samples. Technical error also arises in the reading the fluorescent signals by the detection machine, which may be affected by factors such as misalignment of PCR plate caps or the presence of dust and oil on the PCR plate caps. The machine error is small <0.01%, so care was taken to ensure alignment of PCR plate caps, and all were wiped with a Kim wipe before input to the Opticon machine.

Sample variation is introduced by variations in the efficiency of reverse transcription to cDNA. To curb the variance, multiple RT reactions (n = 2) were run on each RNA samples and UV spec readings taken to determine the actual sample cDNA concentration. Each biological replicate sample is then averaged to minimize these errors.

Further, specificity of primers was addressed by including post-DNase treated RNA and cDNA free control for each run. These controls ensured that there was no primer dimer formation or genomic DNA amplification in processed samples.

3.5.3 Standard Curve Developement

Standard curves were created for each primer by a series of four dilution (1:100, 1:10, 1, 2) of a known quantity of RNA. These dilutions were selected because they represented the most likely range of expression for the selected gene set. Critical threshold, C(t), is plotted versus cDNA concentration on a logarithmic scale in Appendix 1. Linear regression analysis has been preformed to enable quantification of unknown mRNA. Four biological, two sample, and three technical replicates (4x2x3 = 24 samples) were averaged, and their standard deviation calculated and reported. Also, variation in cDNA concentration of each sample arising from the reverse transcription reaction was averaged, and standard deviation calculated and reported. Figure 3.5.3 shows the 18s rRNA standard curve as an example.

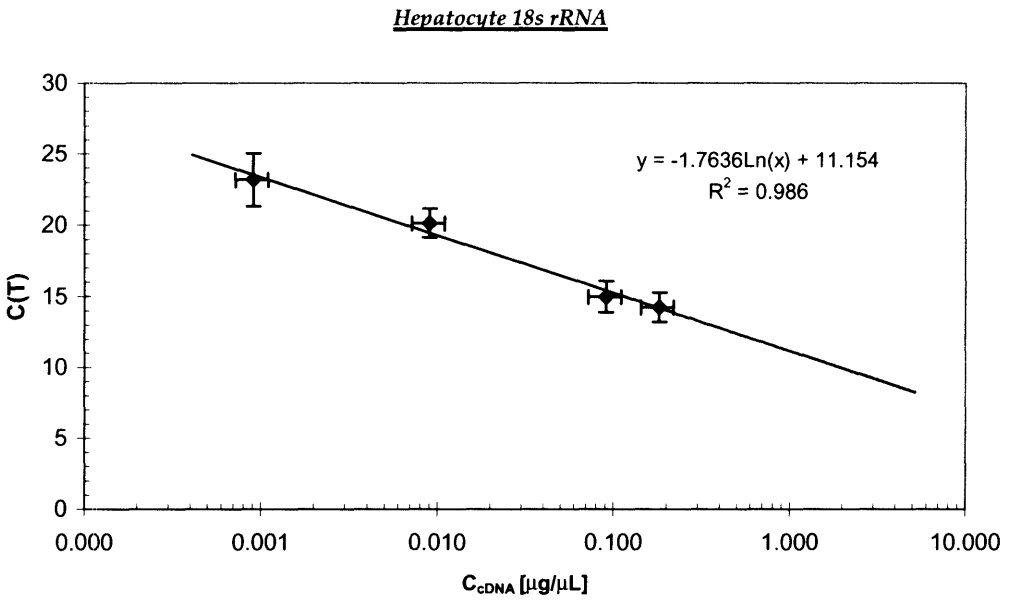

Figure 3.5.3: Real Time RT-PCR Standard Curve for Hepatocyte's 18s rRNA
Dilutions of 1:100, 1:10, 1, & 2 were performed for each primer to generate standard curves. For each point there are four biological, two sample, and three technical replicates (n_{bio}= 4, n_{sample} = 2, n_{tech} = 3). Y-error bars as placed as ± C(t) standard deviation. X-error bars as ± sample C_{cDNA} standard deviation derived from similar RT reactions.

3.6 Gene Selection Rationale

The most crucial step to utilizing gene expression to quantify tissue composition is that the genes selected for study are exclusively specific to phenotype. Existing literature was reviewed to phenotypic markers that are proven to be specific to the desired cell type and whose gene expression is reasonably stable across a different culture systems and culture environments. The desire was to locate whose expression was similar to that of a "housekeeping" gene. This section details the genes selected for analysis in hepatocyte, stellate, endothelial, and kupffer cells.

3.6.1 Housekeeping Gene

The importance of a reference gene for normalization of PCR data was discussed previously in Chapter 2 section 7. Selection of a housekeeping gene focused on finding constitutively expressed gene that was expressed in high levels and whose expression levels were independent of media environment or culture system.

18s rRNA

18s is a ribosomal RNA that is a permanent structural part of a ribosome. 18s demonstrated excellent consistency, reproducibility, and non-regulation by matrigel and collagen compared to β-actin and GAPDH (Selvey et al. 2001). Studies using northern blots on lymphoma cell lines showed that 18s was more stable on temporal and environmental scales than β-actin, GAPDH, β2-microglobulin, α-tubulin (Finnegan et al 1993). The level of 18s rRNA expression is very stabile and high enough such that small

fluctuations will not result in detectable fluctuations in the normalized fluorescence signal of the target gene (Schmid et al. 2003). In addition, studies within the Griffith Lab conducted by Tomo Iida, Anand Sivaraman, Seth Townsend, and Brad Hogan showed that 18s is more stable than GAPDH, albumin, and β-actin across different temporal scales, culture environments and culture systems (unpublished work). Further, 18s was compared to other ribosomal RNA's like 28s and found to possess superior stability across different culture systems (Sivaraman unpublished). Therefore, 18s will be used as the reference "housekeeping" gene due to its' proven stability and in an effort to maintain consistency with ongoing Griffith lab research.

3.6.2 Hepatocyte

Hepatocytes are the main functional cell in the liver and as such have a plethora of specific enzymes. An wide variety of these enzymes (CYP_{450}'s, Phase II) have been studied in depth in our lab, and have been found highly variable in magnitude of expression and extremely sensitive to cell culture system and cell culture environment. Therefore, genes that are highly expressed and more fundamental to the hepatocyte phenotype are targeted.

Albumin

A major function of the liver is the synthesis of albumin. This protein represents a significant portion (~12%) of the total protein that is produced by the normal rat liver. Important roles ascribed to albumin include the maintenance of oncotic pressure in the blood vessels and the maintenance of an endogenous amino acid source. Albumin also acts to transport long chain fatty acids, bilirubin, hormones, calcium, and vitamins. Along with other constitutively expressed genes like 18s rRNA, β-actin and GAPDH, albumin is often used as a "housekeeping gene" for the normalization of mRNA quantification (Bustin et al. 2000). The protein secretion levels of albumin are known to fluctuate greatly in *in vitro* cultures, but are hypothesized to be translationally regulated (Arias, 2001). Albumin has been used as a marker to show differentiation into hepatocytes in hepatic and hematopoietic stem cell cultures (Fiegel et al. 2003, Strain et al. 2000, Vessey et al. 2001). Real time PCR performed on fetal, developing and adult liver has shown that cellular albumin gene expression increases during development. The studies use albumin as a "housekeeping" gene to normalize expression of alpha feto-protein (Cantz et al. 2003, Tollet-Engell et al. 2001). Studies comparing various tissues of the body have shown that albumin gene expression is specific to liver tissue (Arias, 2001). These studies show that albumin is liver specific and its' use as a "housekeeping" gene suggest expression stability. Additionally, microarray experiments conducted inhouse by Tomo Iida showed remarkable correlation between hepatocyte isolate and *in vivo* gene expression levels, which indicates further potential stability of gene expression on a time scale necessary to create standard curves. Further, tissue cultured in the milliF bioreactor has been shown to maintain in vivo-like levels of albumin expression at late time points in culture, thus showing that even if expression levels changed in the intermediate steps the input and output could still be determined. However, no literature was found that compared the expression of albumin in different cell phenotypes of the liver and therefore its' specificity must be validated.

Transferrin

Transferrin is an essential iron-binding protein that is responsible for transporting iron throughout the body and is the most important physiological source of iron for red blood cells (Ponka et al. 1997). The liver specific gene expression level has been shown by Northern blot to be 100x that of the bodies other transferrin expressing organs: brain and testis (Idzerda et al.1986). Researchers have also shown that gene expression of transferrin is significantly higher ($p = 0.001$) in hepatocytes than in Kupffer, SEC, and stellate cells (Zhang et al. 2003). These observations show that transferrin is both specific to the liver and hepatocytes which makes it a solid candidate for analysis. Concerns with transferrin occur because its' expression levels has been shown to vary significantly during partial hepatectomy, in different media environments, and in different culture systems (LeCluyse et al. 1997, Idzerda et al. 1989, Arias, 2001). Therefore, gene expression variation is a concern to investigated further.

3.6.3 Stellate

Stellate cells exhibit two phenotypes, 'quiescent' and 'activated' (Li et al.1999). The presence of these two states has led to the adoption of double-staining protocols in histology studies to identify the entire stellate cell population (Geerts, 2003). Therefore, we aim to find a more fundamental monocyte or fibroblast marker that is highly and constantly expressed in both phenotypes. In addition, we look to validate the gene expression of current "gold standards" of staining for similar juxtaposition studies.

Vimentin

Vimentin is a developmentally regulated intermediate filament protein (IFP) that is widely expressed in cells of mesenchymal origin. It is believed to be involved with the intracellular transport of proteins between the nucleus and plasma membrane. During the development process, vimentin is exchanged for new, tissue-specific IFPs (Arias, 2001). Studies of early liver development have shown that vimentin stains for both stellate cells and endothelium in fetal rat liver and is highly expressed in hematopoietic progenitor cells (Ikeda et al. 1999, Valerius et al. 2002). Vimentin stains for stellate cells in both activated and quiescent states (Geerts et al. 2001) and northern blot analysis showed that this expression level is consistent in the active and quiescent states of both rats and humans (Browm et al. 1995). However, no such studies have been conducted to gauge the extent of expression or lack there of in adult tissues. Therefore, vimentin has the potential to be used as a stable, all-encompassing stellate cell marker if its expression is found to be negligible in endothelial cells.

GFAP & Desmin

GFAP is an intermediate filament protein widely studied as a specific marker for cells of astroglial lineage that was shown to be specific to stellate cells in the normal rat liver (Gard et al. 1985). This marker captures all peri-central and fat storing stellate cells and some (<70%) of activated cells (Geerts, 2003). GFAP has been demonstrated not to co-localize with hepatocyte, kupffer and endothelial cell markers (Neubauer et al. 1996).

Desmin is an intermediate filament protein that differentiates stellate cells from fibroblasts (Yokoi et al. 1984) and has been widely used as a "gold standard" for identifying stellate cells in rodent liver (Palka et al. 2000). This marker has been

instrumental in studying normal and experimentally inured rat liver because 70-80% these cells express desmin (Geerts et al. 1991, Jezequel et al. 1989). Desmin captures most (>90%) of activated cells and the majority (~70%) of quiescent cells, but does not stain peri-central fat storing cells (Geerts, 2003). Overlapping desmin with GFAP allows visualization of >90% of all stellate cells. Further, desmin and GFAP have both been used internally for immuno-staining of stellate cells by Katy Wack and are detailed in her Thesis.

3.6.4 Endothelial

There exist several location specific endothelial cell phenotypes with the liver: sinusoidal, ductile, and vascular (Arias, 2001). Sinusoidal endothelial cells (SEC) are the phenotype of interest, comprising ~70% of liver endothelial cells (Vidal-Vanaclocha, 1997). There is presently a lack of knowledge in the field of SEC genomics, and only recently has a specific antibody (SE-1) been developed. Therefore, we aim to identify potential SEC specific genes and more fundamental, highly expressed endothelial lineage specific markers.

HARE

The hyaluronan receptor for endocytosis (HARE) is an endocytic receptor responsible for the uptake and degradation of hyaluronan (HA) and chondriotin sulfate from the blood stream (P Weigel et al. 2002). The HARE receptor has been identified *in vivo* to only be highly expressed in the liver, spleen, and lymph nodes (Zhou et al. 2000). Additional liver studies showed that HA uptake is specific to endothelial cells and not present in hepatocytes or kupffer cells (Yannariellobrown et al. 1992). Later, labeled monoclonal antibodies were developed against HARE and showed by co-localization with SE-1 that HARE in the liver is specific sinusoidal EC's not just general endothelial cells (Weigel et al. 2003). This level of specificity is very desirable because SE-1 antibodies have only recently been developed and their mechanism for binding is presently unknown. Therefore, HARE is a highly expressed receptor that is specific for sinusoidal endothelial cells. Unfortunately, there are no present studies of variation of HARE gene expression in liver development, adult *in vivo* models, or *in vitro* culture systems. Thus, the stability of HARE expression must be determined internally.

Flk-1 / Flt-1

Fetal liver kinase-1 (Flk-1/KDR / VEGF-R_2) and *fms*-like tyrosine kinase (Flt-1 / VEGF-R_1) are high affinity VEGF receptors localized predominantly to the vascular endothelium in both proliferating and quiescent cells (Ferrara 1999a). Partial hepatectomy studies indicate that flt-1 and flk-1 are associated with VEGF signal transduction in proliferation of endothelial cells. Further hepatic studies have shown that proliferating hepatocytes and kupffer cells highly express VEGF, which indicates cellular communication during proliferation (Kraizer et al. 2001). Northern blot studies confirmed that Flt-1 and Flk-1 expressed on EC's, but not on hepatocytes, kupffer or stellate cells (Yamane et al. 1994). Further studies demonstrated that both Flt-1 and Flk-1 gene expression is upregulated during partial hepatectomy (Mochida et al. 1996). These results imply that both Flt-1 and Flk-1 gene expression is specific to endothelial cells. However, the markers are general vascular markers present in all endothelium of

the body and their expression levels fluctuate significantly following tissue disruption. Correlation between magnitude of cellular increase in gene expression has not been demonstrated and therefore investigation of these genes will serve very useful to determine endothelial cell incorporation and homeostasis in culture.

VE-Cadherin

Vascular endothelial cadherin (VE-Cadherin, CD144) is an adhesive protein that is expressed on endothelial cells of all blood and lymphatic vessels. It is involved in a variety of cell processes involving cell-cell adhesion, including vascular permeability, leukocyte and hematopoietic progenitor cell migration, angiogenesis, tumor vascularization and apoptosis (Yap et al. 1997, Angst et al. 2001). This protein is commonly used as a marker for endothelial lineage differentiation and has been shown via Northern blot and RT-PCR to be "endothelial cell specific" (Kalka et al. 2000, Telo et al. 1998, Takeichi, 1990). More robust microarray analysis have further confirmed this specificity by comparing expression of endothelial cell specific markers to a mixed variety of "non-endothelial" cells (Ho et al. 2003). These studies show that gene expression in endothelial tissue is significantly specific and that VE-cadherin is modestly expressed across a wide variety of other cell types. However, these studies have focused on populations and therefore validation of the magnitude of cell specificity is needed. Further, gene expression of VE-cadherin is induced by shear stress (Re >10) and stable following immortalization in cell monolayer cultures (Kondapalli et al. 2004, Vouret-Craviari et al. 1999). These findings show potential for stability across different culture systems and in our perfused bioreactor (Re~1).

3.6.5 Kupffer

Kupffer cells have been extensively studied because of their role in cytokine secretion and homeostasis in the liver. A variety of specific antibodies have been developed and are considered "gold standards" for identification of these macrophages. Therefore, we aim to validate gene expression of these "gold standards" which were previously shown to be highly expressed, specific, and stable across a wide variety of culture permutations.

CD68 / ED-1

Macrosialin (CD68/ ED-1) is a heavily glycosylated transmembrane protein that is constitutively and ubiquitously expressed in macrophages (Li et al. 1998). CD68 has been proven to be specific to kupffer cells in the liver and along with ED-2 is considered a "gold standard" for immuno-staining of kupffer cells (Jiang et al. 1998). CD68 gene expression was shown to be greater than ED-2 although ED-2 has a higher protein expression, implying translational regulation of these proteins (Fadok et al. 2001). Current researchers use CD68 primarily for immunostaining and subsequently temporal and environmental stability of gene expression have not been extensively validated. Immuno-staining protocols for this family of proteins has been validated in our lab (Appendix 7) and shall be explored for continuity and for its' proven high constitutive macrophage expression.

IL-10Ra

IL10 inhibits macrophage activation through the binding of IL-10 receptor alpha (IL-10Rα) and the subsequent stimulation of transcriptional factors STAT1 and STAT3 (Lim et al. 2004, Ho et al. 1993). The IL-10 receptor gene expression was identified on macrophages, monocytes, T helper cells, and B cells (NCBI). RT-PCR studies focusing on Kupffer cells demonstrated constitutive expression in murine and human cells and showed evidence for translational regulation of protein expression (Knolle et al. 1998). In vivo mouse studies of liver tissue function showed that blocking of the IL-10 receptor shortened life of kupffer cells while showing no effect on other sinusoidal cells (Shi et al. 2003). Presently, there is a dearth of studies of IL-10Rα in rat liver and there are no reported cell specificity studies have reported in rat liver. Further, IL-10Rα expression in porcine liver macrophages was shown to be on the order of 1,000 transcripts per cell (NCBI), which leads to sensitivity concerns. Regardless, the constitutive expression shown in human and murine KC's give this gene large potential for our purposes

CD80

CD80 is a marker for professional antigen presenting cells (APC). This protein enables the activation of T-cells by the binding of CD28. Immunohistochemical double-staining with CD68 in normal rat liver demonstrated that CD80 protein expression is confined to $CD68^{+}$-kupffer cells (Kwekkeboom et al. 2003). Real time RT-PCR showed that variations in gene expression levels were not statistically significant following both *in vivo* liver transplantation and *in vitro* cell immortalization (Kwekkeboom et al. 2003). Additional real time RT-PCR studies showed favorable expression levels of CD80 compared to CD68 (Crispe et al. 2003). These two studies indicate that CD80 is a highly expressed, kupffer cell specific marker with the potential for stability in the culture systems of interest.

CHAPTER 4: DETERMINATION OF TISSUE COMPOSITION VIA REAL-TIME RT-PCR

4.1 Introduction

The liver parenchyma is composed of four primary cell types: hepatocytes; stellate cells (HSC); sinusoidal endothelial cells (SEC); and Kupffer cells (KC), each with a unique function and phenotype. Non-parenchymal cells (NPC's) are considered an essential component of diagnostic long term *in vitro* liver culture systems (Allen et al. 2002). These cells play important roles in creation and maintenance of the hepatic microenvironment through a complex system of cell-matrix interactions, cell-cell interactions, and soluble signaling mechanisms. *In vivo*, each cell phenotype provides different environmental cues necessary to preserve tissue homeostasis. Therefore, it is prudent to develop a system that addresses these mechanisms of intercellular communication. Presently, cellular and molecular biology research has been unable to unveil detailed mechanisms for cell interaction, but the recent decoding of the human genome has spawned new, very promising efforts toward this goal. In the meantime, a wide variety of co-culture systems are being developed and validated by very disparate diagnostic metrics (Chapter 1 section 4). These culture systems each address different operating aspects of cell culture and are very difficult to compare due to uncertainties regarding meaning of results. Few research groups have systematically built culture systems to address composition or even allow for qualitative observation of tissue architecture. Since each NPC is responsible for a particular subset of organoid function, determination of tissue composition (incorporation) is necessary to qualify empirical observations.

The perfused liver bioreactor developed by the Griffith Lab has the unique ability to allow for spontaneous tissue reorganization and *in situ* tissue visualization. This system has demonstrated tremendous ability to maintain stabilized '*in vivo*'-like morphology, function, and drug metabolism of hepatocytes compared to traditional 2D cultures. Incorporation of co-cultured NPC's has been undertaken to further improve the performance of the bioreactor as a viable *in vivo* liver analog. Presently, bioreactor system has demonstrated the ability to maintain co-cultures of hepatocytes with stem cells as well as with a stellate cell-line. However, quantitative determination of cell phenotype has not yet been attained.

The first step in the co-culture process is to develop a methodology to quantitatively perform an input/output analysis of cells in the bioreactor. Such a methodology will allow for systematic study of effects of different substrate, cell ratio's, and spheroid aggregation techniques on the incorporation of NPC's. Initial efforts to quantify tissue composition using scaffold sectioning and immuno-staining failed because current sectioning protocols severely disrupt the tissue and immuno-staining protocols had not been developed (Chapter 2 section 2). Focus then shifted to identifying phenotype specific genes and quantifying cell composition using quantitative real-time RT-PCR.

We have identified a set of cell-specific candidate genes (Chapter 3 section 6) and developed PCR primers for each (Chapter 3 section 5.2). Here, we determine and validate a reference gene for all cell types, demonstrate specificity of each candidate gene, and show cross-reactivity with impure cell populations. Further, we show how well these genes perform at calculating the composition of in vivo tissue and demonstrate their application to collagen gel sandwich, spheroid, and 3D MilliF bioreactor culture systems.

4.2 Materials and Methods

Hepatocytes Isolation

Hepatocytes were isolated from 180-200g male Fischer rats by a modification of Seglen's two-step collagenase perfusion procedure (Block et al. 1996, Seglan et al. 1976) at a perfusion flow rate of 25 mL/min. The resulting cell pellet was centrifuged two times at 40*g (3 min) and the supernatants collected. This hepatocyte fraction was then subjected to the previously described (Chapter 3 section 2.1, Appendix 3) isotonic Percoll gradient and centrifuged at 50*g for 10min. The final cell pellet was re-suspended in hepatocyte growth medium (HGM) without HGF (Block et al. 1996). Cell viability of hepatocytes before cell seeding or homogenization was 85-92% as determined by trypan blue exclusion.

Non-parenchymal Cell Isolation

Non-parenchymal cells were isolated from the supernatants of the first two low gravity spins of as described in Appendix 3. In brief, cells were spun at 100*g for 3 min to pellet residual hepatocytes. This supernatant was then spun at 400*g for 5 min to collect non-parenchymal cells. Remaining cells were collected and then centrifuged in a two-step Percoll gradient at 900*g for 20min (Smedsrod et al. 1985). Respective enriched fractions were re-suspended in HGM and washed of Percoll via centrifugation at 900*g for 5min. Cell viability was >95% as determined by the nuclear stain cell count protocol outlined in Chapter 3 section 1.1 and Appendix 2.

HSC-T6 Cell Isolation

HSC-T6 cells were passaged in T75 flasks supplemented with DMEM + 10% FBS and 5% Pen/Strep. Cells were removed using 2mL of 1x trypsin, washed in PBS, and centrifuged at 400*g for 5 min. Cell viability was >95% as determined by the aforementioned nuclear stain cell count protocol.

Cell Standards

Percolled hepatocytes and HSC-T6 cells were homogenized in TRIzol immediately following isolation and their RNA isolated using a combination of TRIzol and RNeasy kit, as described in Chapter 3 section 3 and Appendix 4. Endothelial and Kupffer cells were first enriched by selective adhesion of substrate as described in Chapter 3 section 2.2, and RNA homogenized and isolated is the same manner as hepatocytes. All samples were homogenized immediately, and stored in TRIzol at –80°C until RNA isolation.

Preparation of Collagen Gel Sandwich Culture

Members of Prof. Steve Tannenbaum's lab at MIT have optimized protocols for collagen gel sandwich cultures. Briefly, isolated hepatocytes and NPC's are seeded in a 1:1 mixture on a collagen gel coated 6-well plates at a total cell density of 50K cells/cm^2 with an appropriate volume of HGM. The cell culture is incubated at 37°C, 5% CO_2 overnight. The following day, media is removed an a collagen gel solution overlay is added. The collagen solution is given ~1 hr to gel at 37°C, then washed with PBS, and the appropriate volume of HGM added. At this point the culture is ready for assay and media is changed every other day.

Spheroid Preparation

Spheroids were formed in suspension culture similar to the methods of Wu et al.(1996). Regular hepatocyte, Percolled hepatocytes, 1:1, and 0.5:1 ratios of NPC:Percolled hepatocytes were suspended in HGM immediately after isolation at a hepatocyte concentration of 150K cells per mL. 100mL of this solution was cultured in a 250 mL spinner flask (Bellco Glass, Vinelan, NJ), which was stirred at 85 rpm for 72 hours. After 72 hours of culturing, spheroids were filtered through a series of 300mm and 100mm filter, the captured cells suspended and centrifuged for 2 min at 40*g, and then either seeded into bioreactors or homogenized in TRIzol and RNA isolated by aforementioned protocol.

Operation of MilliF bioreactor

The MilliF bioreactors were cleaned, assembled, and operated in a manner commensurate with Anand Sivaraman's general protocol and similar to the one described in Powers et al. 2002b. Briefly, day 3 spheroids were seeded into the pre-primed reactor and were allowed to enter the scaffold channels through a combination of sedimentation and slight hydraulic force introduced in the upper chamber from the reversed cross-flow. After seeding, HGM traversed the upper chamber at 0.5 mL/min. The next day the cross flow was established at 60 μL/min in the 'normal' direction and an inline filter attached. Medium was changed every three days.

Two reactors were operated that were seeded with 0.5:1 co-cultured spheroids. At day 7 the reactors were taken down and RNA was isolated separately from each.

RNA Isolation and Quality Control

In order to avoid experimental variation, RNA was isolated from all samples in an identical manner. The protocol used in this experiment was a combination of TRIzol and RNeasy kit, as described in Chapter 3 section 3 and Appendix 4. RNA quality was checked for all samples using UV Spec as previously described in Chapter 3 section 3.

Real-Time RT-PCR

Reverse transcription reactions were performed at various concentrations as described in Chapter 3 section 4, but diluted normalize cDNA stock concentration at 10 μg/mL. PCR was performed using SYBR Green master mix analysis as described in Chapter 3 section 5. cDNA was loaded using identical pipetting techniques to minimize technical error. Three technical replicates were run in each reaction and averaged from the data generation.

Standard Curve Development

Standard curves were created using 1:100x, 1:10x, 1x and 2x serial dilutions of cDNA template, as described in Chapter 3 section 5.3. Each data sample was tested for the presence of genomic DNA. Those testing positive were discarded and new cDNA reverse transcribed.

Cross-Reactivity and Specificity Study

0.75 μg/mL of contaminant cDNA was mixed with 0.25 μg/mL of target cDNA. PCR was then performed on the samples as per the protocol outlined in Appendix 5.

PCR was run for 1x cDNA of each cell isolate fraction against each designed primer as per the protocol outlined in Appendix 5.

4.3 Results & Discussion

4.3.1 Standard Curves

Compositions of the cell suspensions used for standard curve development of primers are detailed in Chapter 3 section 2. In brief, stellate cell samples are known to be 100% pure because they were derived from the HSC-T6 cell line. Isolated hepatocytes did not stain for any ED-2, GFAP, or SE-1 and are considered to be >99% pure. Endothelial and Kupffer were unable to be purified, but were enriched to purities of 87% and 68% respectively.

Standard curves were developed for each designed primer using 1:100, 1:10, 1, and 2 serial dilutions of a known volume of concentrated cDNA. Each point represents the average of 24 data sets (n_{bio}= 4 [$n_{passage}$= 4 for stellate], n_{sample} = 2, n_{tech} = 3). Variations in cDNA concentration were detected following reverse transcription and consequently, the cDNA concentrations represent an average of eight data sets (n_{bio} = 4, n_{sample}= 2). The threshold for C(t) determination was set to a value ~ 10 standard deviations above the mean baseline (α = 0.025) fluorescence following global baseline normalization. Quality and validity of each sample were determined by replacing cDNA with DNase treated RNA and by running another sample with no cDNA at all. Amplification of these control samples is an indicator genomic DNA contamination or primer dimer formation. Samples testing positive for genomic DNA contaminant were discarded and fresh cDNA prepared. Evidence of primer dimers resulted in the redesign of the gene specific primer. All samples have been screened and results represent data that has passed these filters. Logarithmic regression analysis was performed on data sets to generate a standard curve of the form, $C(t)=m*\ln(C_{cDNA})+b$.

18s rRNA

First, the reference gene, 18s rRNA, was evaluated for its expression levels in the different cell phenotypes. The parameters fit by logarithmic regression are reported in Table 4.1. Different biological, sample, and technical replicated showed excellent correlation (all R^2 > 0.985). This remarkable correlation signifies minimal gene

expression differences between rats, precise and accurate experimental technique, and sufficient normalization of cDNA concentration to explain the variance.

Table 4.1: Logarithmic Regression Statistics of 18s Standard Curves

	m	*b*	R^2
Hepatocyte	-1.76	11.15	0.986
Stellate	-1.60	10.77	0.996
Kupffer	-2.11	10.78	0.995
Endothelial	-1.81	10.38	0.994

Standard curve slopes varied between cell types between -1.6 and -2.1. A slope of -1.7 is indicative of 100% PCR efficiency or said differently, an increase in one C(t) unit per doubling of cDNA. Hepatocytes, stellate cells, and endothelial cells' slopes were not statistically different from this ideal slope ($p > 0.3$) and very similar to the slope of -1.84 determined by Seth Townsend and Anand Sivaraman for Percolled hepatocytes. This harmony in the standard curves slopes confirms that the 18s primer efficiently amplifies its target cDNA.

The Kupffer cell fraction was also not statistically different from the ideal slope ($p > 0.1$), but showed much greater variance of individual samples. Two separate UV spec readings of Kupffer cell cDNA sample replicates yielded three-fold different concentrations. These observed variances were likely caused the previously discussed inefficiencies in the reverse transcription reaction. Propagation of such an error has been shown to lead such a result.

The logarithmic regression parameter, '*b*', is a representation of the cycle threshold at a cDNA concentration of 1μg/μL. '*b*' parameter values varied from 11.1 in hepatocytes to 10.4 in endothelial cells. These values were not statistically different from one another ($p > 0.2$), which is expected considering the reasonable threshold for real-time PCR experimental variation is ± 0.5 C(t) (Walker, 2001). This synchronization in '*b*' parameter values shows that 18s rRNA is expressed at a constant level relative to the total amount of RNA regardless of hepatic cell type. In other words, hepatic cell types can contain different amounts of total RNA, but the amount of 18s rRNA/total RNA is constant. This observation validates 18s rRNA as a standard "housekeeping gene" for NPC's and further implies the direct calculation of cell number of each cell with the determination of total RNA per cell for each phenotype. Such back of the envelope calculations were attempted, however, inefficiencies in aforementioned cell counting, RNA loss during isolation, and variations in reverse transcription efficiency made correlation of cDNA to cell number impossible. Such an approach will be possible and much more meaningful when NPC isolation and counting protocols are developed that allow precise control of purity and numerical number of cells used for standard development. It is also important to note the absolute quantification methods such as this are extremely sensitive to errors in standard curves. As such, a great deal of attention

should be given in future research to improving the purity and cell count accuracy of the isolated cell fractions used for standard curve development.

Further, we realized that 18s rRNA does not posses a poly-A tail like mRNA's and as such, there may be no mechanism for the landing of T-7 oligo dT primer to the rRNA transcript during the reverse transcription to cDNA. Anand Sivaraman exhaustively tested this hypothesis by performing PCR on a hepatocyte sample, running the resulting PCR products on a Northern blot, and sequencing the collected product band. The PCR product was confirmed to the desired 18s rRNA. Additionally, random hexamers were added to the reverse transcription to ensure synthesis of cDNA from all present RNA's (messenger, viral and ribosomal) and comparative real-time PCR performed on both cDNA samples. This study showed no significant difference in the expression level of 18s rRNA using T7-oligo dT or T7 supplemented with random hexamers (Data not shown)

Cell Specific Genes

Results of logarithmic regression parameter fit for all cell specific genes is reported in Table 4.2. Biological, sample, and technical data sets again demonstrated excellent correlation ($R^2 > 0.99$). Standard curve slopes ranged in value from –1.57 in Desmin (stellate) to –2.01 in CD68 (Kupffer). These slope variations mirrored the previously described phenomenon seen in 18s rRNA samples regarding sample specific variations and were not statistically different from one another ($p > 0.3$). This harmonization of data gives further support to the idea that the variations in slope were an artifact of the propagation of error caused by variations in the RT reaction and not indicative of actual significant variations in PCR efficiency from unity.

Table 4.2: Logarithmic Regression Statistics of Gene Standard Curves

	m	*b*	R^2
Albumin	-1.85 ± 0.15	17.51	0.993
Transferrin	-1.66 ± 0.04	19.44	0.997
Desmin	-1.56 ± 0.12	24.85	0.997
Vimentin	-1.72 ± 0.02	19.46	0.999
HARE	-1.57 ± 0.13	24.80	0.995
Flk-1	-1.68 ± 0.03	21.21	0.996
Flt-1	-1.61 ± 0.07	22.25	0.998
CD68	-2.01 ± 0.31	20.16	0.998
IL10Ra	-1.98 ± 0.29	29.15	0.998

Analysis of 'b' value in the case of cell specific standards is a measure of relative magnitude of gene expression by a given cell type. This quantity was further measured by normalizing the entire data set of 96 samples ($n_{dilution}$=4, n_{bio}= 4, n_{sample}=2, n_{tech} = 3) to 18s rRNA [$\Delta C(t) = C(t)_{gene} - C(t)_{18s}$]. This normalization determines the number of 18s rRNA transcripts present per transcript of target gene. Such a relative quantification magnitude of gene expression is not necessary for the absolute quantification of composition, but a useful qualitative tool for comparison of standards to tested culture

samples and culture systems. Figure 4.1 shows that Albumin, transferrin, vimentin and CD68 (macrosialin) are highly expressed in their respective cell type, while IL-10Ra, desmin and HARE are expressed in much lower magnitudes. It should be noted that an ideal target should have sufficiently high expression that small deviations in gene expression do not significantly effect the determined tissue composition. However, genes that are expressed in lower magnitude can still be successful for this purpose if they demonstrate stability of expression on a temporal scale and across different culture systems. Standard curve development has shown that a set of primers has been identified that has the ability to specifically and reproducibly amplify target gene sequences.

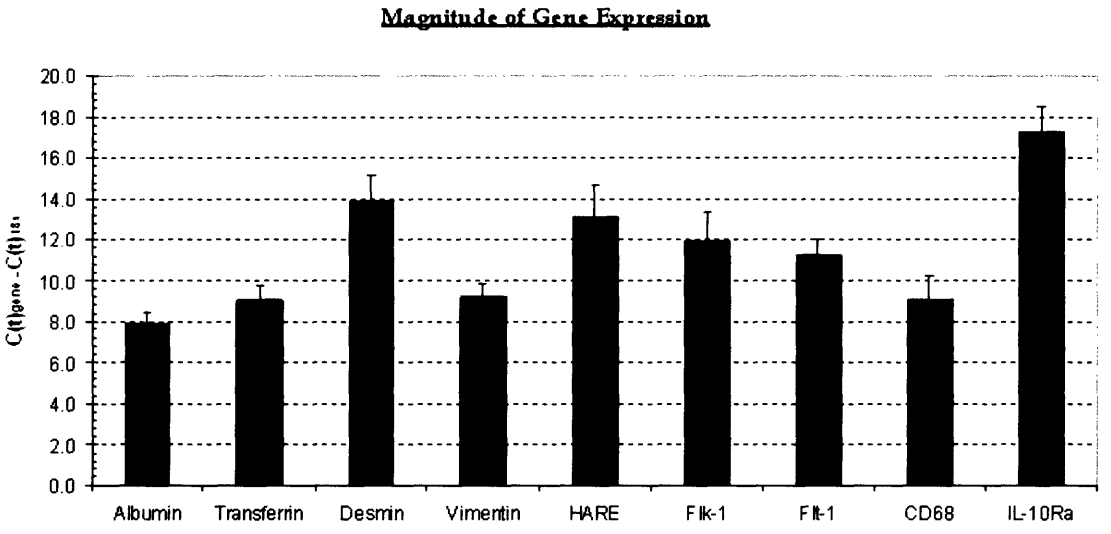

Figure 4.1: Normalized Magnitude of Cell-Specific Gene Expression, $\Delta C(t)_{gene}$

Unsuccessful Markers of Gene Expression

Standard curve development was successful for ten of thirteen target compounds. Effective primers for GFAP, VE-Cadherin, and CD80 were unable to be designed. Three different primer designs were tested for each gene, none showing the ability to specifically amplify the target cDNA.

Melting and amplification fluorescence curves for a sample GFAP primer are shown in Figure 4.2. These curves depict the amplification of the 1X dilution for passage replicates of pure stellate cells ($n_{passage}$ = 4). Melting curve analysis of three different primer designs showed the amplification of three distinct products. Primer design was initially performed using the aforementioned Primer3 software, with the GC purity and sequence length constraints outlined by Qiagen's RT-PCR Manual. A second primer design aimed to target a sequence specific to an intron-intron boundary. The final iteration added a melting temperature constraint (Sato et al. 2003) intended to limit the GCAT composition. Genomic DNA and primer dimer controls were negative for this gene. This suggests genetic redundancy within the GFAP gene sequence leading to nonspecific binding of primers to undesired targets. Amplification curves show large replicate deviation ($\sigma_{C(t),GFAP}$= 2.4 vs. $\sigma_{C(t),vimentin}$= 0.25) compared to those seen with vimentin. Such deviation devalues the significance of the data and does not allow meaningful standard curve development (R^2 <0.60). Further, fluorescence was observed

to decrease following amplification, which implies a reduction in the number of double stranded DNA's. The exact mechanism and meaning of this phenomenon have not yet been elucidated, but its' presence is considered to signify an unreliable data (Giulietti et al. 2001). Northern blot and gene sequencing need to be performed to investigate the identity of the different products before a new, more effective GFAP primer can be designed. Therefore, GFAP has been omitted from further study.

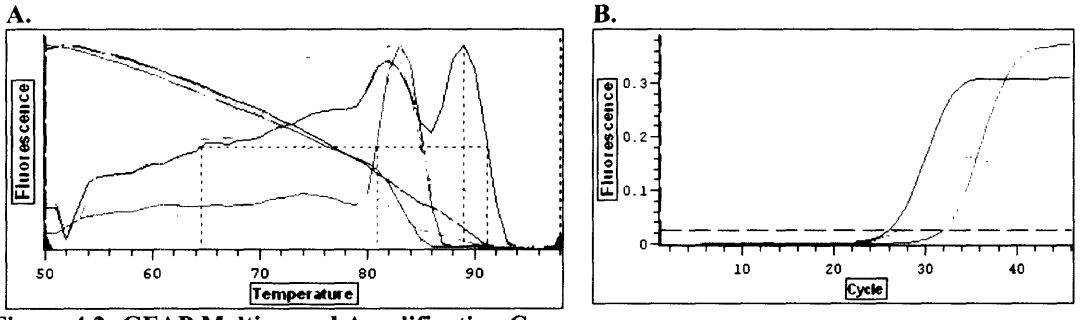

Figure 4.2: GFAP Melting and Amplification Curve

(A) Melting curves across four passage replicates ($n_{passage}$ = 4) and three GFAP primer designs (n_{primer} =3) showed the inability to selectively amplify dsDNA GFAP products.

(B) Amplification curve of GFAP primers show large deviations ($\sigma_{C(t),GFAP}$= 2.4) and a decrease in fluorescence during the constant 'primer-limited' regime.

Similar primer design strategies attempted for VE-Cadherin and CD80 were also unsuccessful. Tested CD80 primers behaved in the same way as those previously described for GFAP and its' melting and amplification curves are shown in Figure 4.4. Desired VE-Cadherin melting curves were attained (Figure 4.3 green curve), but not maintained across biological replicates. This primer does not appear to amplify multiple products, but rather to create different sized amplicons of the same target. The exact mechanism for this observation is unknown, but its presence renders use of CD80 for absolute quantification of PCR data useless.

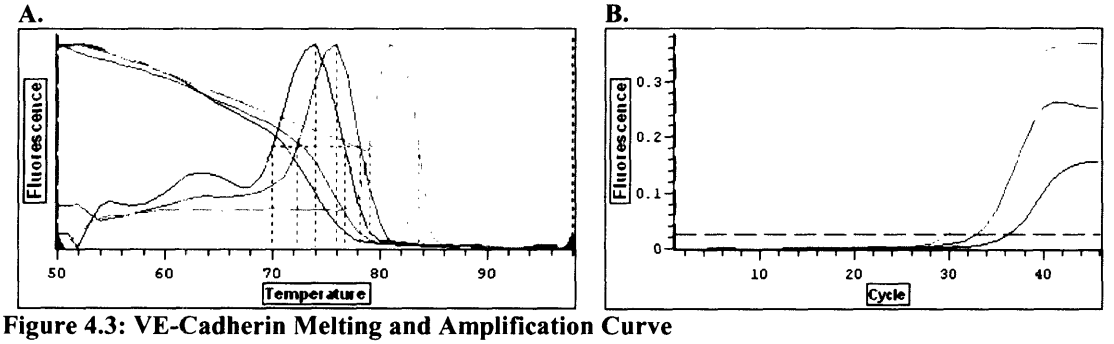

Figure 4.3: VE-Cadherin Melting and Amplification Curve

(A) Melting curves across four biological replicates (n_{bio} = 4) and three VE-Cadherin primer designs (n_{primer} =3) showed the inability to selectively amplify dsDNA VE-Cadherin products. The green curve is the expected target specific curve.

(B) Amplification curve of VE-Cadherin primers show large deviations ($\sigma_{C(t),VE\text{-}Cad}$= 2.1) and a decrease in fluorescence during the constant 'primer-limited' regime.

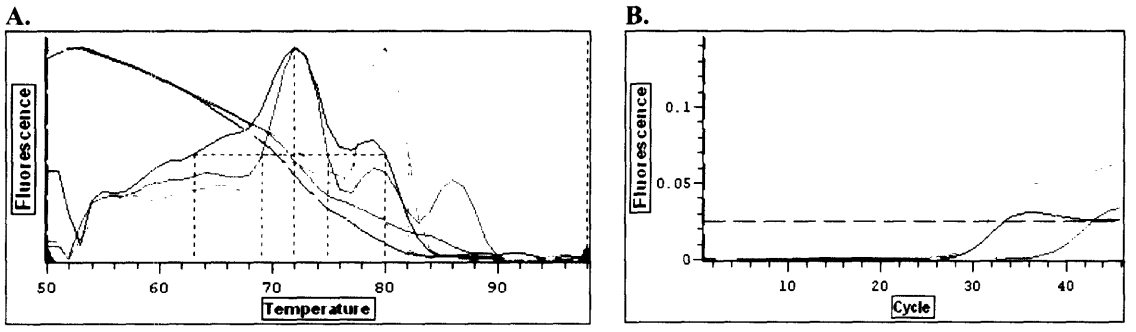

Figure 4.4: CD80 Melting and Amplification Curve

(A) Melting curves across four biological replicates ($n_{bio} = 4$) and three CD80 primer designs ($n_{primer} = 3$) showed the inability to selectively amplify dsDNA CD80 products. The green curve is the expected target specific curve.

(B) Amplification curve of CD80 primers show large deviations ($\sigma_{C(t),CD80} = 2.8$) and a decrease in fluorescence during the constant 'primer-limited' regime.

4.3.2 Validation of Specificity of Phenotype Markers

Specificity of a candidate gene primer was determined by performing real-time PCR on negative controls ($n_{bio} = 4$, $n_{tech} = 2$) of each enriched cell population ($n_{control} = 3$). These data sets were normalized to reflect the number of 18s rRNA transcripts present per transcript of target. Further, cross-reactivity experiments were conducted by mixing the gene specific cDNA sample with 3x contaminant of one undesired cell sample$\left(C_{cDNA} = \frac{3*C_{cDNA,(-)}+C_{cDNA,(+)}}{4}\right)$, (representing the potential for a two-fold reduction of C(t)) and comparing absolute gene expression to that of a representative positive control sample which was contaminated with water$\left(C_{(+)control} = \frac{3*H_2O+C_{cDNA,(+)}}{4}\right)$. So every sample was one part target and three parts contaminant, where the contaminant was either water (positive control) or another cell type. Thus, a specific marker should return the same cycle threshold regardless of the nature of the contaminant. Contaminant concentration was selected based on the maximum contamination possible given the volume of stock cDNA remaining for each sample. Regardless, these studies were undertaken to further validate specificity in a mixed population of cells. These data are presented in the form of $C(t)_{gene}$ because the aforementioned sample volume constraints did not permit determination of 18s C(t), and as such are subject to additional variation arising from previously mentioned differences in sample cDNA concentration.

Hepatocytes

Albumin and transferrin specificity and cross-reactivity results are detailed in Figure 4.5. Albumin gene expression by hepatocytes was significantly different from NPC's ($p < 0.0001$). Enriched Kupffer cell controls expressed significantly more albumin than endothelial cells and stellate cells ($p < 0.01$). This observation implies low levels of albumin expression by kupffer cells. However, kupffer cells have never been proven to express albumin (Li et al. 1999). A more likely explanation for the low-level

of albumin mRNA transcripts is that they were present in the parenchymal cell blebs that heavily contaminated the kupffer cell isolate. This data therefore shows that parenchymal cell blebs in the kupffer cell isolate are essentially inert.

Albumin cross-reactivity experiments showed that contamination by NPC's resulted in no significant variations in gene expression ($p > 0.8$). Said differently, contaminant NPC's do not expression sufficient levels of albumin to appreciably alter C(t) from that of the positive control. Therefore, albumin gene expression is specific to hepatocytes.

A.

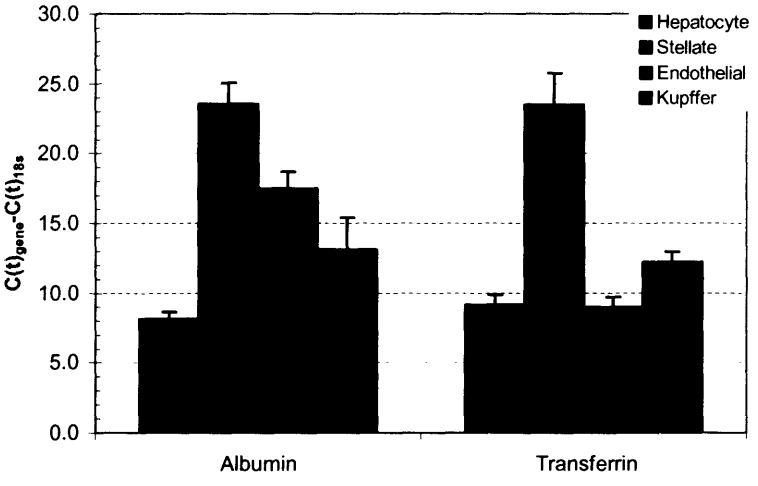

B.

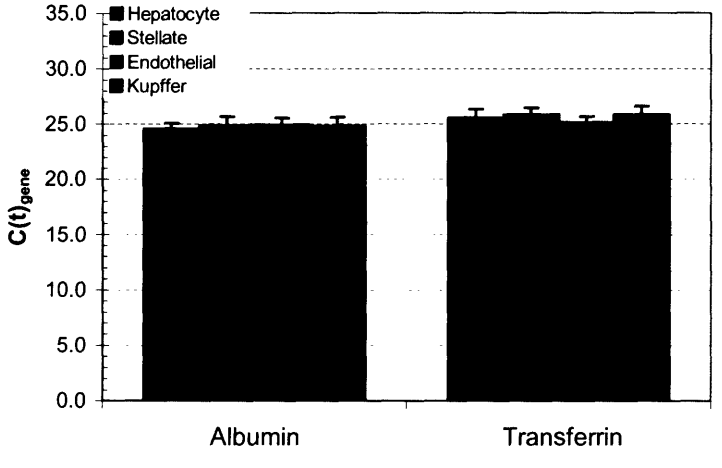

Figure 4.5: Albumin and Transferrin Specificity and Cross-Reactivity Screening
(A) Normalized gene expression of Albumin and Transferrin in hepatic cells show hepatocytes to be specific for albumin and endothelial cells to show slight expression of transferrin
(B) Cross reactivity of 1x hepatocytes with 3x various NPC contaminant shows no significant variation in expression levels

Transferrin gene expression in hepatocytes is significantly different from that of stellate cells and Kupffer cells ($p < 0.0001$) (Figure 4.5). Kupffer cells demonstrated similar low levels of transferrin gene expression as was previously seen with albumin. The same parenchymal cell bleb contaminants are believed to be responsible for this expression. However, endothelial cells showed a significant transferrin expression. This observation is surprising because gene expression levels of transferrin in hepatocytes have previously been reported as statistically different from NPC's ($p < 0.01$) and most statistically significant ($p < 0.0001$) from endothelial cells (Zhang et al. 2003). Careful inspection of the melting curves unveils the formation of a second PCR product in endothelial cell controls ($n = 3$) (Figure 4.6A). However, in all other transferrin cell standards, negative controls, and culture samples, normal melting curves were observed (Figure 4.6B). Upon this discovery, endothelial cell samples were re-run using transferrin primers and again, the same phenomenon was observed. This observation was truly perplexing since kupffer cell samples, which are known to contain endothelial cell contaminant, demonstrated normal melting curve phenomena, as did one of the endothelial cell negative controls. This leads to two possible conclusions. First, the samples could have become polluted with genomic DNA after the original screens were run, and thus be corrupted. Alternatively, these melting curves could imply the need for redesign of transferrin primers. New primers have been designed and are presently being re-evaluated to determine if this observation was true endothelial cell gene expression or simply and artifact of polluted samples.

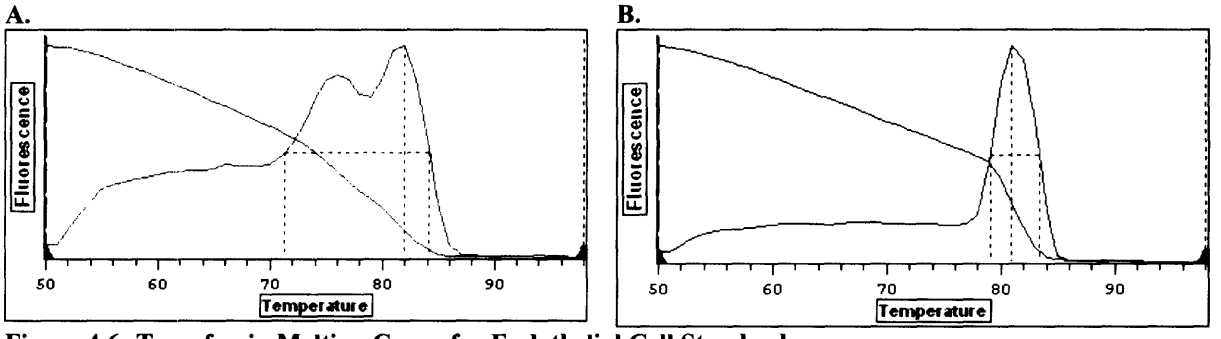

Figure 4.6: Transferrin Melting Curve for Endothelial Cell Standards
(A) Transferrin melting curve for pure endothelial sample.
(B) Transferrin melting curve for kupffer cell samples.

Cross-reactivity experiments showed that the absolute expression of mixed cell populations was not significantly different from the positive hepatocyte control ($p > 0.2$). This observation gives support to the belief that expression of transferrin by EC's is an artifact of contamination and not an intrinsic property. Therefore, for the purpose of this work, transferrin shall be considered a hepatocyte specific marker.

Stellate Cells

Desmin and vimentin gene expression were statistically disparate from that of hepatocytes, EC's, and KC's ($p < 0.01$) (Figure 4.7A). The endothelial cell enriched samples, previously described as containing 3% primary stellate cells, demonstrated the most pronounced non-stellate expression levels. These levels of gene expression ($\Delta C(t) \sim 3.1$) are not statistically different ($p = 0.27$) from back of the envelope estimations

3% stellate cell expression made from the standard curves ($\Delta C(t) \sim 3.4$). This agreement of between empirical expression of primary cells and calculations made from cell-line derived standards shows strong promise for stability of Cross-reactivity experiments (Figure 4.7B) further confirmed that mixing with non-stellate cells does not cause significant variations in gene expression from positive control ($p > 0.2$). Therefore, both desmin and vimentin are markers that are specific to a stellate cell phenotype.

A.

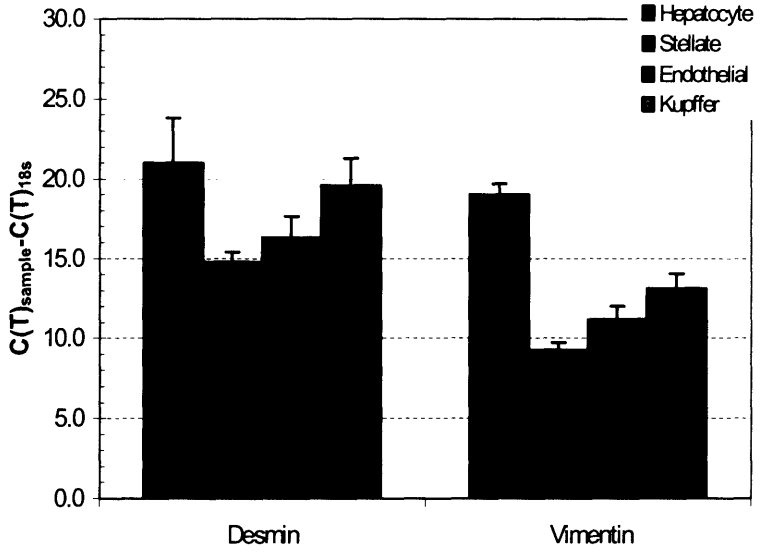

B.

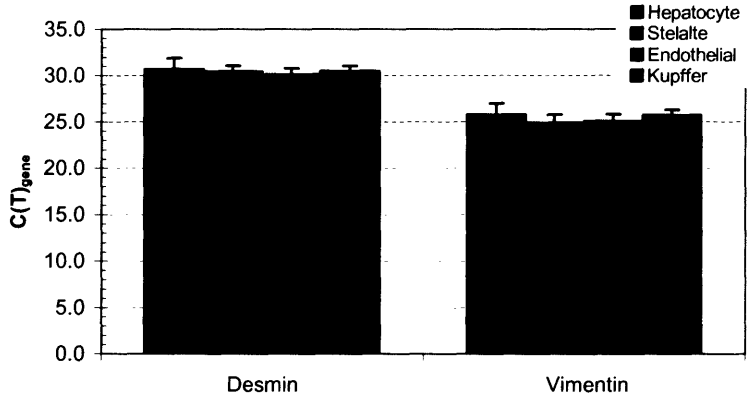

Figure 4.7: Desmin and Vimentin Specificity Screening for Stellate Cells
(A) Normalized gene expression of desmin and vimentin shows stellate cells to display significant specificity against other liver cell types.
(B) Cross reactivity of 1x stellate with 3x various hepatic cell contaminant shows no significant variation in expression levels.

Endothelial Cells

Endothelial cell gene expression of HARE, Flk-1, and Flt-1 was statistically greater than that of hepatocytes, and stellate cells ($p < 0.001$) (Figure 4.8A). However, KC samples demonstrated appreciable amplification of these EC targets. This outcome is expected because of significant cross-contamination between KC and EC standard cell fractions (Chapter 3 section 2.2). KC:EC ratios of KC and EC samples was determined to be 68 : 32 and 10 : 87 respectively. Therefore, there is 55% difference between the EC content of these two samples ($\Delta P_{EC} = P_{EC/EC} - P_{EC/KC}$). This difference in EC content should correlate to approximately a 0.9 difference in $\Delta C(t)$ [$\Delta C(t) = \log_2(\Delta P_{EC})$]. Empirical $\Delta C(t)$ was equal to 1.11 ± 0.86, 0.57 ± 0.62, and 1.37 ± 0.47 for HARE, Flk-1 and Flt-1 respectively. Thus, it can be seen that empirical results are not significantly different from those expected by calculation ($p > 0.3$). This hypothesis was further corroborated by cross-reactivity studies (Figure 4.9B).

A.

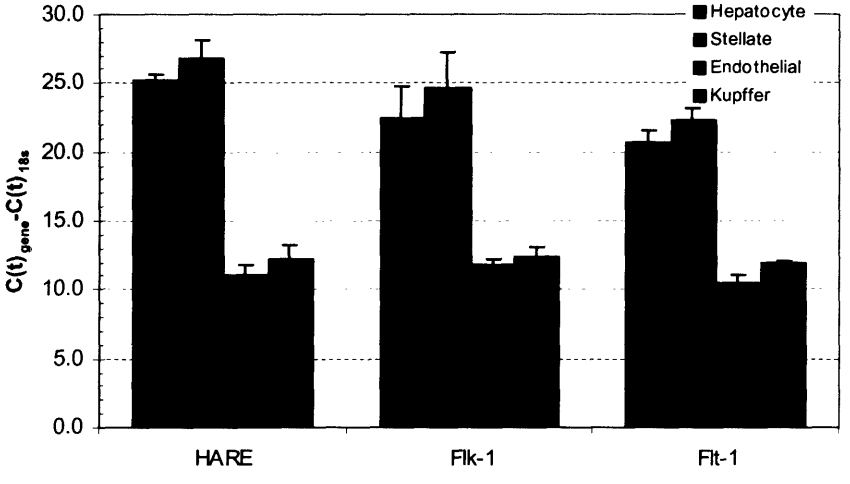

B.

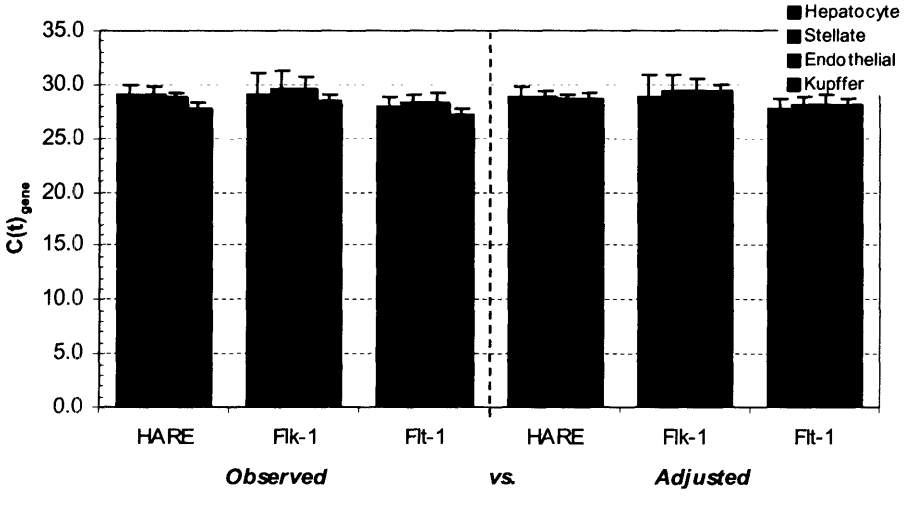

Figure 4.8: HARE, Flk-1, & Flt-1 Specificity and Cross-Reactivity Screening
(A) Normalized gene expression of HARE, Flk-1 and Flt-1 shows endothelial cells to display significant specificity against hepatocytes and stellate cells, but cross-contamination of cell isolate perturbs validation of specificity against Kupffer cells
(B) Cross reactivity of 1x endothelial with 3x various hepatic cell contaminant shows no significant variation in expression levels ($p > 0.2$) and mathematical corrections for cross-contamination shows remarkable sample correlation ($p > 0.65$), insinuating actual specificity of EC markers against KC's.

These, cross-reactivity studies showed significant correlation of endothelial cell gene expression ($p > 0.2$) in initial studies and even more similarity of gene expression ($p>0.65$) when corrected for observed cross-contamination $\left(C(t)_{adj}=C(t)_o+\log_2(C_{cDNA,EC}+3*C_{cDNA,ECj})\right)$. Hence, sufficient evidence does not exist to contradict previously reported specificity of these mRNA transcripts to endothelial cells (Yannariellobrown et al. 1992, Yamane et al. 1994). Thus, all tested EC target genes are specific against hepatocytes and stellate cells, and sufficient evidence does not exists to contradict previous reports of specificity against Kupffer cells.

Kupffer Cells

Kupffer cell gene expression of CD68 and IL-10Ra was statistically greater than that of hepatocytes, and stellate cells ($p < 0.0001$) (Figure 4.9A). The same cross-contamination previously described for endothelial cells was observed. Recapitulating the previous analysis for KC's, there is 58% difference between the KC content of KC and EC samples. This difference in KC content should correlate to approximately a 0.8 difference in C(t). Empirical $\Delta C(t)$ was 0.63 ± 1.07, and 1.60 ± 1.04 for CD68 and IL-10Ra respectively. Thus, it can be seen that empirical results are not significantly different from those expected by calculation correcting for cross-contamination ($p > 0.2$). This hypothesis was further corroborated by cross-reactivity studies (Figure 4.9B).

A.

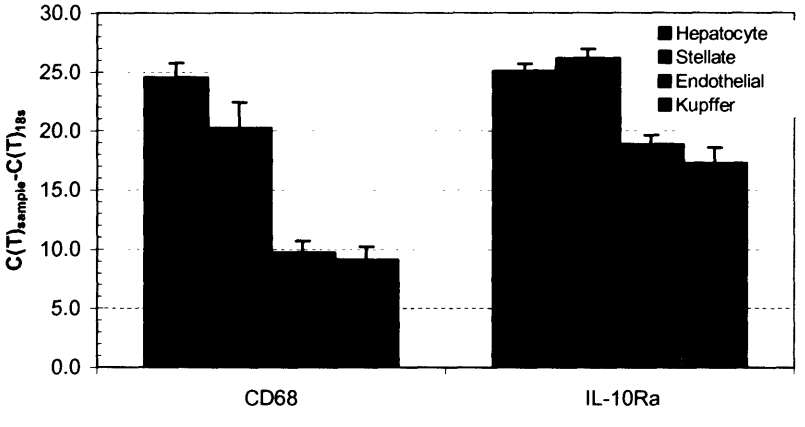

B.

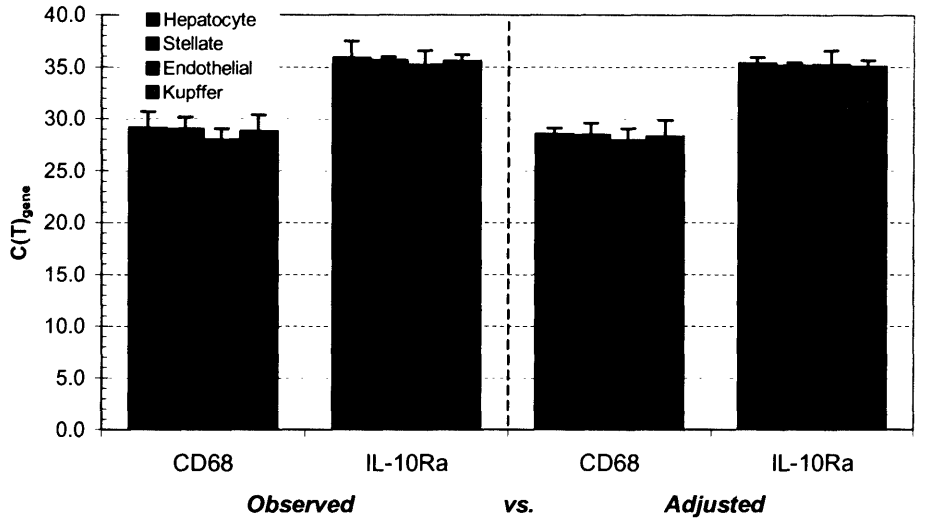

Figure 4.9: CD68 and IL-10Ra Specificity Screening for Kupffer Cells
(A) Normalized gene expression of CD68 and IL-10Ra shows Kupffer cells to display significant specificity against hepatocytes and stellate cells, but cross-contamination of cell isolate perturbs validation of specificity against endothelial cells
(B) Cross reactivity of 1x Kupffer with 3x various hepatic cell contaminant shows no significant variation in expression levels ($p > 0.15$) and mathematical corrections for cross-contamination shows remarkable sample correlation ($p > 0.75$), insinuating actual specificity of KC markers against EC's.

These, cross-reactivity studies showed significant correlation of Kupffer cell gene expression ($p > 0.15$) in initial studies and even more similarity of gene expression ($p > 0.75$) when corrected for observed cross-contamination $\left(C(t)_{adj} = C(t)_o + \log_2(C_{cDNA,KC} + 3 * C_{cDNA,KC_i})\right)$. These studies indicate that sufficient evidence does not exist to contradict reports claiming significant specificity of CD68 to Kupffer cells (Jiang et al.1998). However, since specificity of IL-10Ra in KC's has not yet been proven, sufficient evidence does not exist to validate IL-10Ra as only expressed in Kupffer cells. Thus, CD68 and IL-10Ra transcripts are not appreciably expressed in hepatocytes or stellate cells, and no evidence exists to contradict previous reports of insignificant CD68 presence in EC's, nor does any evidence exist to claim IL-10Ra specificity in KC's.

4.3.3 NPC Incorporation in Cell-Culture

Tissue composition in *in vivo*, post perfused liver isolate, 2D collagen gel sandwiches, spheroid aggregates, and the 3D MilliF bioreactor cultures has been determined via absolute quantification using the newly developed standard curves. Real-time PCR was run to determine the cycle threshold of all validated cell specific genes. For this analysis, IL-10Ra has been treated as transcript specific to Kupffer cells. C(t) values of each gene were related to standard curves to determine the concentration of each probes cDNA present in the sample. cDNA concentrations for each set of cell specific markers were then averaged to generate the 'mean' presence phenotypic cDNA:

$$C_{cDNA,X} = \frac{\sum_{i=1}^{n} e^{\left(\frac{C(t)-b_i}{m_i}\right)}}{n}$$

These mean phenotypic cDNA concentration were then combined to determine tissue composition as follows:

$$f_i = \frac{C_{cDNA,i}}{\sum_{i=1}^{4} C_{cDNA,i}} \qquad i = \{PC, SC, EC, KC\}$$

This composition is a cell number fraction because the standard curves used are correlated to cell number. Also, because it is calculated without normalizing to a housekeeping gene like 18s discrepancies in the RNA content of each cell type are avoided. Essentially, we are just taking the ratio of the number of cells present in a representative sample

In Vivo

In vivo samples represent the average of an 18-sample data set (n_{bio} = 3, n_{sample} = 2, n_{tech} = 3). Figure 4.9 shows a graphic representation of published *in vivo* hepatic tissue composition and our calculated tissue compositions. Biological replicates were analyzed separately and the compositions determined by each averaged. The two data sets show that our gene library does not succeed at estimating *in vivo* tissue composition.

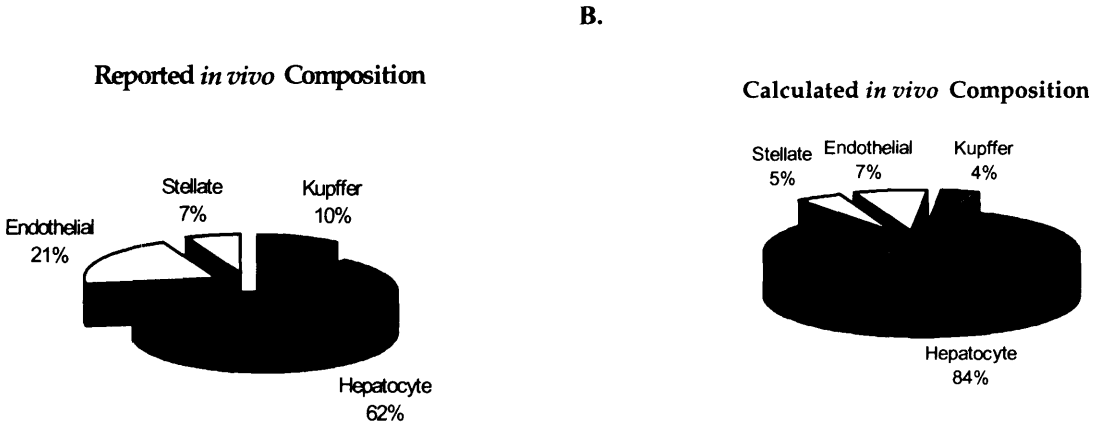

Figure 4.9: Predicted and Calculated *in vivo* Tissue Composition from Full Gene Set
(A) Reported composition of in vivo liver (data pooled from Gebhardt et al. 1992, Malik et al. 2002, Geerts et al. 2003, Smedsrod et al. 1994)
(B) Prediction of in vivo tissue composition using arithmetic mean of phenotype specific markers fails to replicate reported data.

This disparity implies that our standard curves derived from isolated cell fractions is either overestimating the presence of hepatocytes or underestimating NPC's. Comparing the normalized gene expression of our *in vivo* data set to the magnitudes of gene expression seen in the isolated cell fractions (Figure 4.10), significant variations are present. All NPC's demonstrate a lower magnitude of gene expression *in vivo* than in their standards. Such a variation is expected since NPC isolate standards represent purified cell fractions whereas their respective concentrations *in vivo* are proportionally less with their concentration. However, albumin and transferrin demonstrated notably higher levels of gene expression *in vivo* than in their purified cell standards. These genes'

expression levels have been shown to be regulated by similar mechanisms (Li et al.1999), and are both known to vary significantly in different *in vitro* culture systems. Such an observation implies significant down-regulation of gene expression stemming from the Percoll isolation process. Slight variations were expected, but the hope was that the time scale for gene expression regulation would be sufficiently long such that the isolation process (~30min post-perfusion) would not result in major changes of their relative gene expression.

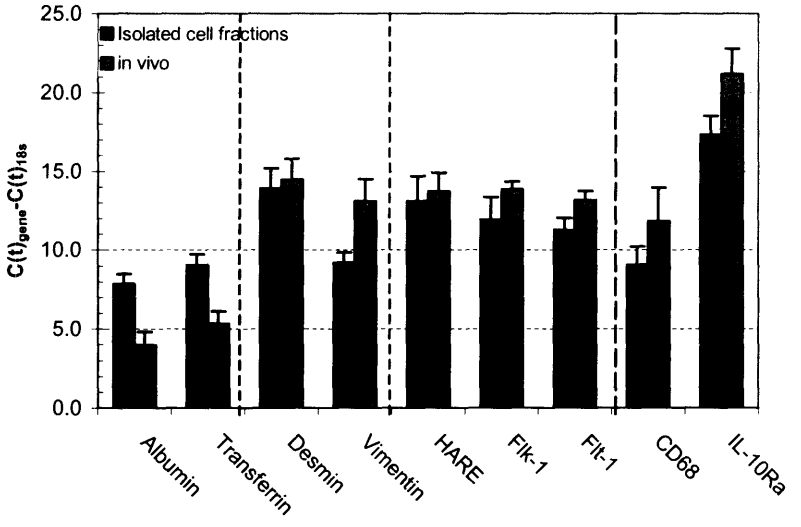

Figure 4.10: Comparison of Cell Isolate Fraction used for Standard Curves to *in vivo*
Normalized gene expression levels ($\Delta C(t)=C(t)_{gene}-C(t)_{18s}$)of full gene set in cell isolate fractions used for standard curve development versus *in vivo* tissue samples

To further analyze these data; the $\log_2$ fold change between *in vivo* and our cell isolate standards has been compared to the theoretical $\log_2(FC)$ necessary to replicate *in vivo* composition (Figure 4.11) [$\log_2(FC)_{calc}=\log_2(P_{standard}/P_{in\ vivo}$]. This comparison is a direct measure of how effective each gene standard is at predicting *in vivo* data. Such comparison is a useful estimation of stability of a gene because variations in expression between freshly isolated primary cells and *in vivo* will likely become more pronounced in culture.

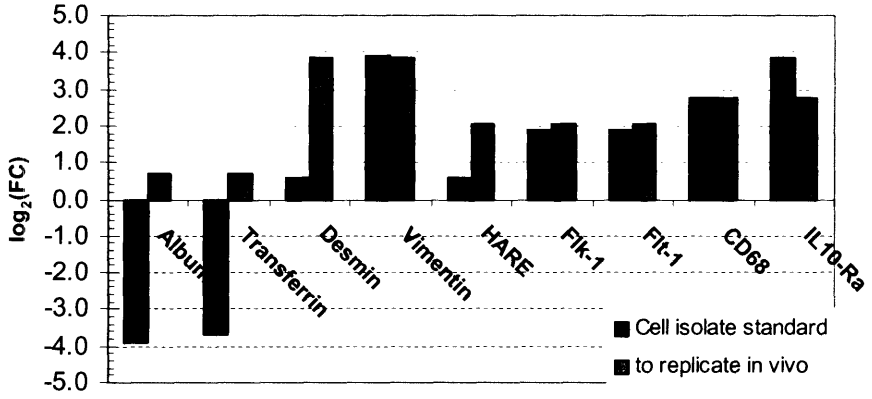

Figure 4.11: Stability of Gene Set Expression – Observed vs. Theoretical
Log2 Fold Change of gene expression in cell isolate fractions used for standard curves compared to theoretical $\log_2(FC)$ of gene expression level needed to replicate in vivo data

This comparison confirms that hepatocyte expression of albumin and transferrin is underestimated in hepatocyte standards. Such underestimation leads to a vertical shift in the standard curve and an overestimation of the regression constant, 'b'. Absolute quantitation calculations assume a fixed standard curve position and thus are inflexible to irregularity in gene expression. In essence a mixture of cells having a C_{cDNA} of 0.1 would yield a C(t) value of 10 *in vivo*. However, the isolated hepatocyte standard curves yield a C(t) of 13. Thus, when the *in vivo* data is applied to the isolated hepatocyte standard curve, it is falsely identified as having a cDNA concentration of 1.0, which leads to overestimation of tissue composition. Figure 4.12 shows a graphic representation of this phenomenon.

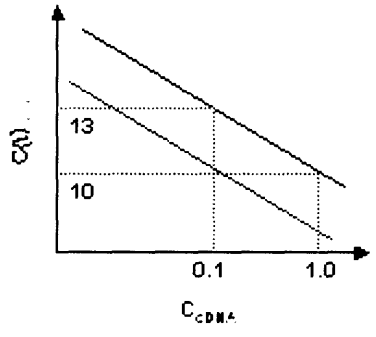

Figure 4.12: Sensitivity of Standard Curves to Gene Expression Variability

Stability of gene expression is a fundamental requirement of absolute quantitation for a cell population. Therefore, the gene set has been further screened for markers that demonstrate said stability. Stable genes have been defined as those who demonstrate less than a one fold change between standards and *in vivo* ($\log_2(FC) < \pm 0.5$). Figure 4.11 shows that only vimentin, Flk-1, Flt-1 and CD68 pass this filter. This data supports our prior assumption of the phenotypic specificity of Flk-1, Flt-1 and CD68. These genes

represent stellate, endothelial, and kupffer phenotypes and show very good ability to predict *in vivo* cDNA concentrations. The stability displayed by vimentin is particularly positive because the cell standards were derived from a cell line cultured on tissue culture plastic in the presence of serum, showing considerable resilience of gene expression to disparate culture systems.

Unfortunately, no hepatocyte markers passed this stability check. However, 18s expression has been validated as a general "house-keeping" gene that is consistently expressed relative to total RNA expression. Therefore, we can reliably define the total amount of cDNA present in a sample and the cDNA concentration contributed from each non-parenchymal phenotype. Thus, hepatocyte cDNA concentration can be backed calculated as follows:

$$C_{cDNA,Hep} = C_{cDNA,18s} - \sum_{i=1}^{3} C_{cDNA,NPC_i}$$

This data manipulation implies that all cells that are not non-parenchymal are hepatocytes. Consequently, the hepatocyte cDNA concentration includes all present pit, biliary, and other cell types in liver. These cell types account for < 1% of the total population, and as such can be considered negligible.

In vivo tissue compositions calculated using this filtered gene set were very similar to those previously reported for *in vivo* tissue (Figure 4.13). This data demonstrates that we have defined a gene set capable of estimating the reported composition of *in vivo* tissue using standard curves derived from isolated cell fractions of post perfused liver. Thus, the selected genes show significant stability and expression levels despite exposure to shear stress, removal from the hepatic microenvironment, traumatic cell enrichment procedures, and harsh enzyme conditions, and as such show strong promise to not be affected in long-term cell culture systems.

A.

Reported *in vivo* Composition

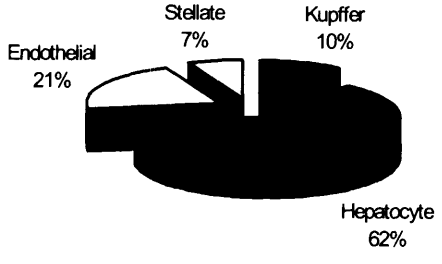

B.

Calculated *in vivo* tissue composition

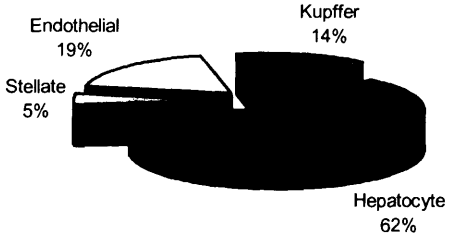

Figure 4.13: Predicted and Calculated *in vivo* Tissue Composition from Filtered Gene Set
(A) Reported composition of in vivo liver (data pooled from Gebhardt et al. 1992, Malik et al. 2002, Geerts et al. 2003, Smedsrod et al. 1994)
(B) 18s rRNA, Flk-1, Flt-1, Vimentin, & CD68 show the ability to replicate reported *in vivo* tissue composition within reported error ranges.

Post-Perfused Liver Isolate

Using the previously described gene set and mathematical construct, the cellular composition of post-perfused liver isolate was determined at two operating flow rats. Liver isolate was collected from three rats (n_{flow}=2, n_{bio}= 3, n_{sample}= 2, n_{tech}= 3) pre-centrifugation and immediately homogenized. Figure 4.14 shows the resulting calculated isolate composition as calculated using the filtered gene set. Liver isolate is an intermediate step between *in vivo* tissue and the isolated cell fractions used to develop standard curves and as such is believed to be accurately estimated by the filtered gene set.

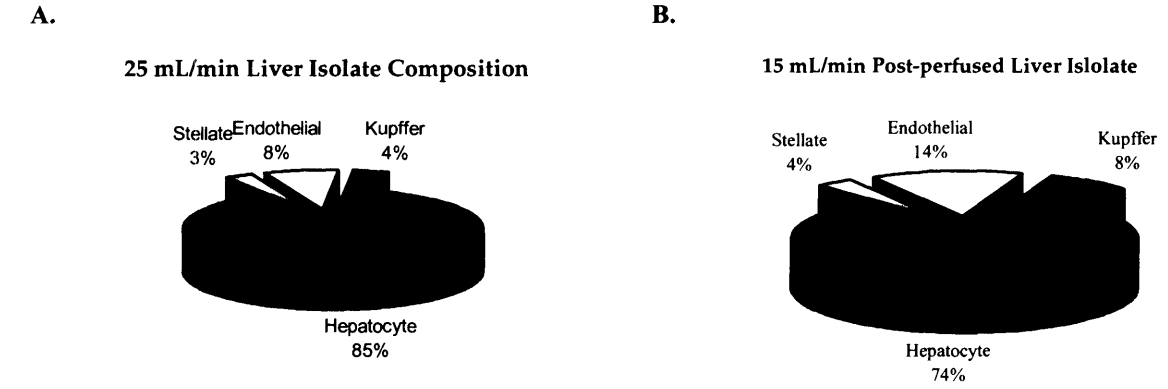

Figure 4.14: Estimated Composition of Post-perfused Liver Isolate at High and Low Flow Rates
(A) Post-perfused liver isolate (n = 3) composition at 'high' 25 mL/min perfusion flow rate as determined by filtered gene set
(B) Post-perfused liver isolate (n = 2) composition at 'low' 15 mL/min perfusion flow rate as determined by filtered gene set

This data is a means to gauge the impact of our perfusion procedure on the relative loss of cell type, and compare said impact between perfusion flow rates. Said differently, we can estimate what cells are lost by blendzyme digestion and perfusion. Such information allows the determination of input in mass balance and efficiency calculations of the isolation procedure and is less time and labor intensive to attain than previously attempted cyto-spinning and staining methods. Kupffer and endothelial cells show significant loss of their initial cell population. This cell loss is expected because these cells are physiologically exposed to the greatest perfusion trauma. However, this data confirms results of nuclear staining (Chapter 3 section 1.2) that indicated a low flow rate (15 mL/min) perfusion allows greater recovery of NPC's. This observation has been speculated for some time, but this data shows quantitatively that a low flow rate isolation procedure is preferred for the recovery on NPC's.

Post-Percoll Centrifugation NPC Isolate

The gene set was further applied to establish the composition of purified NPC isolate that is added to co-culture. NPC isolate was collected from three rats (n_{flow}=2, n_{bio}= 3, n_{sample}= 2, n_{tech}= 3) post-Percoll gradient isolation and immediately homogenized. Figure 4.15 shows the resulting calculated isolate composition as calculated using the filtered gene set. NPC isolate is an intermediate step between *in vivo* tissue and the enriched cell fractions used to develop standard curves and as such is believed to be accurately estimated by the filtered gene set.

A.

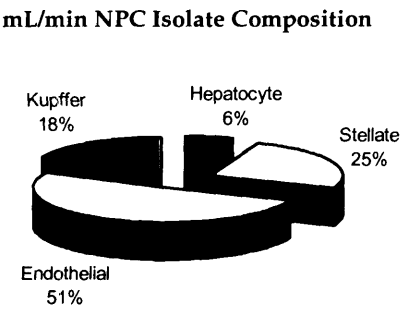

B.

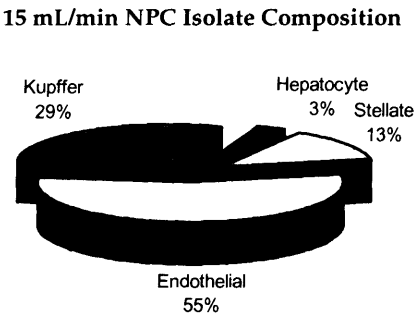

Figure 4.15: Estimated Composition of Post-perfused Liver Isolate at High and Low Flow Rates
(A) Post-perfused NPC isolate ($n = 3$) composition at 'high' 25 mL/min perfusion flow rate as determined by filtered gene set
(B) Post-perfused NPC isolate ($n = 2$) composition at 'low' 15 mL/min perfusion flow rate as determined by filtered gene set

This data establishes the composition of NPC's derived at different perfusion flowrates. This data coupled with the results of the nuclear staining cell-count provides a full, quantitative characterization of the cell population input to an *in vitro* co-culture system. Application of the gene set at the endpoint of the culture will provide the output. Thus, we can begin to perform quantitative engineering analyses to determine the efficiency of cell separations and cell incorporation in each step of our process. This analysis will be invaluable in pinpointing the limiting steps in our process and furthering its biological and physiological optimization.

Application in 2D Collagen Gel Sandwich Culture

Percolled hepatocytes were co-cultured in a 1:1 ratio with the isolated primary NPC fraction in collagen gel sandwich and analyzed on Day 2, 4 & 7 post-overlay. This experiment was only conducted on one biological replicate perfused at 25 mL/min and data represents the average of three culture wells. Figure 4.15 shows the calculated compositions of collagen gel cultures on Day 2, 4 & 7 (A) and compares them to the overall RNA recovered on each respective day (B). The RNA recovered from these experiments was high quality ($1.9>P_{col}>2.1$) and is indicative of the number of cells in a culture. This claim assumes the total amount of RNA expressed in NPC's is constant overtime, which has been validated in hepatocytes (Iida et al. 2003). Immuno-staining was attempted on these cultures, but due to high background fluorescence was unable to be quantified. Thus this data represents a qualitative observation of the behavior of co-cultured hepatic primary cells.

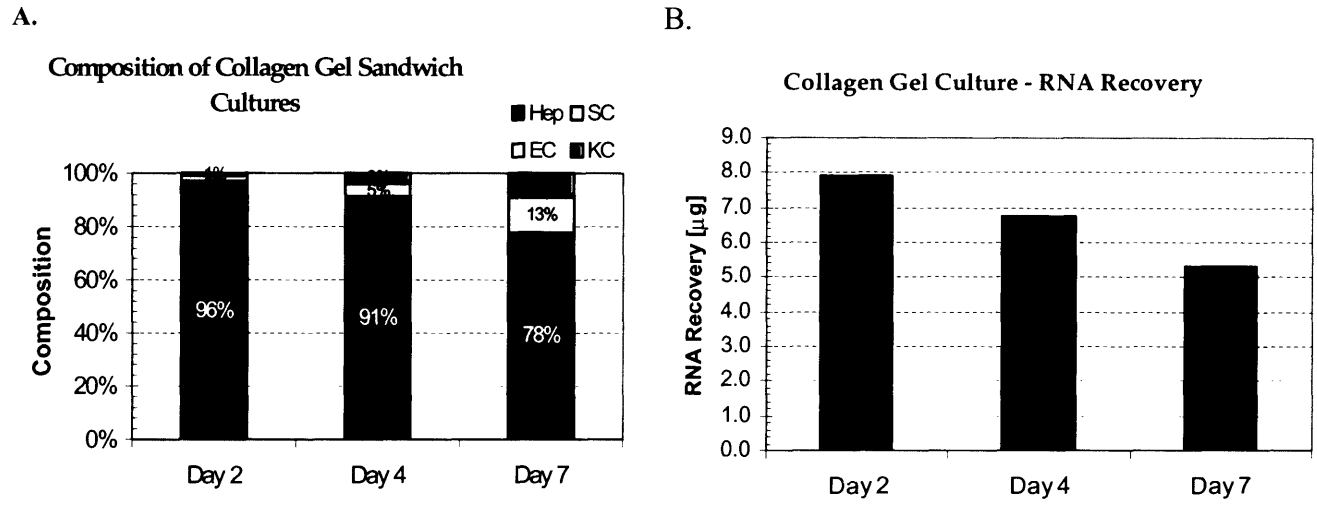

Figure 4.16: Estimated Composition of Collagen Gel Sandwich Cultures
(A) Temporal composition of NPC's co-cultured in a 1:1 ratio with hepatocytes at a seeding density of 50K/cm^2
(B) Total RNA recovered from collagen sandwich cultures

The RNA recovery data implies a constant decline in the overall number of viable cells in culture. This phenomenon was previously reported by LeCluyse et al. (1997). Such a decrease shows that cells are dying and is corroborated by observation that the number of hepatocytes is also decreasing. However, the composition data implies that the rate of death of the more RNA abundant hepatocytes is considerable at day 7, whereas the proliferation of NPC's seems to keep the rate of RNA loss constant. Interestingly, NPC's do not appear incorporate well in the collagen gel construct, but once incorporated seem to maintain viability. Further, it appears that the total relative composition of Kupffer and stellate cells is increasing. This observed proliferation is significantly different from artificial relative composition increase from the death of hepatocytes $\left(P_{NPC,adj} = \frac{P_{NPC,o}}{P_{Hep,o} - \Delta P_{Hep}}\right)$. Hence, it appears that the kupffer and stellate cells undergo a phenotypic change into the 'active', proliferative form. Endothelial cells appear to maintain their cell population throughout the 7-day culture.

The overall population size is too small (n_{bio}=1, n_{well}= 3) is to make any definitive conclusions. The temporal stability of these genes has not been definitely proven and as such we cannot be sure that the observed trends represent what is truly taking place in culture. Additional studies that couple estimations made by immuno-staining with estimations made by our gene set will be instrumental in establishing the temporal stability and accuracy of our gene set. Regardless this study shows that our gene set can be applied to a 2D collagen sandwich culture system.

Application in 3D Spheroid Aggregates and MilliF bioreactor

Percolled hepatocytes were co-cultured NPC's in various ratios (0%, ~5%, 33%, & 50%) for three days in spinner flasks cultures. This experiment was conducted on the

same rat as the 2D collagen gel sandwiches perfused at 25mL/min to eliminate biological variation between experiments (n_{col} = n_{sph} =1, n_{sample}=3, n_{tech}=3). The RNA recovered from these experiments was high quality (1.9>P_{col}>2.1) and all reported data is on spheroids a 'normal' size (100 < D < 300μm) sufficient to maintain ample O_2 transfer to cells in the spheroid core. Figure 4.16 shows the resulting compositions of these spheroids.

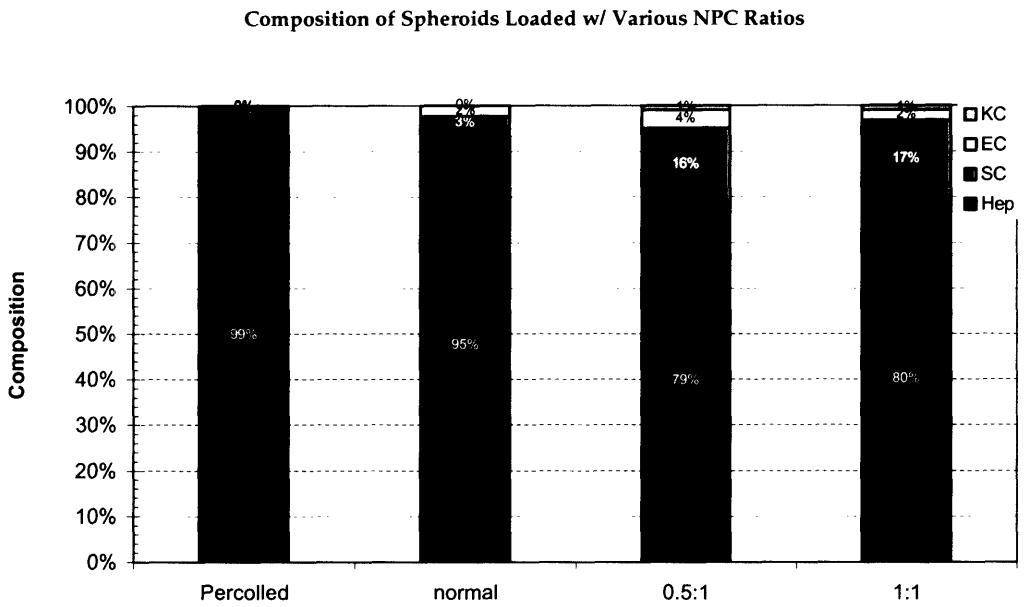

Figure 4.17: NPC Incorporation in Spheriod Aggregates
NPC-hepatocytes co-cultured in spinner flasks for three days in different NPC proportions (0%, ~5%, 33%, 50% NPC) (n_{bio} = 1, n_{sample} = 2, n_{tech} = 3).

Although temporal studies have not been conducted to confirm stability of the filtered gene set in spinner flask culture, these experiments offer a qualitative sense of NPC incorporation into spheroid aggregates. Magnitude of incorporation cannot be considered significant, but this data does demonstrate the presence or absence of particular cell phenotypes. Kupffer cells are not being incorporated into spheroids and that incorporation of endothelial cells is also very minor. However, stellate cells do appear to be appreciably incorporating in all cultures where they are present. This data also seems to imply an NPC incorporation maximum as 0.5:1 and 1:1 NPC seeding ratios yield the same NPC incorporation. However, the overall population size is too small (n_{bio}=1, n_{well}= 3) is to make any definitive conclusions. It should be noted that these stellate cells are primary and not the HSC-T6 cell line that was used for the stellate cell standard, and thus stellate cells represent a small fraction of the initially co-cultured NPC's. This observation makes sense biologically because stellate cells are the only non-parenchymal cells that form cell-cell junctions (gap junction) with hepatocytes. Endothelial and kupffer cells form cellular junctions with one another, but communicate with hepatocytes and stellate cells primarily through soluble signaling mechanisms. Cells form spheroid aggregates by junction formation (tight or gap) caused by random cellular collisions in the spinning culture. Thus, endothelial cells and kupffer cells have no

mechanism to incorporate in spheroids and there presence is likely an artifact of random entrapment instead of actual cell-cell contacts.

Seeding 0.5:1 spheroid aggregates into the MilliF bioreactor further corroborated this phenomenon. This bioreactor was run for seven days post-seeding, medium changed every other day, and homogenized immediately following removal from culture ($t < 5$min) Figure 4.17 confirms that Kupffer cells and endothelial cell markers are not present in the bioreactor whereas there is significant presence of primary stellate cell markers.

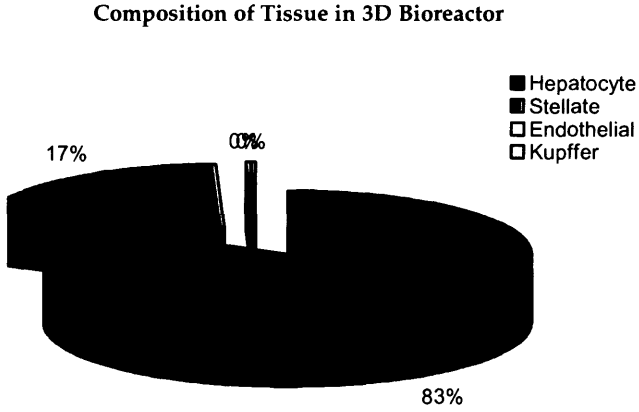

Figure 4.18: NPC Incorporation in the MilliF Bioreactor
Tissue Composition calculations of day 7 bioreactors seeded with 0.5:1 NPC:Hepatocytes co-cultured day 3 spheroids (n_{bio}= 1, n_{sample} = 2, n_{tech} = 3). This tissue composition is the same as the 0.5:1 spheriods seeded into the bioreactor when correcting for apparent loss of endothelial cells.

Additionally, the calculated composition of spheroids seeded into the bioreactor is the same as the composition of incorporated tissue within the bioreactor when corrected for the loss of endothelial cells ($P_{rxr,i} = P_{sph,I} / (1-P_{sph,EC})$). This data implies that stellate cells are capable of being incorporated into spheroids and integrated into tissue within the bioreactor, but a different incorporation strategy must be developed to incorporate endothelial and Kupffer cells.

4.4 Conclusions

In this chapter, the previously identified set of phenotype-specific candidate genes (Chapter 3 section 6) was tested for specificity and expression stability. In order to evaluate specificity and stability, enriched cell fractions of each liver cell phenotype were collected and standard curves developed for each designed gene primer. The entire gene set was then tested in each cell fraction to validate specificity. Cross-reactivity studies were then conducted on mixed cell populations to confirm specificity results and gauge the magnitude of error caused by gene expression in undesired cell types. Genes that were shown to be phenotype-specific were examined for stability by their ability to successfully recreate known *in vivo* tissue composition. Genes that were demonstrated to be both specific to a cell phenotype, possess high magnitude of expression, and have

stable expression levels in post-perfusion cell isolate fractions and *in vivo* were used to estimate the tissue composition of samples taken from the following culture systems: post-perfused liver isolate; 2D collagen gel sandwich; 3D spheroid aggregates; and MilliF bioreactor.

Standard curve development confirmed that 18s primers are efficiently amplified during PCR in all hepatic phenotypes. Additionally, though each cell type was shown to have varying amounts of total RNA, the amount of 18s rRNA relative to the total RNA was found to be constant (C_{18s}/C_{RNA}=constant). Thus, 18s rRNA is consistently maintained in all cell types and can be used both as a housekeeping gene for normalization of data and to eventually correlate to the total number of each cell type present in culture. Presently, there exist inefficiencies in RNA isolation, reverse transcription of RNA to cDNA, and purity of cell isolate standards that perturb such calculations on the present data.

Primers were unable to be designed for CD80, GFAP, and VE-Cadherin. Three iterations of primer sequence failed to eliminate the presence of multiple PCR products. Standard curves were successfully developed for albumin, transferrin, desmin, vimentin, Flk-1, Flt-1, HARE, CD68, and IL-10Ra primers. These standard curves demonstrate that a two-fold increase in cDNA concentration resulted in a one-fold increase in C(t), and thus, that these primers are highly efficient at amplifying cDNA during PCR. The magnitude of gene expression levels varied significantly between selected target genes.

Hepatocyte and stellate targets' gene expression were found to be statistically specific to their respective phenotype. Cross-contamination in endothelial and Kupffer cell standards prevented direct validation of target gene specificity, though all targets were statistically specific from stellate cells and hepatocytes. However, cross-reactivity studies show remarkable correlation of gene expression when corrected for the cross-contamination. Thus, our experiments showed no significant evidence to disprove previous reports of EC and KC target specificity made on pure cell populations.

There were significant fluctuations in many of the gene expression levels between cell isolate fraction and *in vivo*. Albumin and transferrin showed particularly extreme instability and, contrary to previous reports, are incongruous as hepatocyte 'house-keeping' genes to quantify cell number (Tollet-Engell et al. 2001). Only vimentin, CD68, Flt-1, and Flk-1 exhibited stable and high levels of gene expression in the post-perfused cell isolate and *in vivo*. These genes represented each NPC phenotype and when combined with 18s rRNA were capable of replicating reported *in vivo* liver composition within an acceptable range of biological deviation. Thus, we have defined a gene set whose expression levels are consistent with *in vivo* tissue as well as post-perfused isolated cell fractions.

Application of this gene set to liver isolate confirmed that perfusion flow rate inversely impacts the relative yield of sinusoidal NPC's. This result agrees with the findings of nuclear staining and proves that there exists a significant inverse correlation between perfusion flow rate and NPC yield. Further application of the gene set to the

NPC isolate determined the composition of non-parenchymal cells being added to co-culture. NPC isolate composition is the first component in completing a process mass balance, calculating cellular incorporation efficiencies, and detecting incorporation limiting steps in the process.

The gene expression stability of the final gene set has not yet been validated in *in vitro* culture, so no definitive quantitative conclusions can be drawn. However, these markers were used to detect the presence of cell types and to loosely speculate on trends in cell growth and NPC incorporation. Application of these methods to collagen gel sandwich cultures showed a decrease in total cell number present, but definite incorporation of all NPC types into culture. There was a significant temporal increase in the relative expression of stellate and Kupffer cell markers, and a stable maintenance of endothelial cell markers. Further, application of the gene set to co-culture spheroids with various physiological NPC ratios showed that Kupffer and endothelial cell markers are not expressed, insinuating that they do not incorporate well in spinning cultures. However, stellate cell markers were expressed in high levels and maintained relative expression levels after the seeding of the spheroids into the milliF bioreactor, insinuating the retention of relative tissue composition, independent of adherence to the reactor scaffold and exposure to perfused flow.

CHAPTER 5: CONCLUSIONS AND RECOMMENDATIONS

Non-parenchymal cells (NPC's) are considered an essential component of diagnostic long term *in vitro* liver culture systems (Allen et al. 2002). These cells play important roles in creation and maintenance of the hepatic microenvironment through a complex system of cell-matrix interactions, cell-cell interactions, and soluble signaling mechanisms. *In vivo*, each cell phenotype provides different environmental cues necessary to preserve tissue homeostasis. Therefore, it is prudent to develop a system that addresses these mechanisms of intercellular communication. Presently, a wide variety of co-culture systems are being developed and validated by very disparate diagnostic metrics. These culture systems each address different operating aspects of cell culture and are very difficult to compare due to uncertainties regarding interpretation of results. Few research groups have systematically built culture systems to address composition or even allow for qualitative observation of tissue architecture. Since each NPC is responsible for a particular subset of organoid function, determination of tissue composition is necessary to draw meaningful correlation between operational system design parameters and their influence on the replication of *in vivo* tissue function.

The objective of this thesis was to identify, develop, and implement a technique to quantify the relative tissue composition of non-parenchymal cells co-cultured in various *in vitro* systems. The development of such a quantitative method allows a mass balance analysis to be performed on different culture systems. This analysis provides valuable insight into the capabilities and limitations of existing *in vitro* co-culture systems.

Gene expression has been exploited as a means to determine tissue composition. A set of target genes was identified based on their documented potential to be cell-type specific, highly expressed, and stable across a range of culture environments and their primers carefully designed. Expression levels were determined using real-time RT-PCR. This technique was selected from several candidates because it is highly quantitative; high throughput; easily implemented, time, labor and economically feasible assay capable of simultaneously generating data on tissue composition and tissue function.

The first step in the co-culture of non-parenchymal cells is accurate estimation of cell number for input into *in vitro* systems. We have developed a new fluorescent nuclear staining protocol for cell counting that circumvents the resolution and accuracy limitations that have led to overestimation by current techniques. This protocol was capable of estimating NPC yields consistent with theoretical calculations of perfusion NPC yield, and further demonstrated the correlation inverse between perfusion flow rate and cell yield and viability.

Cell purification protocols were established to acquire cell populations adequate for real-time RT-PCR standard curve development. Hepatocytes were purified to >99% using an isotonic Percoll® density gradient. Stellate cell isolates were derived from the HSC-T6 stellate cell line and, as such, are 100% pure. Kupffer and endothelial cells were separated via a two-step Percoll® density gradient followed by selective adhesion to

substrate. Endothelial cells were able to be isolated to ~87% purity exploiting preferential adhesion to collagen (t = 2.5 hrs). Kupffer cells were separated to ~ 67% purity utilizing selective adhesion for 0.5 hrs to non tissue culture treated plastic. Impurities in KC and EC isolates are a result of inefficiencies in the selectivity of respective substrate for the target cell type, and were unable to be eradicated.

Standard curve development confirmed that 18s primers are efficiently amplified during PCR in all hepatic phenotypes. Additionally, though each cell type was shown to have varying amounts of total RNA, the amount of 18s rRNA relative to the total RNA was found to be constant (C_{18s}/C_{RNA}=constant). Thus, 18s rRNA is consistently maintained in all cell types and can be used both as a housekeeping gene for normalization of data and to eventually correlate to the total number of each cell type present in culture. Presently, there exist inefficiencies in RNA isolation, reverse transcription of RNA to cDNA, and purity of cell isolate standards that perturb such calculations on the present data.

Primers were unable to be designed for CD80, GFAP, and VE-Cadherin. Three iterations of primer sequence failed to eliminate the presence of multiple PCR products. Standard curves were successfully developed for albumin, transferrin, desmin, vimentin, Flk-1, Flt-1, HARE, CD68, and IL-10Ra primers. These standard curves demonstrate that a two-fold increase in cDNA concentration resulted in a one-fold increase in C(t), and thus, that these primers are highly efficient at amplifying cDNA during PCR. The magnitude of gene expression levels varied significantly between selected target genes.

Hepatocyte and stellate targets' gene expression were found to be statistically specific to their respective phenotype. Cross-contamination in endothelial and Kupffer cell standards prevented direct validation of target gene specificity, though all targets were statistically specific from stellate cells and hepatocytes. However, cross-reactivity studies show remarkable correlation of gene expression when corrected for the cross-contamination. Thus, our experiments showed no significant evidence to disprove previous reports of EC and KC target specificity made on pure cell populations.

There were significant fluctuations in many of the gene expression levels between cell isolate fraction and *in vivo*. Albumin and transferrin showed particularly extreme instability and, contrary to previous reports, are incongruous as hepatocyte 'house-keeping' genes to quantify cell number (Tollet-Engell et al. 2001). Only vimentin, CD68, Flt-1, and Flk-1 exhibited stable and high levels of gene expression in the post-perfused cell isolate and *in vivo*. These genes represented each NPC phenotype and when combined with 18s rRNA were capable of replicating reported *in vivo* liver composition within an acceptable range of biological deviation. Thus, we have defined a gene set whose expression levels are consistent with *in vivo* tissue as well as post-perfused isolated cell fractions.

Application of this gene set to liver isolate confirmed that perfusion flow rate inversely impacts the relative yield of sinusoidal NPC's. This result agrees with the findings of nuclear staining and proves that there exists a significant inverse correlation

between perfusion flow rate and NPC yield. Further application of the gene set to the NPC isolate determined the composition of non-parenchymal cells being added to co-culture. NPC isolate composition is the first component in completing a process mass balance, calculating cellular incorporation efficiencies, and detecting incorporation limiting steps in the process.

The gene expression stability of the final gene set has not yet been validated in *in vitro* culture, so no definitive quantitative conclusions can be drawn. However, these markers were used to detect the presence of cell types and to loosely speculate on trends in cell growth and NPC incorporation. Application of these methods to collagen gel sandwich cultures showed a decrease in total cell number present, but definite incorporation of all NPC types into culture. There was a significant temporal increase in the relative expression of stellate and Kupffer cell markers, and a stable maintenance of endothelial cell markers. Further, application of the gene set to co-culture spheroids with various physiological NPC ratios showed that Kupffer and endothelial cell markers are not expressed, insinuating that they do not incorporate well in spinning cultures. However, stellate cell markers were expressed in high levels and maintained relative expression levels after the seeding of the spheroids into the milliF bioreactor, insinuating the retention of relative tissue composition, independent of adherence to the reactor scaffold and exposure to perfused flow.

Herein, **I have developed a high throughput quantitative methodology that can be used to attain <u>both</u> tissue composition and tissue function data**. This method has been validated and applied to characterize material balance from the native in vivo liver, to the cell isolation process, and through the input of non-parenchymal cells to *in vitro* co-culture. In the course of this development, protocols have been developed to accurately count and isolate an enriched fraction of primary NPC's. This work enables the systematic addition of a characterized non-parenchymal population to co-culture, and permits analysis of the limiting steps to their incorporation in our process.

Further investigation is recommended to optimize limitations of the current protocol. The defined gene sets' expression levels and temporal stability must be validated in controlled experiments in each of the applied culture systems and culture environments (media formulation, O_2 concentration, etc...) to ensure that no significant fluctuations in expression exist that will corrupt results. The completion of these experiments will complete the material balance and allow more meaningfully modeling to be performed on correlation between system design parameters and tissue function.

Additionally, the precision and accuracy of this methodology would be improved by the development better EC, KC, and primary stellate cell isolation procedures. Well-defined, pure cell populations will allow the determination of variables necessary to calculate species incorporation yield in addition to composition and further demonstrate the quality of current standard curves. Moreover, further characterization and optimization is needed to define a protocol that reverse transcribes RNA into cDNA at constant reaction efficiencies.

Finally, more genes need to be identified and investigated that meet the defined criteria so that averages of component results can be used to minimize potential variance in expression levels (i.e. hepatocyte CK-18, KC CD86, etc).

REFERENCES

Allen, J. W. and S. N. Bhatia (2002). "Engineering liver therapies for the future." Tissue Engineering **8**(5): 725-737.

Allen, J. W. and S. N. Bhatia (2002). "Improving the next generation of bioartificial liver devices." Seminars in Cell & Developmental Biology **13**(6): 447-454.

Allen, J. W., T. Hassanein, et al. (2001). "Advances in bioartificial liver devices." Hepatology **34**(3): 447-455.

Angst, B. D., C. Marcozzi, et al. (2001). "The cadherin superfamily: diversity in form and function." Journal of Cell Science **114**(4): 629-641.

Arias, I. M., J. L. Boyer, et al. (2001). The Liver: Biology and Pathobiology. New York, Lippincott.

Bader, A., E. Knop, et al. (1996). "3-D coculture of hepatic sinusoidal cells with primary hepatocytes - Design of an organotypical model." Experimental Cell Research **226**(1): 223-233.

Barret, C. e. a. (2003). "Microarrays: the use of oligonucleotides and cDNA for the analysis of gene expression." Drug Discovery Today **8**: 134-141.

Bhadriraju, K. and C. S. Chen (2002). "Engineering cellular microenvironments to cell-based drug testing improve." Drug Discovery Today **7**(11): 612-620.

Bhatia, S. N., U. Balis, et al. (1998). "Development of microfabricated hepatocyte co-cultures." Abstracts of Papers of the American Chemical Society **216**: U289-U289.

Bhatia, S. N., U. J. Balis, et al. (1998). "Microfabrication of hepatocyte/fibroblast co-cultures: Role of homotypic cell interactions." Biotechnology Progress **14**(3): 378-387.

Bhatia, S. N., U. J. Balis, et al. (1999). "Effect of cell-cell interactions in preservation of cellular phenotype: cocultivation of hepatocytes and nonparenchymal cells." Faseb Journal **13**(14): 1883-1900.

Block, G. D., J. Locker, et al. (1996). "Population expansion, clonal growth, and specific differentiation patterns in primary cultures of hepatocytes induced by HGF/SF, EGF and TGF alpha in a chemically defined (HGM) medium." Journal of Cell Biology **132**(6): 1133-1149.

Block, G. D., J. Locker, et al. (1996). "Population expansion, clonal growth, and specific differentiation patterns in primary cultures of hepatocytes induced by

HGF/SF, EGF and TGF alpha in a chemically defined (HGM) medium." Journal of Cell Biology **132**(6): 1133-1149.

Braet, F., P. H. H. Bomans, et al. (2003). "The observation of intact hepatic endothelial cells by cryo-electron microscopy." Journal of Microscopy-Oxford **212**: 175-185.

Browm, J. C. and R. Timpl (1995). "The Collagen Superfamily." International Archives of Allergy and Immunology **107**(4): 484-490.

Bustin, S. A. (2000). "Absolute quantification of mRNA using real-time reverse transcriptional polymerase chain reaction assays." Journal of Molecular Endocrinology(25): 169-193.

Cantz, T., D. M. Zuckerman, et al. (2003). "Quantitative gene expression analysis reveals transition of fetal liver progenitor cells to mature hepatocytes after transplantation in uPA/RAG-2 mice." American Journal of Pathology **162**(1): 37-45.

Churchill, G. A. (2002). "Fundamentals of experimental design for cDNA microarrays." Nature Genetics **32**: 490-495.

Crispe, I. N. (2003). "Hepatic T cells and liver tolerance." Nature Reviews Immunology **3**(1): 51-62.

Deleeuw, A. M., S. P. Mccarthy, et al. (1984). "Purified Rat-Liver Fat-Storing Cells in Culture Divide and Contain Collagen." Hepatology **4**(3): 392-403.

Duff, B., J. A. Weigel, et al. (2002). "Endothelium in hepatic cavernous hemangiomas does not express the hyaluronan receptor for endocytosis." Human Pathology **33**(3): 265-269.

Dunn, J. C. Y., R. G. Tompkins, et al. (1992). "Hepatocytes in Collagen Sandwich - Evidence for Transcriptional and Translational Regulation." Journal of Cell Biology **116**(4): 1043-1053.

Fadok, V. A., D. L. Bratton, et al. (2001). "Phagocyte receptors for apoptotic cells: recognition, uptake, and consequences." Journal of Clinical Investigation **108**(7): 957-962.

Fahrig, R., M. Rupp, et al. (1998). "Use of primary rat and human hepatocyte sandwich cultures for activation of indirect carcinogens: Monitoring of DNA strand breaks and gene mutations in co-cultured cells." Toxicology in Vitro **12**(4): 431-444.

Ferrara, N. (1999). "Molecular and biological properties of vascular endothelial growth factor." Journal of Molecular Medicine-Jmm **77**(7): 527-543.

Fiegel, H. C., M. V. Lioznov, et al. (2003). "Liver-specific gene expression in cultured human hematopoietic stem cells." Stem Cells **21**(1): 98-104.

Fiegel, H. C., J. J. H. Park, et al. (2003). "Characterization of cell types during rat liver development." Hepatology **37**(1): 148-154.

Finnegan, M. C. M., J. R. Goepel, et al. (1993). "Investigation of the Expression of Housekeeping Genes in Non-Hodgkins-Lymphoma." Leukemia & Lymphoma **10**(4-5): 387-393.

Friedman, S. L. and F. J. Roll (1987). "Isolation and Culture of Hepatic Lipocytes, Kupffer Cells, and Sinusoidal Endothelial-Cells by Density Gradient Centrifugation with Stractan." Analytical Biochemistry **161**(1): 207-218.

Gabig, M. (2001). "An introduction to DNA chips: Principles, Technology, Applications, and Analysis." Acta Biochimica Polonic **48**: 615-622.

Gard, A. L., F. P. White, et al. (1985). "Extra-Neural Glial Fibrillary Acidic Protein (Gfap) Immunoreactivity in Perisinusoidal Stellate Cells of Rat-Liver." Journal of Neuroimmunology **8**(4-6): 359-375.

Gavin, T. P. and P. D. Wagner (2002). "Attenuation of the exercise-induced increase in skeletal muscle Flt-1 mRNA by nitric oxide synthase inhibition." Acta Physiologica Scandinavica **175**(3): 201-209.

Gebhardt, R. (1992). "Cell-Cell Interactions - Clues to Hepatocyte Heterogeneity and Beyond." Hepatology **16**(3): 843-845.

Gebhardt, R. (1992). "Metabolic Zonation of the Liver - Regulation and Implications for Liver-Function." Pharmacology & Therapeutics **53**(3): 275-354.

Geerts, A. (2001). "History, heterogeneity, developmental biology, and functions of quiescent hepatic stellate cells." Seminars in Liver Disease **21**(3): 311-335.

Gerlach, J. C. (1997). "Long-term liver cell cultures in bioreactors and possible application for liver support." Cell Biology and Toxicology **13**(4-5): 349-355.

Ginzinger, D. G. (2002). "Gene quantification using real-time quantitative PCR: An emerging technology hits the mainstream." Experimental Hematology **30**(6): 503-512.

Giulietti, A., L. Overbergh, et al. (2001). "An overview of real-time quantitative PCR: Applications to quantify cytokine gene expression." Methods **25**(4): 386-401.

Ho, A. S. Y., Y. Liu, et al. (1993). "A Receptor for Interleukin-10 Is Related to Interferon Receptors." Proceedings of the National Academy of Sciences of the United States of America **90**(23): 11267-11271.

Ho, M., E. Yang, et al. (2003). "Identification of endothelial cell genes by combined database mining and microarray analysis." Physiological Genomics **13**(3): 249-262.

Holmstrom, P., V. Dzikaite, et al. (2003). "Structure and liver cell expression pattern of the HFE gene in the rat." Journal of Hepatology **39**(3): 308-314.

Idzerda, R. L., R. R. Behringer, et al. (1989). "Expression from the Transferrin Gene Promoter in Transgenic Mice." Molecular and Cellular Biology **9**(11): 5154-5162.

Idzerda, R. L., H. Huebers, et al. (1986). "Rat Transferrin Gene-Expression - Tissue-Specific Regulation by Iron-Deficiency." Proceedings of the National Academy of Sciences of the United States of America **83**(11): 3723-3727.

Ikeda, D., S. Wada, et al. (1999). "Carnosine stimulates vimentin expression in cultured rat fibroblasts." Cell Structure and Function **24**(2): 79-87.

Jasmund, I., A. Langsch, et al. (2002). "Cultivation of primary porcine hepatocytes in an OXY-HFB for use as a bioartificial liver device." Biotechnology Progress **18**(4): 839-846.

Jezequel, A. M., R. Mancini, et al. (1989). "Dimethylnitrosamine-Induced Cirrhosis - Evidence for an Immunological Mechanism." Journal of Hepatology **8**(1): 42-52.

Junquiera, L. C., J. Carneiro, et al. (1999). Basic Histology. Stamford, CT, Appleton and Lange.

Kim, Y., V. Ratziu, et al. (1998). "Transcriptional activation of transforming growth factor beta 1 and its receptors by the Kruppel-like factor Zf9/core promoter-binding protein and Sp1 - Potential mechanisms for autocrine fibrogenesis in response to injury." Journal of Biological Chemistry **273**(50): 33750-33758.

Klassen, C. D. (2001). Casarett and Doul's Toxicology: The Basic Science of Poisons. NY, McGraw-Hill Medical Publishing Division.

Knittel, T., M. Mehde, et al. (1999). "Expression patterns of matrix metalloproteinases and their inhibitors in parenchymal and non-parenchymal cells of rat liver: regulation by TNF-alpha and TGF-beta 1." Journal of Hepatology **30**(1): 48-60.

Knolle, P. A., A. Uhrig, et al. (1998). "Interleukin-10 expression is autoregulated at the transcriptional level in human and murine Kupffer cells." Hepatology **27**(1): 93-99.

Koide, N., K. Sakaguchi, et al. (1990). "Formation of Multicellular Spheroids Composed of Adult-Rat Hepatocytes in Dishes with Positively Charged Surfaces and under Other Nonadherent Environments." Experimental Cell Research **186**(2): 227-235.

Kondapalli, J., A. S. Flozak, et al. (2004). "Laminar shear stress differentially modulates gene expression of p120 catenin, Kaiso transcription factor, and vascular endothelial cadherin in human coronary artery endothelial cells." Journal of Biological Chemistry **279**(12): 11417-11424.

Kraizer, Y., N. Mawasi, et al. (2001). "Vascular endothelial growth factor and angiopoietin in liver regeneration." Biochemical and Biophysical Research Communications **287**(1): 209-215.

Kuckuck, F. W., B. S. Edwards, et al. (2001). "High throughput flow cytometry." Cytometry **44**(1): 83-90.

Kulig, K. and J. P. Vacanti (2004). "Hepatic tissue engineering." Transplant Immunology.

LeCluyse, E. L., P. L. Bullock, et al. (1996). "Strategies for restoration and maintenance of normal hepatic structure and function in long-term cultures of rat hepatocytes." Advanced Drug Delivery Reviews **22**(1-2): 133-186.

LeCluyse, E. L. and S. C. Sutton (1997). "In vitro models for selection of development candidates. Permeability studies to define mechanisms of absorption enhancement." Advanced Drug Delivery Reviews **23**(1-3): 163-183.

Lee, M., J. Kwon, et al. (2003). "cDNA microarray gene expression profiling of hydroxyurea, paclitaxel, and p-anisidine, genotoxic compounds with differing tumorigenicity results." Environmental and Molecular Mutagenesis **42**(2): 91-97.

Lee, S. J. and T. D. Boyer (1993). "The Effect of Hepatic Regeneration on the Expression of the Glutathione S-Transferases." Biochemical Journal **293**: 137-142.

Li, A. C., F. R. B. Guidez, et al. (1998). "The macrosialin promoter directs high levels of transcriptional activity in macrophages dependent on combinatorial interactions between PU.1 and c-Jun." Journal of Biological Chemistry **273**(9): 5389-5399.

Li, D. and S. L. Friedman (1999). "Liver fibrogenesis and the role of hepatic stellate cells: New insights and prospects for therapy." Journal of Gastroenterology and Hepatology **14**(7): 618-633.

Lim, S., G. Caramori, et al. (2004). "Differential expression of IL-10 receptor by epithelial cells and alveolar macrophages." Allergy **59**(5): 505-513.

Liu, W. H. and D. A. Saint (2002). "Validation of a quantitative method for real time PCR kinetics." Biochemical and Biophysical Research Communications **294**(2): 347-353.

Malik, R., C. Selden, et al. (2002). "The role of non-parenchymal cells in liver growth." Seminars in Cell & Developmental Biology **13**(6): 425-431.

Manhani, A. R., R. Manhani, et al. (2001). "CK-19 expression by RT-PCR in the peripheral blood of breast cancer patients correlates with response to chemotherapy." Breast Cancer Res Treat **66**(3): 249-54.

McCuskey, R. (1994). The Hepatic Microenvironment. The Liver: Biology and Pathobiology: 1089-1106.

Michalopoulos, G. K., W. C. Bowen, et al. (2001). "Histological organization in hepatocyte organoid cultures." American Journal of Pathology **159**(5): 1877-1887.

Michalopoulos, G. K. and M. C. DeFrances (1997). "Liver regeneration." Science **276**(5309): 60-66.

Mochida, S., K. Ishikawa, et al. (1996). "Increased expressions of vascular endothelial growth factor and its receptors, flt-1 and KDR/flk-1, in regenerating rat liver." Biochemical and Biophysical Research Communications **226**(1): 176-179.

Morris, D. L. and J. C. Davila (1996). "Analysis of rat cytochrome P450 isoenzyme expression using semi-quantitative reverse transcriptase-polymerase chain reaction (RT-PCR)." Biochemical Pharmacology **52**(5): 781-792.

Murray, H. W., C. M. Lu, et al. (2002). "Interleukin-10 (IL-10) in experimental visceral leishmaniasis and IL-10 receptor blockade as immunotherapy." Infection and Immunity **70**(11): 6284-6293.

Neubauer, K., T. Knittel, et al. (1996). "Glial fibrillary acidic protein - A cell type specific marker for Ito cells in vivo and in vitro." Journal of Hepatology **24**(6): 719-730.

Nitsch, R., E. E. Pohl, et al. (2004). "Direct impact of T cells on neurons revealed by two-photon microscopy in living brain tissue." Journal of Neuroscience **24**(10): 2458-2464.

Ochoa, E. R. and J. P. Vacanti (2002). "An overview of the pathology and approaches to tissue engineering." Lymphatic Continuum: Lymphatic Biology and Disease **979**: 10-26.

Palka, J., E. Banikowski, et al. (2000). "An accumulation of IGF-I and IGF-binding proteins in human umbilical cord." Molecular and Cellular Biochemistry **206**(1-2): 133-139.

Pierce M, C. W., M Rebentisch, M Endo, M Stump, A Kamb (2003). "A high-throughput, homogeneous microplate assay for agents that kill mammalian tissue culture cells." J Biomol Screen(8): 283-291.

Ponka, P. (1997). "Tissue-specific regulation of iron metabolism and heme synthesis: Distinct control mechanisms in erythroid cells." Blood **89**(1): 1-25.

Powers, M. J., K. Domansky, et al. (2002). "A microfabricated array bioreactor for perfused 3D liver culture." Biotechnology and Bioengineering **78**(3): 257-269.

Powers, M. J. and L. G. Griffith (1998). "Adhesion-guided in vitro morphogenesis in pure and mixed cell cultures." Microscopy Research and Technique **43**(5): 379-384.

Powers, M. J., D. M. Janigian, et al. (2002). "Functional behavior of primary rat liver cells in a three-dimensional perfused microarray bioreactor." Tissue Engineering **8**(3): 499-513.

Powers, M. J., S. S. Kim, et al. (1997). "Adhesion phenomena in the organization and morphogenesis of liver cells." Abstracts of Papers of the American Chemical Society **213**: 335-Coll.

Powers, M. J., R. E. Rodriguez, et al. (1997). "Cell-substratum adhesion strength as a determinant of hepatocyte aggregate morphology." Biotechnology and Bioengineering **53**(4): 415-426.

Redig, A. (2002). "Microarray: A Technique Review." Journal of Young Investigators **5**: 123-245.

Sato, M., S. Suzuki, et al. (2003). "Hepatic stellate cells: Unique characteristics in cell biology and phenotype." Cell Structure and Function **28**(2): 105-112.

Schena, M., R. A. Heller, et al. (1998). "Microarrays: biotechnology's discovery platform for functional genomics." Trends in Biotechnology **16**(7): 301-306.

Schmid, H., C. D. Cohen, et al. (2003). "Validation of endogenous controls for gene expression analysis in microdissected human renal biopsies." Kidney International **64**(1): 356-360.

Seglen, P. (1976). "Preparation of isolated rat liver cells." Meth Cell Biol(13): 29-83.

Selvey, S., E. W. Thompson, et al. (2001). "beta-actin - an unsuitable internal control for RT-PCR." Molecular and Cellular Probes **15**(5): 307-311.

Shackel, N. A., M. D. Gorrell, et al. (2002). "Gene array analysis and the liver." Hepatology **36**(6): 1313-1325.

Shankey, T. V., P. S. Rabinovitch, et al. (1993). "Guidelines for the Implementation of Clinical DNA Cytometry." Breast Cancer Research and Treatment **28**(1): 61-68.

Shi, M. Q., W. L. Pan, et al. (2003). "Experimental African trypanosomiasis: IFN-gamma mediates early mortality." European Journal of Immunology **33**(1): 108-118.

Shimizu, H., M. Miyazaki, et al. (2001). "Vascular endothelial growth factor secreted by replicating hepatocytes induces sinusoidal endothelial cell proliferation during regeneration after partial hepatectomy in rats." Journal of Hepatology **34**(5): 683-689.

Slonim, D. K. (2002). "From patterns to pathways: gene expression data analysis comes of age." Nature Genetics **32**: 502-508.

Smedsrod, B., P. J. Debleser, et al. (1994). "Cell Biology of Liver Endothelial and Kupffer Cells." Gut **35**(11): 1509-1516.

Smedsrod, B. and H. Pertoft (1985). "Preparation of pure hepatocytes and reticuloendothelial cells in high yield from a single rat liver by means of Percoll centrifugation and selective adherence." J Leukoc Biol **38**(2): 213-30.

Strain, A. J. and H. A. Crosby (2000). "Hepatic stem cells." Gut **46**(6): 743-745.

Sun, Z. L., T. Wada, et al. (2003). "Hepatic allograft-derived Kupffer cells regulate T cell response in rats." Liver Transplantation **9**(5): 489-497.

Takeichi, M., H. Inuzuka, et al. (1990). "Cadherin-Mediated Cell Cell-Adhesion and Neurogenesis." Neuroscience Research: S92-S96.

Telo, P., F. Breviario, et al. (1998). "Identification of a novel cadherin (vascular endothelial cadherin-2) located at intercellular junctions in endothelial cells." Journal of Biological Chemistry **273**(28): 17565-17572.

Tollet-Egnell, P., A. Flores-Morales, et al. (2001). "Gene expression profile of the aging process in rat liver: Normalizing effects of growth hormone replacement." Molecular Endocrinology **15**(2): 308-318.

Tzanakakis, E. S., D. J. Hess, et al. (2000). "Extracorporeal tissue engineered liver-assist devices." Annual Review of Biomedical Engineering **2**: 607-632.

Uyama, N., N. Kawada, et al. (2000). "The interaction between hepatocytes and stellate cells on individual cell proliferation and differentiation." Hepatology **32**(4): 465a-465a.

Uyama, N., N. Kawada, et al. (2001). "Regulation of the proliferation of cultured rat hepatocytes by stellate cells." Hepatology **34**(4): 260a-260a.

Vacanti, J., W. Cheung, et al. (2003). "Hepatocyte and endothelial cell survival in a tissue engineered human liver device with its own vascular network." Journal of the American College of Surgeons **197**(3): S86-S86.

Valatas, V., C. Xidakis, et al. (2003). "Isolation of rat Kupffer cells: a combined methodology for highly purified primary cultures." Cell Biology International **27**(1): 67-73.

Valerius, A. T., L. T. Patterson, et al. (2002). "Microarray analysis of novel cell lines representing two stages of metanephric mesenchyme differentiation." Mechanisms of Development **110**(1-2): 151-164.

Vessey, C. J. and P. D. L. M. Hall (2001). "Hepatic stem cells: A review." Pathology **33**(2): 130-141.

Vidal-Vanaclocha, F. (1997). The Hepatic Sinusoidal Endothelium: Functional Aspects and Phenotypic Hetergeneity. Functional Heterogeneity of Liver Tissue. New Yorl, R.G. Landes Company: 71-108.

Vogel, S., R. Piantedosi, et al. (2000). "An immortalized rat liver stellate cell line (HSC-T6): a new cell model for the study of retinoid metabolism in vitro." Journal of Lipid Research **41**(6): 882-893.

Vouret-Craviari, V., D. Grall, et al. (1999). "Effects of cytotoxic necrotizing factor 1 and lethal toxin on actin cytoskeleton and VE-cadherin localization in human endothelial cell monolayers." Infection and Immunity **67**(6): 3002-3008.

Walker, N. J. (2001). "Real-time and quantitative PCR: Applications to mechanism-based toxicology." Journal of Biochemical and Molecular Toxicology **15**(3): 121-127.

Weigel, J. A., R. C. Raymond, et al. (2002). "The hyaluronan receptor for endocytosis (HARE) is not CD44 or CD54 (ICAM-1)." Biochemical and Biophysical Research Communications **294**(4): 918-922.

Weigel, P. H. and J. H. N. Yik (2002). "Glycans as endocytosis signals: the cases of the asialoglycoprotein and hyaluronan/chondroitin sulfate receptors." Biochimica Et Biophysica Acta-General Subjects **1572**(2-3): 341-363.

Wisse, E., F. Braet, et al. (1996). "Structure and function of sinusoidal lining cells in the liver." Toxicologic Pathology **24**(1): 100-111.

Wu, F. J., J. R. Friend, et al. (1996). "Efficient assembly of rat hepatocyte spheroids for tissue engineering applications." Biotechnology and Bioengineering **50**(4): 404-415.

Yagi, K., N. Sumiyoshi, et al. (1995). "In vitro maintenance of liver function in hierarchical co-culture of hepatocytes and non-parenchymal liver cells." Journal of Fermentation and Bioengineering **80**(6): 575-579.

Yamada, K., M. Kamihira, et al. (2001). "Self-organization of liver constitutive cells mediated by artificial matrix and improvement of liver functions in long-term culture." Biochemical Engineering Journal **8**(2): 135-143.

Yamane, A., L. Seetharam, et al. (1994). "A New Communication-System between Hepatocytes and Sinusoidal Endothelial-Cells in Liver through Vascular Endothelial Growth-Factor and Flt Tyrosine Kinase Receptor Family (Flt-1 and Kdr/Flk-1)." Oncogene **9**(9): 2683-2690.

Yang, Y. and e. t. al. (2002). "Design Issues for cDNA Microarray Experiments." Nature Genetics **3**: 579-588.

Yannariellobrown, J., C. T. Mcgary, et al. (1992). "The Endocytic Hyaluronan Receptor in Rat-Liver Sinusoidal Endothelial-Cells Is Ca+2-Independent and Distinct from a Ca+2-Dependent Hyaluronan Binding-Activity." Journal of Cellular Biochemistry **48**(1): 73-80.

Yap, A. S., W. M. Brieher, et al. (1997). "Molecular determinants of cadherin adhesive function." Molecular Biology of the Cell **8**: 1079-1079.

Yokoi, Y., T. Namihisa, et al. (1984). "Immunocytochemical Detection of Desmin in Fat-Storing Cells (Ito-Cells)." Hepatology **4**(4): 709-714.

Zhang, A. S., S. G. Xiong, et al. (2004). "Localization of iron metabolism-related mRNAs in rat liver indicate that HFE is expressed predominantly in hepatocytes." Blood **103**(4): 1509-1514.

Zhou, B., J. A. Weigel, et al. (2002). "Molecular cloning and functional expression of the rat 175-kDa hyaluronan receptor for endocytosis." Molecular Biology of the Cell **13**(8): 2853-2868.

APPENDICES

Appendix 1: Primer Standard Curves

A.

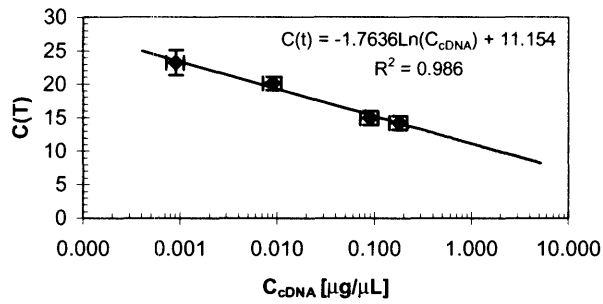

B.

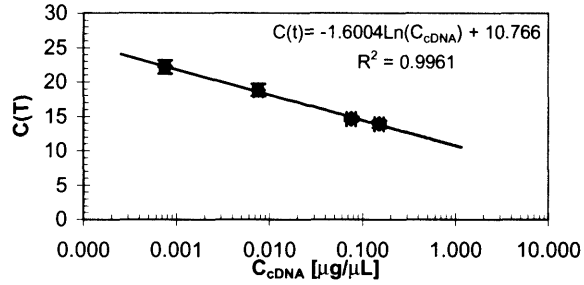

C.

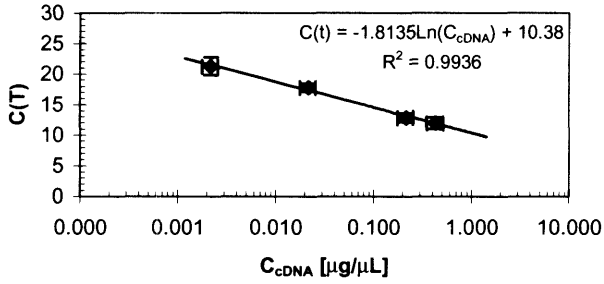

D.

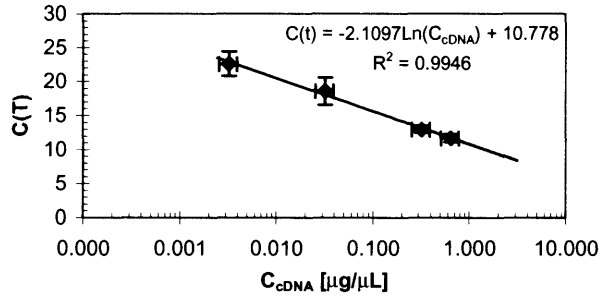

Albumin

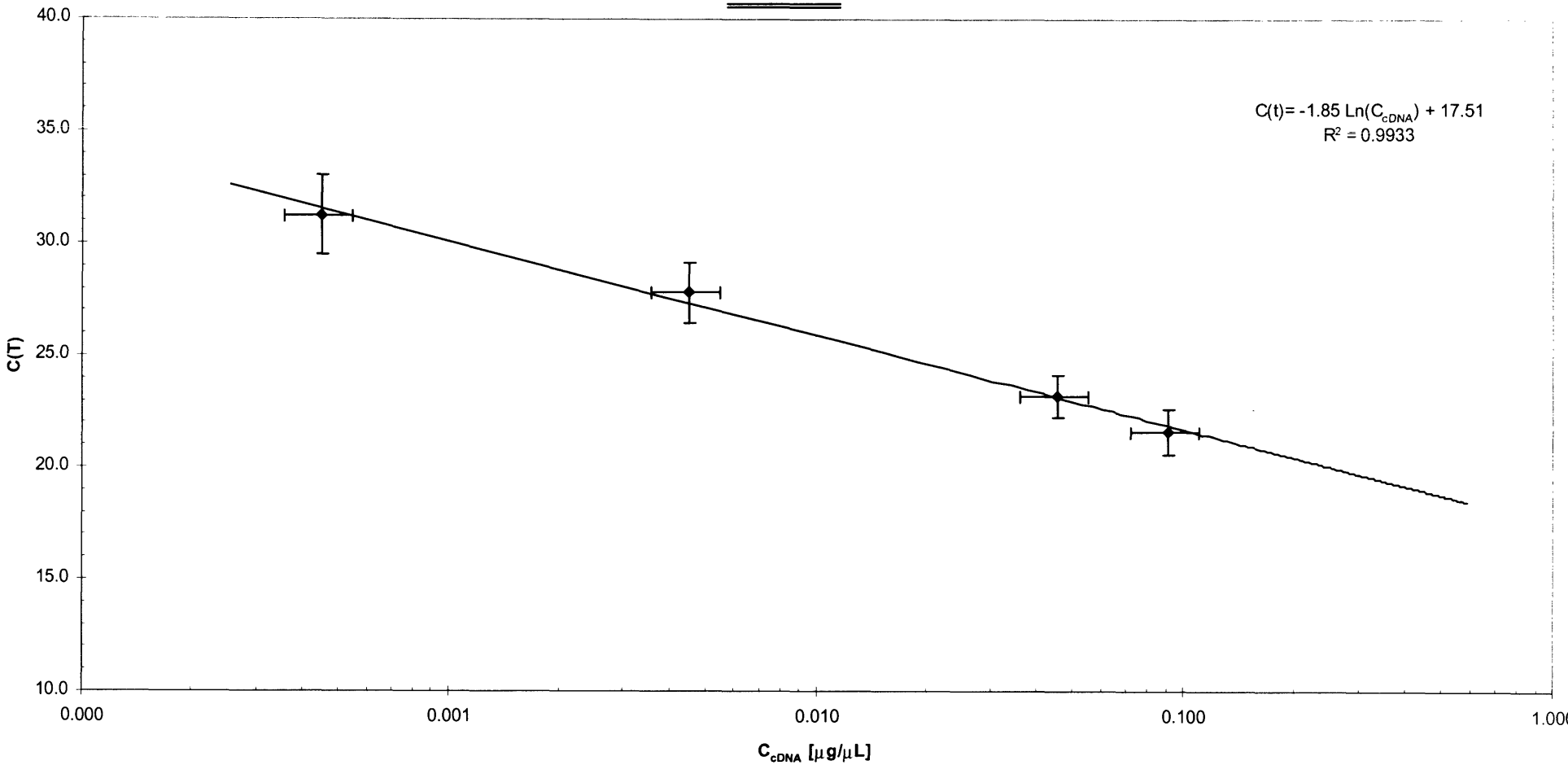
C(t)= -1.85 Ln(C_cDNA) + 17.51
R² = 0.9933
C(T)
40.0
35.0
30.0
25.0
20.0
15.0
10.0
0.000
0.001
0.010
0.100
1.000
C_cDNA [µg/µL]

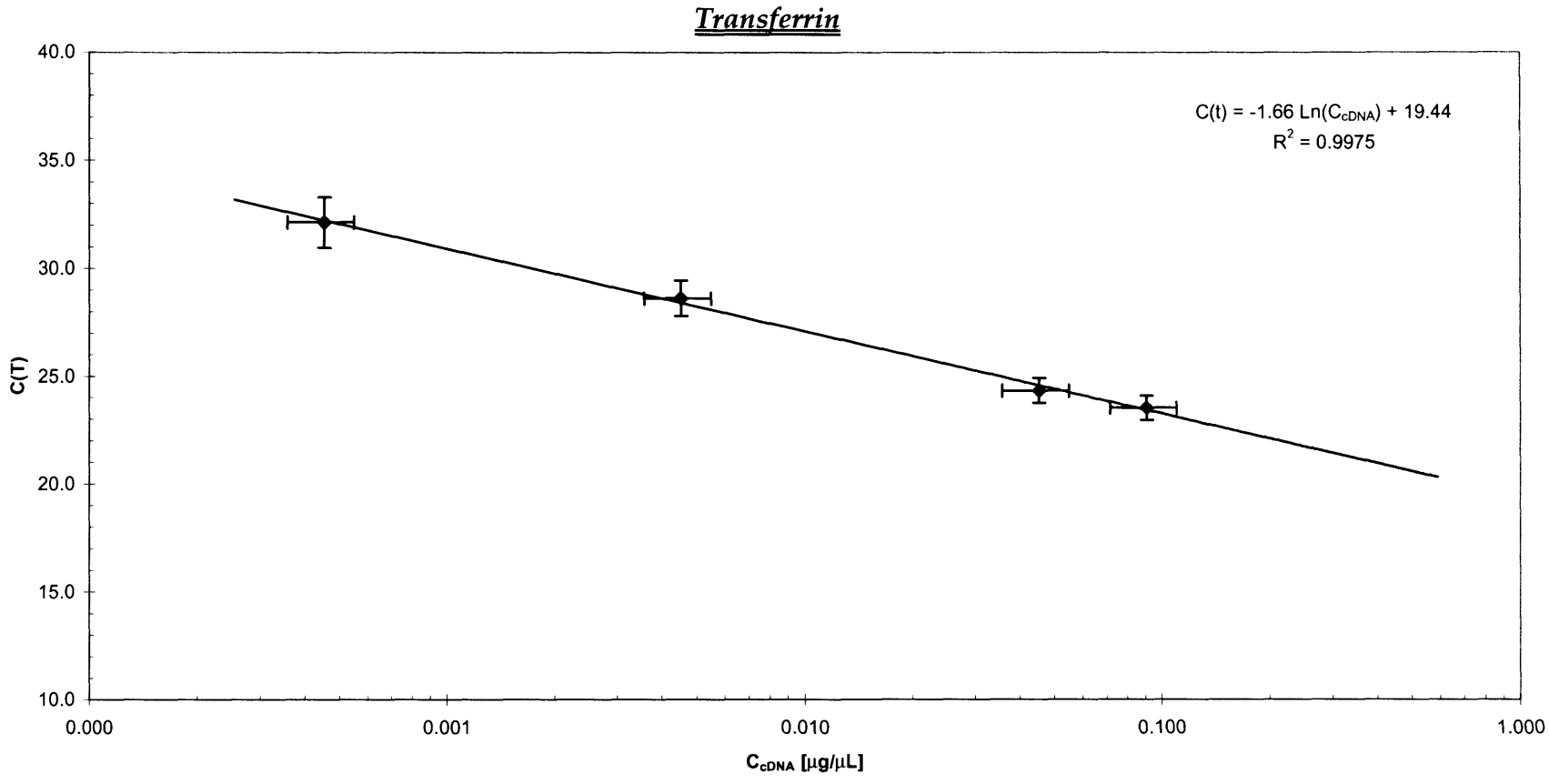
Transferrin
C(t) = -1.66 Ln(CcDNA) + 19.44
R2 = 0.9975
C(T)
40.0
35.0
30.0
25.0
20.0
15.0
10.0
0.000
0.001
0.010
0.100
1.000
CcDNA [µg/µL]

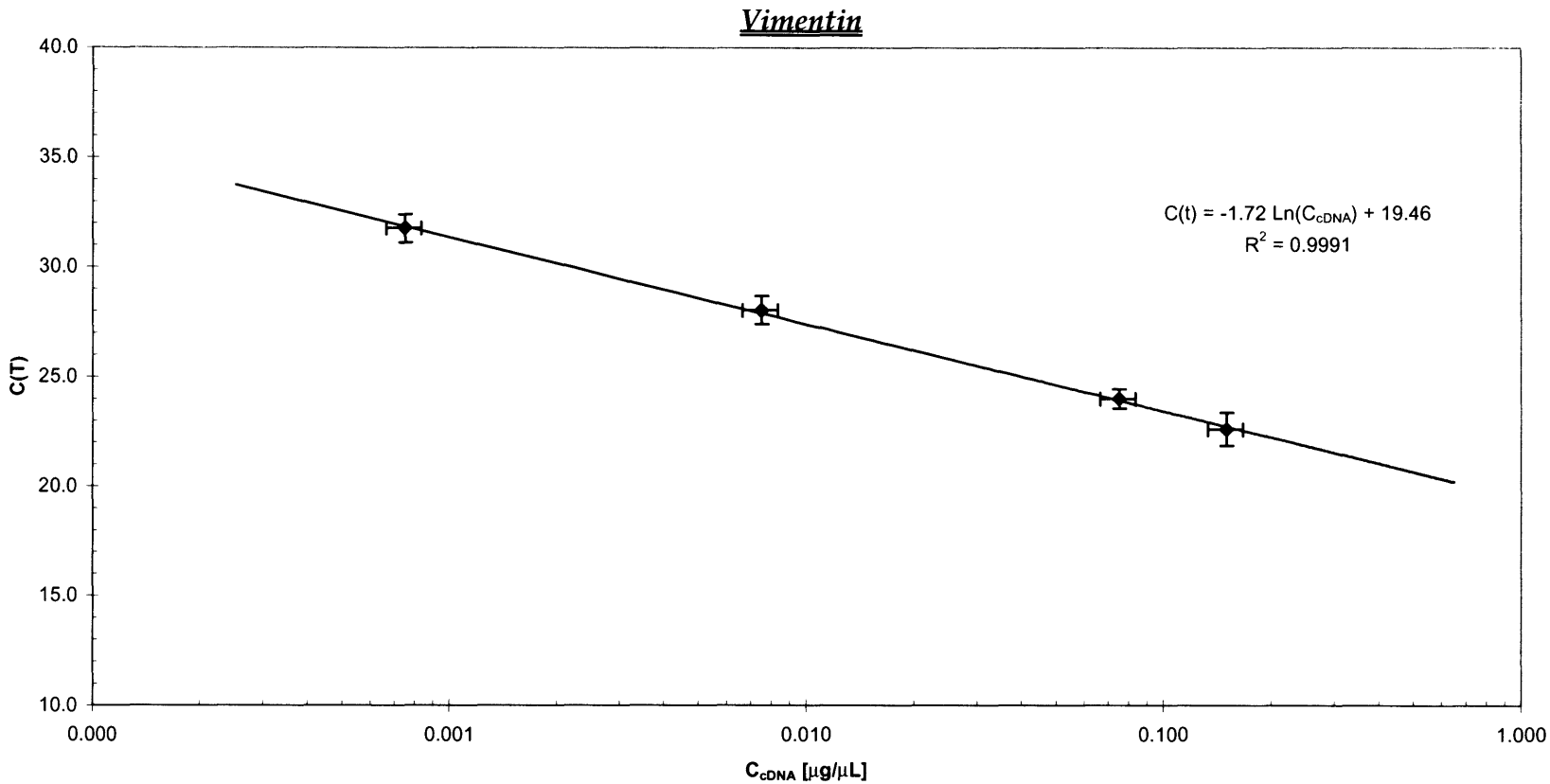
Vimentin
40.0
35.0
30.0
25.0
20.0
15.0
10.0
C(T)
C(t) = -1.72 Ln(CcDNA) + 19.46
R2 = 0.9991
0.000
0.001
0.010
0.100
1.000
CcDNA [µg/µL]

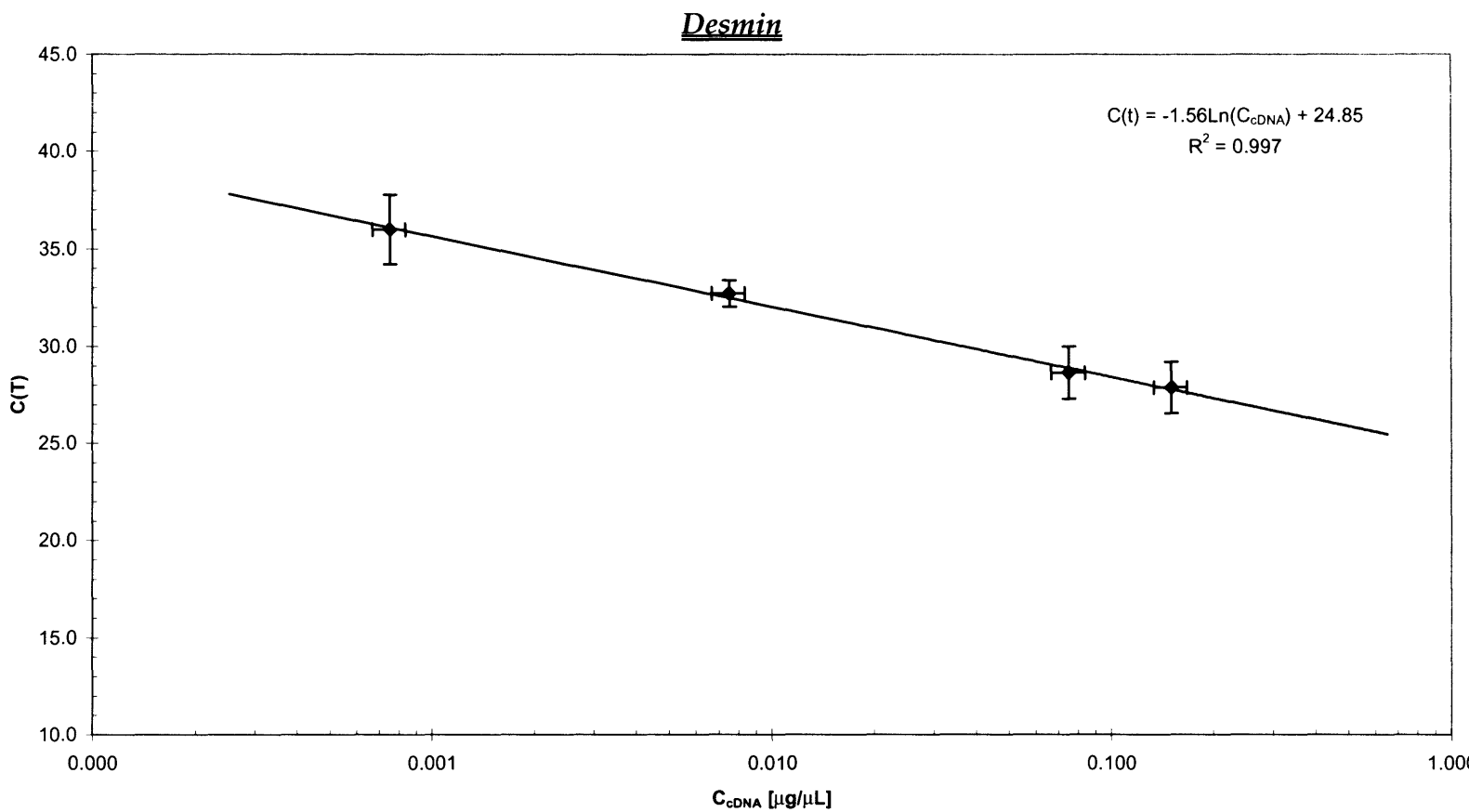
Desmin
C(t) = -1.56Ln(CcDNA) + 24.85
R2 = 0.997
45.0
40.0
35.0
30.0
25.0
20.0
15.0
10.0
C(T)
0.000
0.001
0.010
0.100
1.000
CcDNA [µg/µL]

Hyaluronic Acid Receptor for Endocytosis (HARE)

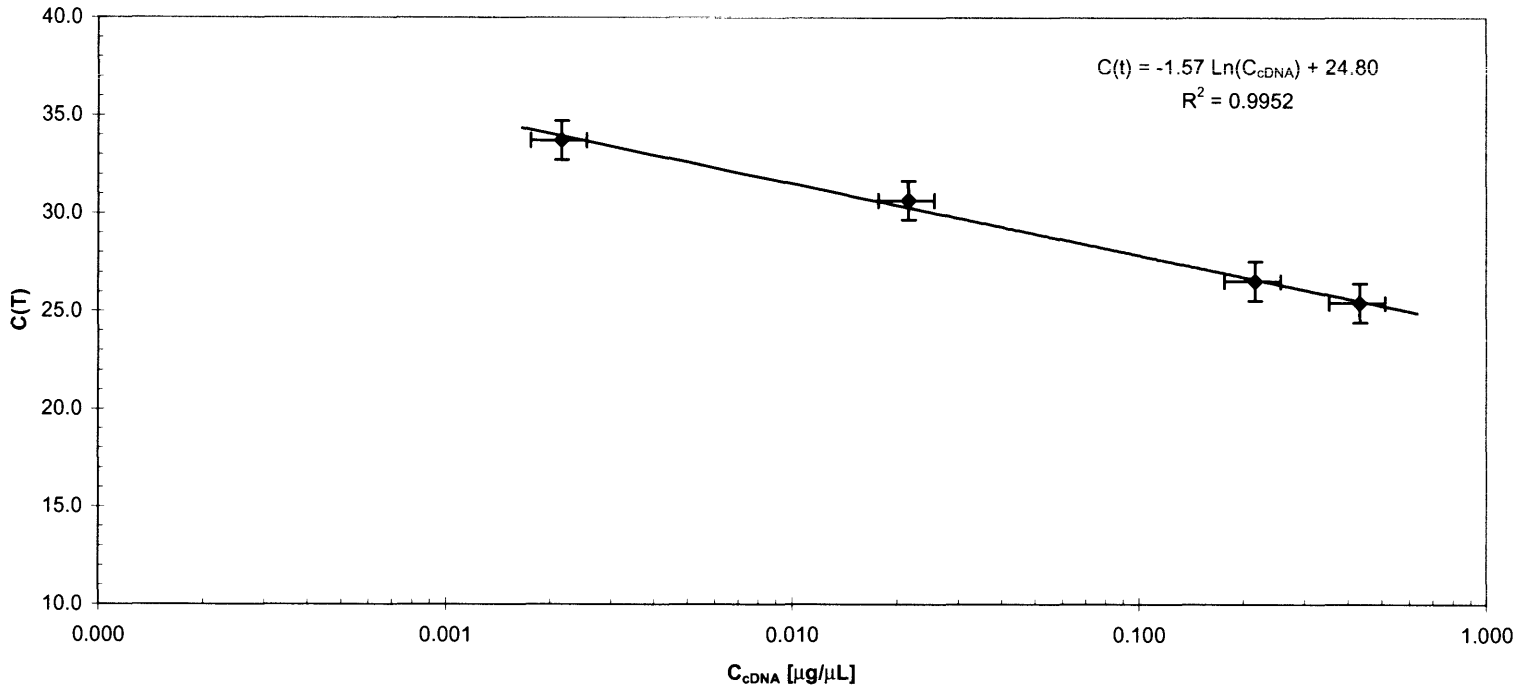

Flk-1 / VEGF-R2

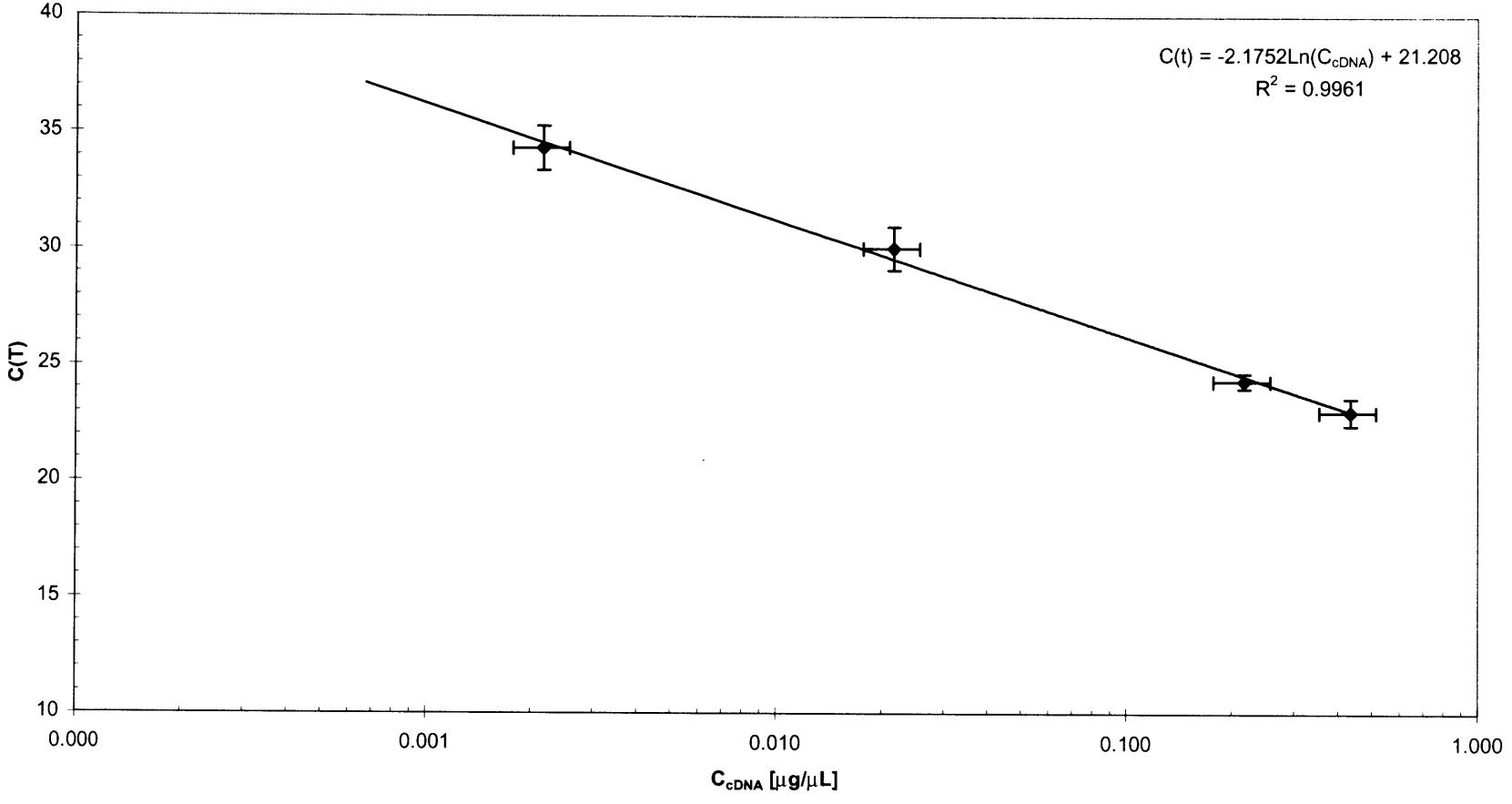
C(t) = -2.1752Ln(C_cDNA) + 21.208
R² = 0.9961
C(T)
40
35
30
25
20
15
10
0.000
0.001
0.010
0.100
1.000
C_cDNA [µg/µL]

Flt-1 / VEGF-R1

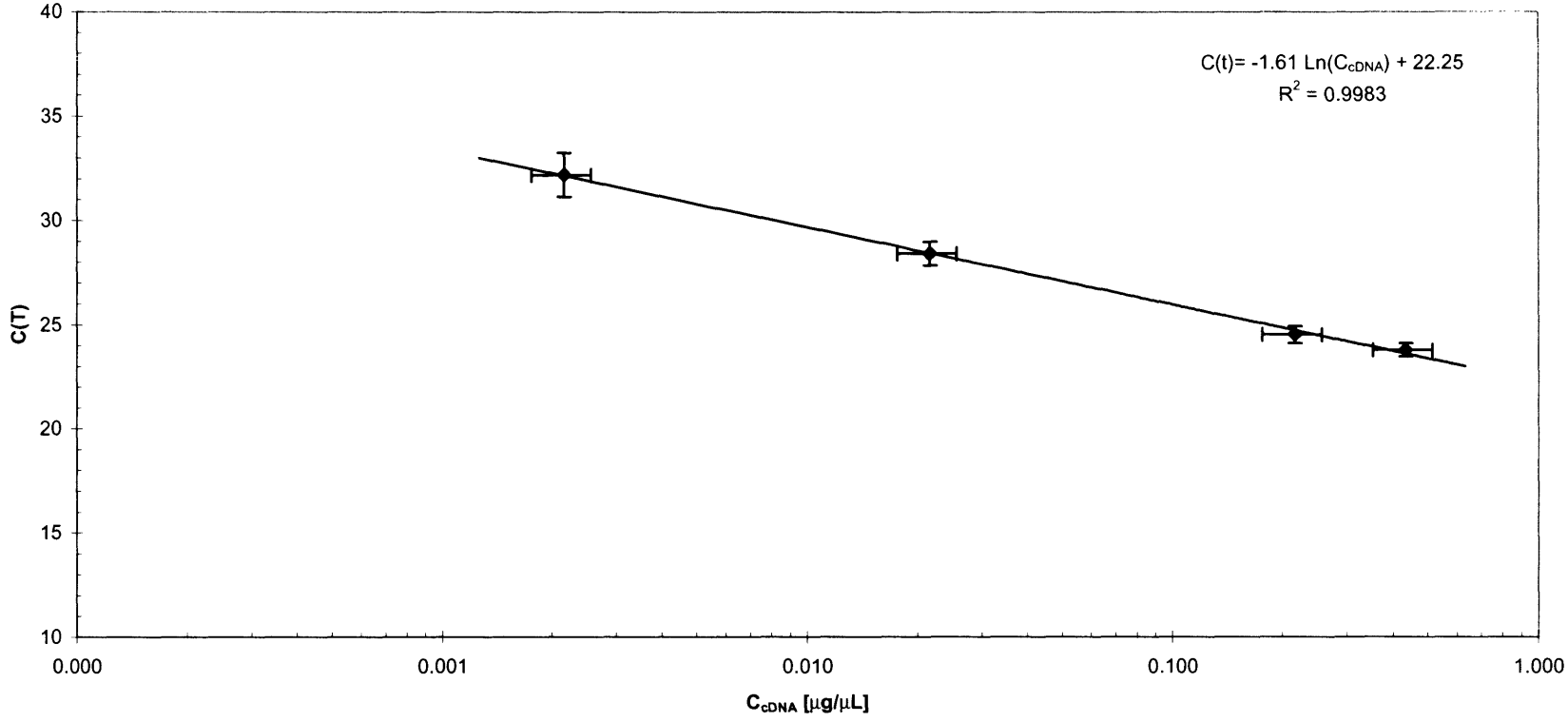
C(t)= -1.61 Ln(CcDNA) + 22.25
R2 = 0.9983
C(T)
40
35
30
25
20
15
10
0.000
0.001
0.010
0.100
1.000
CcDNA [µg/µL]

Macrosialin (CD68 / ED-1)

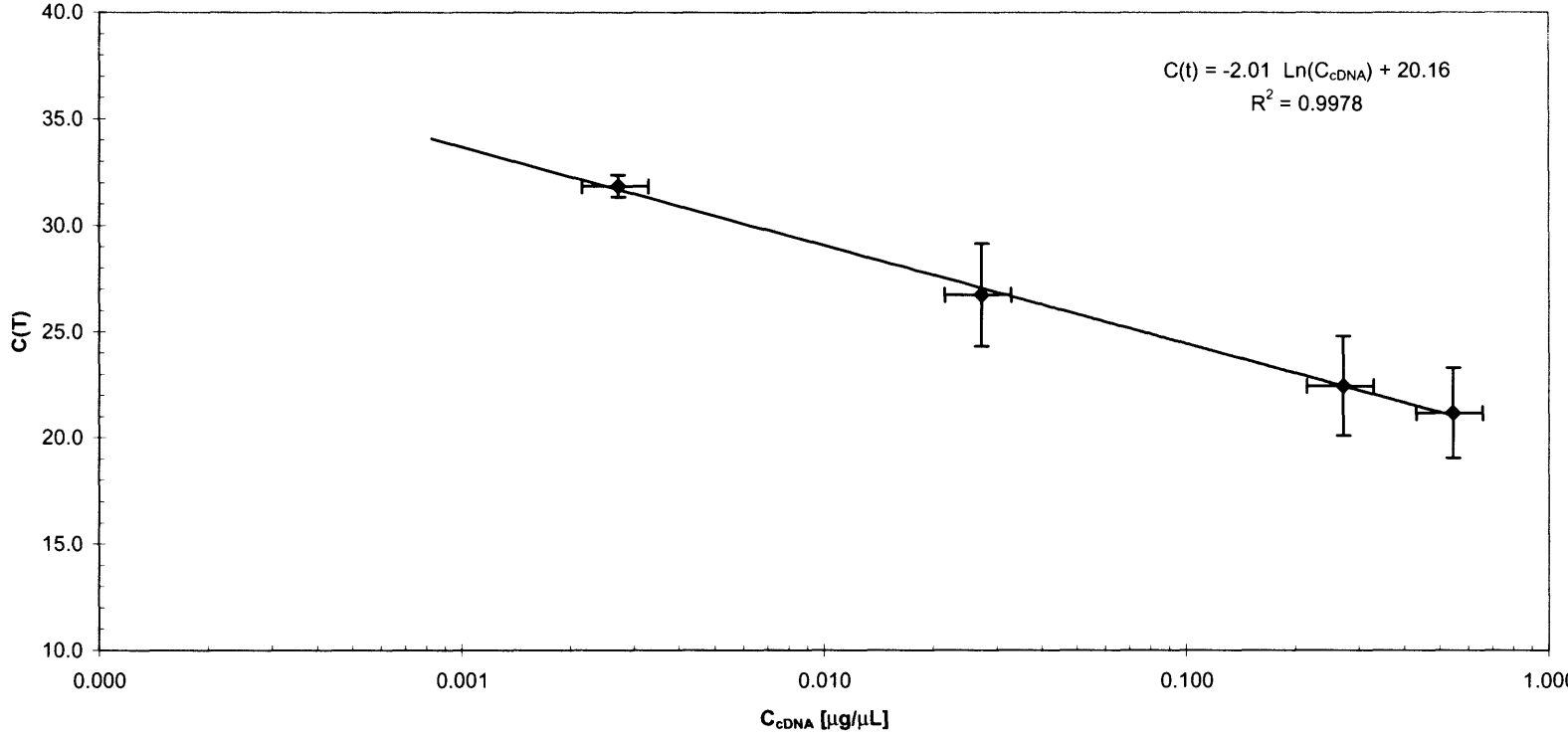

IL-10Ra

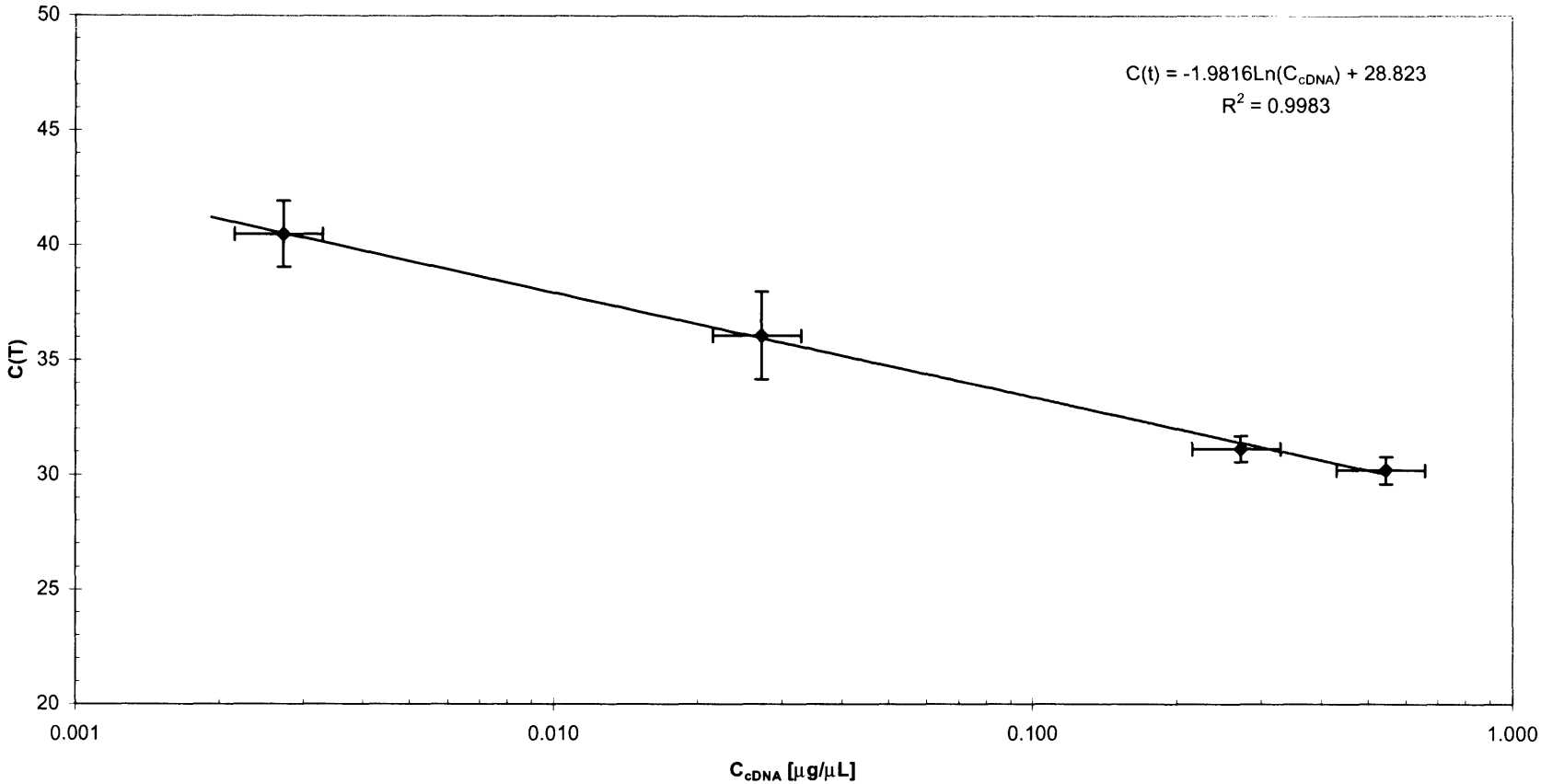
C(t) = -1.9816Ln(C_cDNA) + 28.823
R² = 0.9983
C(T)
50
45
40
35
30
25
20
0.001
0.010
0.100
1.000
C_cDNA [µg/µL]

Appendix 2: Hoechst & SYTOX© Orange Cell Counting Protocol

Material Needed: Hoechst 33342 (Molecular Probes, #H-3570) , SYTOX© Orange (Molecular Probes, #S-11368), aluminum foil, haemacytometer

Step 1: *Stain Cells*

1) In a 1.5 mL eppendorf tube add the following:
    - 800 µL of PBS
    - 200 µL of Cell Suspension

    (in the dark)
    - 1µL of Hoechst 33342
    - 1µL of SYTOX Orange
2) Cover in aluminum foil and mix by gentle inversion
3) Let sit covered for 5 minutes

Step 2: *Count Cells*

1) Mix again by gentle inversion
2) Add 10µL of resulting solution to each side of haemacytometer and count by conventional methods
3) View and image under DAPI with an exposure time, $t_{exposure} < 1$sec, and the digital gain set to 1x

(note – live cells will appear blue, while dead cells will be visually green…$t_{exposure} > 1$sec pick up cell debris and background fluorescence)

Appendix 3A: Hepatocyte Isolation Protocol

Material Needed: Percoll® Solution (Sigma, P1644-1L), 10X HBSS (Gibco #14025-076), Trypan Blue (Gibco #15250-0), aluminum foil, haemacytometer

1) Add 21.6mL of Percoll to 2.4mL of 10X Hank's Balanced Salt Solution in a 50mL conical tube to create a Percoll concentration of 90% v/v and put on ice.

(This must be done the day of the isolation because the salt in the HBSS begins to dissolve the Percoll silica beads when stored)

2) Dilute hepatocytes to a density of 5-7 million cells/mL in 24 mL of HGM (Need minimum 125 million hepatocytes).

(higher cell densities decrease the efficiency of separation as contaminant cells are carried through the gradient and lower densities reduce the yield)

3) Gently mix 24 mL of cell suspension with 24 mL of the 90% Percoll suspension to form a uniform isotonic gradient.

4) Centrifuge at 50 x g for 10 min at 4°C in a swinging bucket centrifuge (maximum acceleration and brake setting of 3)

5) Aspirate the dead and compromised cell from suspension, and resuspend the resulting pellet in 45 mL of HGM.

6) Centrifuge at 50 x g for 3 min at 4°C in a swinging bucket centrifuge

7) Remove the supernatant and resuspend cells in the appropriate volume of HGM.

8) Determine cell count and viability using trypan blue exclusion on a hemacytometer.

9) Keep cells on ice until use, but try to process hepatocytes immediately, as they begin to dedifferentiate rapidly in suspension

Appendix 3B: NPC Isolation Protocol

Material Needed: Percoll® Solution (Sigma, P1644-1L), 10X HBSS (Gibco #14025-076), non-TC treated 6-well Plate, Vitrogen (Cohesion #FXP-019), 50mL centrifuge tubes, Hoechst 33342 (Molecular Probes, #H-3570) , SYTOX© Orange (Molecular Probes, #S-11368) , aluminum foil, haemacytometer

Step 1: *Prepare the Percoll Layers*

1) Add 20mL Percoll to 20mL 10X HBSS in a 50mL conical tube and mix to create a uniform suspension with a concentration of 50% v/v Percoll.

(Percoll has also been successfully mixed with PBS)

2) In a separate 50mL conical tube add 10mL Percoll to 30mL 10X HBSS to create a uniform suspension with a concentration of 25% v/v Percoll.

3) Add 20 mL of 25% Percoll into each of two separate 50mL conical tubes.

4) Slowly pipette 15mL of 50% Percoll solution underneath the 25% layer. (You should be able to visually see an interface if you tilt the tube 45°)

(Be very careful not mix layers as it will decrease the efficiency of separation. If you don not see an interface remark the Percoll gradient)

Step 2: *Preparation of NPC cell Suspension*

5) Centrifuge the supernatants ($n = 4$) at 100 x g for 3 min to further separate out residual hepatocytes and debris

6) Collect the supernatants into fresh 50mL conical tubes, discard pellets or use them to acquire small hepatocytes.

7) Centrifuge these new supernatants at 400 x g for 5min @ 4°C in a swinging bucket centrifuge with the brake off, to spin down the NPC's.

8) Aspirate the resulting supernatant; suspend cells in one tube in 10mL of media (media formulation is experiment specific). Transfer this media to each of the other three tubes to resuspend the NPC's and concentrate the suspension.

9) Add 10mL more of media to the tube to collect residual cells by the same procedure in 8).

10) Count the resulting cell population using the nuclear staining technique described in Appendix 2.

Step 3: *Isolate the NPC's*

11) Slowly and gently add 10mL of NPC's at a density of 5-7 million cells per mL to the top of the 25% Percoll layer.

(Again, be careful not to mix layers or force the cells too deep in the layer as they will stay creating contaminant)

12) Centrifuge at 900 x g for 20min @ 4°C with the brake off (brake on will lead to mixing)

13) Aspirate off 25 mL of medium.

14) The cell layer lying in the 5 mL range near the layer interface is rich in non-parenchymal cells and should be separated into a separate tube and resuspended in maximal amount of medium.

15) Centrifuge at 900 x g for 5 min @ 4°C with the brake off.

16) Resuspend in appropriate amount of media and count cells using the nuclear staining protocol described in Appendix 2

Appendix 3C: EC & KC Isolation Protocol for Standard Curve Development

Material Needed: Percoll® Solution (Sigma, P1644-1L), non-TC treated 6-well Plate, Vitrogen (Cohesion #FXP-019), 50mL centrifuge tubes, Hoechst 33342 (Molecular Probes, #H-3570) , SYTOX© Orange (Molecular Probes, #S-11368), aluminum foil, haemacytometer

Step 1: *Prepare the Adhesion Substrate*

1) Add 100mL of Vitrogen to 10mL of PBS and mix thoroughly to create a collagen concentration of 30μg/mL.

2) Lay this collagen on two EC labeled non-TC treated plastic 6-well plates.

3) Incubate plates for 30 minutes @ 37°C

4) Wash the collagen monolayer 2X with PBS and stored with PBS on ice until further use

5) Put two no fresh KC labeled non-TC treated plastic plates on ice until further use as well

Step 2: *Prepare the Percoll Layers*

6) Add 20mL Percoll to 20mL 10X HBSS in a 50mL conical tube and mix to create a uniform suspension with a concentration of 50% v/v Percoll.

(Percoll has also been successfully mixed with PBS)

7) In a separate 50mL conical tube add 10mL Percoll to 30mL 10X HBSS to create a uniform suspension with a concentration of 25% v/v Percoll.

8) Add 20 mL of 25% Percoll into each of two separate 50mL conical tubes.

9) Slowly pipette 15mL of 50% Percoll solution underneath the 25% layer. (You should be able to visually see an interface if you tilt the tube 45°)

(Be very careful not mix layers as it will decrease the efficiency of separation. If you don not see an interface remark the Percoll gradient)

Step 3: *Preparation of NPC cell Suspension*

10) Centrifuge the supernatants ($n = 4$) at 100 x g for 3 min to further separate out residual hepatocytes and debris

11) Collect the supernatants into fresh 50mL conical tubes, discard pellets or use them to acquire small hepatocytes.

12) Centrifuge these new supernatants at 400 x g for 5min @ 4°C in a swinging bucket centrifuge with the brake off, to spin down the NPC's.

13) Aspirate the resulting supernatant; suspend cells in one tube in 10mL of media (media formulation is experiment specific). Transfer this media to each of the other three tubes to resuspend the NPC's and concentrate the suspension.

14) Add 10mL more of media to the tube to collect residual cells by the same procedure in 8).

15) Count the resulting cell population using the nuclear staining technique described in Appendix 2.

Step 4: *Isolate the NPC's*

16) Slowly and gently add 10mL of NPC's at a density of 5-7 million cells per mL to the top of the 25% Percoll layer.

(Again, be careful not to mix layers or force the cells too deep in the layer as they will stay there creating contaminant)

17) Centrifuge at 900 x g for 20min @ 4°C with the brake off (brake on will lead to mixing)

18) Aspirate off 25 mL of medium.

19) The cell layer lying in the 5 mL range near the layer interface (fraction 1) is rich in non-parenchymal cells and should be separated into a separate tube and resuspended in maximal amount of medium. The next 10 mL (Fraction II) is rich in Kupffer cells specifically and showed be similarly separated and resuspended.

20) Centrifuge at 900 x g for 5 min @ 4°C with the brake off.

21) Resuspend both in appropriate amounts of media and count cells using the nuclear staining protocol described in Appendix 2

Step 5: *Selective Adhesion to Substrate*

17) Cells derived from fraction I are then seeded at a seeded on collagen monolayer at a density of 2 million cells/well.

18) These EC are then allowed to adhere to the substrate for 2.5 hrs @37°C, 5% O_2

19) Cells derived from fraction II are then seeded on non-TC treated plastic at a density of $\rho \rightarrow 2$ million cells/well.

(Yield is low for Fraction II and as such the 2 million cell density is rarely meet)

20) These KC are then allowed to adhere to the substrate for 0.5 hrs @37°C, 5% O_2

21) After the appropriate adhesion time one plate of each type is fixed in 2% paraformaldehyde for 30 minutes and then stored at 4oC until immunostained. The other plate is immediately processed to isolate RNA.

Appendix 4A: RNA Isolation for Hepatic Cell Pellet (TRIzol+Qiagen)

Material Needed: Trizol Reagent (Gibco #15596-026), Chloroform, Qiagen RNeasy Mini Kit (Qiagen #74104), Ethanol, RNase-free water (such as DEPC-treated water), and RNase-free tips and tubes

Day 1: *Cell Pellet Preparation and Homogenizaiton*

1) Re-suspend final counted cell isolate in HGM at a density of ~1 million cells/mL and place in a 1.5 mL eppindorf tube.
2) Centrifuge at 1000 x g for 15sec at room temperature
3) Suction medium using a 1000 µL pipetteman set to 800 µL being very careful not to touch or suction the media-cell interface.
4) Add **1 mL** of Trizol reagent to the eppindorf tube
5) Homogenize via vortexing for 2 minutes or until the sample is sufficiently homogenized
6) *** store sample for further processing in the –80°C for upto 1 month **OR** ****

(note – TRIzol has stabilizing agents that maintain the integrity of RNA much better than simple storage in medium)

Day 2: *RNA Preparation from TRIzol and RNeasy Kit*

7) Add **200 µL** of Chloroform per 1 mL of TRIzol
8) Vortex for 30 sec (Solution should become cloudy pink and be consistent throughout)
9) Centrifuge in Cold Room (4°C) at 12,000 rpm for 15 min
10) Take **upper aqueous phase** into a new 1.5 mL eppidorf tube paying particular attention not to suction any TRIzol reagent using a 200 µL pipetteman (Should aquire 400-700 µL of solution)

(note – The bottom organic phase contains protein and DNA that will reduce the quality/purity of you RNA sample)

11) Add an equal volume of 70% EtOH to the aqueous phase and vortex for 15 sec
12) Label RNeasy columns, add 700 µL of RNA solution, and centrifuge for 15 sec
13) Capture the 700 µL column ellutant and repeat step 12, then discard ellutant.
14) Repeat steps 12 & 13 until all RNA solution has been passed twice through the column
15) Discard collection tube, replace with a clean RNase-free collection tube
16) Add 500 µL of RPE Buffer to the column and spin for 15 sec.

(notes — Double check that it has been equilibrated with EtOH, if a fresh bottle equilibrate as per the Qiagen manual, pg 80
— Replacing the collection tube is essential because the RNA in EtOH is 'dirty' from the isolation process. The RPE buffer is cleaning the RNA, and if same collection tube is used, the cleansing can be contaminated)

17) Add 500 µL more of RPE buffer, spin for 1 min (or until the column is dry), and discard collection tube.
18) Place column in eppindorf, add **30 µL** of RT-PCR grade water, and spin for ~30 sec @ 10,000 rpm
19) Add **20 µL** more of RT-PCR grade water, and spin for ~30 sec @ 10,000 rpm (RNA is being solublized in the water
20) Collect RNA solution and store at **–80°C** for up to 1 month.

(note – RNA is more stable in TRIzol than water, so try to process RNA samples as quickly as possible)

Appendix 4B: RNA Isolation from monolayer and Collagen Gel Sandwich

Material Needed: Trizol Reagent (Gibco #15596-026), Chloroform, Qiagen RNeasy Mini Kit (Qiagen #74104), Ethanol, RNase-free water (such as DEPC-treated water), RNase-free tips and tubes, 25 gauge needle and 3mL syringe, sterile plastic scapper

Day 1: *Hepatocyte Cell Pellet Preparation and Homogenizaiton*

1) Aspirate medium
2) Add **1 mL** of TRIzol reagent to each well (6-well plate)
3) Remove collagen or monolayer from the plate with a sterile plastic scrapper
4) Transfer the solution to a fresh eppendorf or can leave in the well (personal preference)
5) Homogenize using a 25 gauge needle and 3mL syringe until the sample is homogeneous (~10min/well)
6) *** store sample for further processing in the –80°C for upto 1 month **OR** ****

(note – TRIzol has stabilizing agents that maintain the integrity of RNA much better than simple storage in medium)

Day 2: *RNA Preparation from TRIzol and RNeasy Kit*

7) Add **200 µL** of Chloroform per 1 mL of TRIzol
8) Vortex for 30 sec (Solution should become cloudy pink and be consistent throughout)
9) Centrifuge in Cold Room (4°C) at 12,000 rpm for 15 min
10) Take **upper aqueous phase** into a new 1.5 mL eppidorf tube paying particular attention not to suction any TRIzol reagent using a 200 µL pipetteman (Should aquire 400-700 µL of solution)

(note – The bottom organic phase contains protein and DNA that will reduce the quality/purity of you RNA sample)

11) Add an equal volume of 70% EtOH to the aqueous phase and vortex for 15 sec
12) Label RNeasy columns, add 700 µL of RNA solution, and centrifuge for 15 sec
13) Capture the 700 µL column ellutant and repeat step 12, then discard ellutant.
14) Repeat steps 12 & 13 until all RNA solution has been passed twice through the column
15) Discard collection tube, replace with a clean RNase-free collection tube
16) Add 500 µL of RPE Buffer to the column and spin for 15 sec.

(notes — Double check that it has been equilibrated with EtOH, if a fresh bottle equilibrate as per the Qiagen manual, pg 80
— Replacing the collection tube is essential because the RNA in EtOH is 'dirty' from the isolation process. The RPE buffer is cleaning the RNA, and if same collection tube is used, the cleansing can be contaminated)

17) Add 500 µL more of RPE buffer, spin for 1 min (or until the column is dry), and discard collection tube.
18) Place column in eppendorf, add **30 µL** of RT-PCR grade water, and spin for ~30 sec @ 10,000 rpm
19) Add **20 µL** more of RT-PCR grade water, and spin for ~30 sec @ 10,000 rpm (RNA is being solublized in the water
20) Collect RNA solution and store at **–80°C** for up to 1 month.

(note – RNA is more stable in TRIzol than water, so try to process RNA samples as quickly as possible)

Appendix 4C: RNA Isolation from Spheroids Cultured in Spinner Flask

Material Needed: TRIzol Reagent (Gibco #15596-026), Chloroform, Qiagen RNeasy Mini Kit (Qiagen #74104), Ethanol, RNase-free water (such as DEPC-treated water), RNase-free tips and tubes, 25 gauge needle and 3mL syringe, sterile plastic scapper

Day 1A: *Spheroid Preparation from spinner flask*
1) Transfer purified spheroid suspension (3~5 million cells) to 50mL conical tube
2) Centrifuge @ 40 x g for 3 min, 4°C

Day 1B: *RNA Preparation in TRIzol*
3) Aspirate medium from tube
4) Add **2 mL** of TRIzol reagent to each tube
5) Homogenize via vortexing for 2 minutes or until the sample is sufficiently homogenized
6) *** store sample for further processing in the –80°C for upto 1 month **OR** ****

Day 2: *RNA Preparation from TRIzol and RNeasy Kit*
7) Add **200 µL** of Chloroform per 1 mL of TRIzol
8) Vortex for 30 sec (Solution should become cloudy pink and be consistent throughout)
9) Centrifuge in Cold Room (4°C) at 12,000 rpm for 15 min
10) Take **upper aqueous phase** into a new 1.5 mL eppendorf tube paying particular attention not to suction any TRIzol reagent using a 200 µL pipetteman (Should aquire 400-700 µL of solution)

(note – The bottom organic phase contains protein and DNA that will reduce the quality/purity of you RNA sample)

11) Add an equal volume of 70% EtOH to the aqueous phase and vortex for 15 sec
12) Label RNeasy columns, add 700 µL of RNA solution, and centrifuge for 15 sec
13) Capture the 700 µL column ellutant and repeat step 12, then discard ellutant.
14) Repeat steps 12 & 13 until all RNA solution has been passed twice through the column
15) Discard collection tube, replace with a clean RNase-free collection tube
16) Add 500 µL of RPE Buffer to the column and spin for 15 sec.

(notes — Double check that it has been equilibrated with EtOH, if a fresh bottle equilibrate as per the Qiagen manual, pg 80
— Replacing the collection tube is essential because the RNA in EtOH is 'dirty' from the isolation process. The RPE buffer is cleaning the RNA, and if same collection tube is used, the cleansing can be contaminated)

17) Add 500 µL more of RPE buffer, spin for 1 min (or until the column is dry), and discard collection tube.
18) Place column in eppindorf, add **30 µL** of RT-PCR grade water, and spin for ~30 sec @ 10,000 rpm
19) Add **20 µL** more of RT-PCR grade water, and spin for ~30 sec @ 10,000 rpm (RNA is being solublized in the water
20) Collect RNA solution and store at **–80°C** for up to 1 month.

(note – RNA is more stable in TRIzol than water, so try to process RNA samples as quickly as possible)

Appendix 4D: RNA Isolation from MilliF Bioreactor

Material Needed: TRIzol Reagent (Gibco #15596-026), Chloroform, Qiagen RNeasy Mini Kit (Qiagen #74104), Ethanol, RNase-free water (such as DEPC-treated water), RNase-free tips and tubes, 25 gauge needle and 3mL syringe, sterile plastic scapper

Day 1: *Scaffold Sample Preparation*

1) Take scaffold and filter from the reactor and place in an 1.5mL eppendorf tube
2) Add **1 mL** of TRIzol reagent to the tube
3) Use 25 gauge needle and 3mL syringe to force the TRIzol through the scaffold channels and filter for ~2 min (Try to lyse as many cells as possible from the reactor, check with Karel to make sure that the scaffold has no inverse effects from the phenol based TRIzol)
5) Homogenize syringe and needle to homogenize lysate solution ~5 min
6) *** store sample for further processing in the –80°C for upto 1 month **OR** ****

Day 2: *RNA Preparation from TRIzol and RNeasy Kit*

7) Add **200 µL** of Chloroform per 1 mL of TRIzol
8) Vortex for 30 sec (Solution should become cloudy pink and be consistent throughout)
9) Centrifuge in Cold Room (4°C) at 12,000 rpm for 15 min
10) Take **upper aqueous phase** into a new 1.5 mL eppidorf tube paying particular attention not to suction any TRIzol reagent using a 200 µL pipetteman (Should aquire 400-700 µL of solution)

(note – The bottom organic phase contains protein and DNA that will reduce the quality/purity of you RNA sample)

11) Add an equal volume of 70% EtOH to the aqueous phase and vortex for 15 sec
12) Label RNeasy columns, add 700 µL of RNA solution, and centrifuge for 15 sec
13) Capture the 700 µL column ellutant and repeat step 12, then discard ellutant.
14) Repeat steps 12 & 13 until all RNA solution has been passed twice through the column
15) Discard collection tube, replace with a clean RNase-free collection tube
16) Add 500 µL of RPE Buffer to the column and spin for 15 sec.

(notes — Double check that it has been equilibrated with EtOH, if a fresh bottle equilibrate as per the Qiagen manual, pg 80
— Replacing the collection tube is essential because the RNA in EtOH is 'dirty' from the isolation process. The RPE buffer is cleaning the RNA, and if same collection tube is used, the cleansing can be contaminated)

17) Add 500 µL more of RPE buffer, spin for 1 min (or until the column is dry), and discard collection tube.
18) Place column in eppindorf, add **30 µL** of RT-PCR grade water, and spin for ~30 sec @ 10,000 rpm
19) Add **20 µL** more of RT-PCR grade water, and spin for ~30 sec @ 10,000 rpm (RNA is being solublized in the water
20) Collect RNA solution and store at **–80°C** for up to 1 month.

(note – RNA is more stable in TRIzol than water, so try to process RNA samples as quickly as possible)

Appendix 5: Primer Design Procedure and Guidelines

Step 1: *Identify Gene Sequence*

- Use NCBI Nucleotide Search to find the target genes' sequence
- Include species (*rattus norvegicus*) and RNA type (i.e. mRNA, rRNA, etc.) in your search

Step 2: *Remove Exon Sequence*

- Use Exon/Gene search engine or StrataGene search engine to identify the exon runs in your target gene sequence
- Remove exons from target gene sequence

Step 3: *Design Initial Primer*

- Input the resulting gene sequence into MIT's Primer3 software (Whitehead Institute)

Specify the following conditions (shown in the field below as well)

- 100-200 basepair target sequence
- 18-30 nucleotides in length
- 45-55% GC content

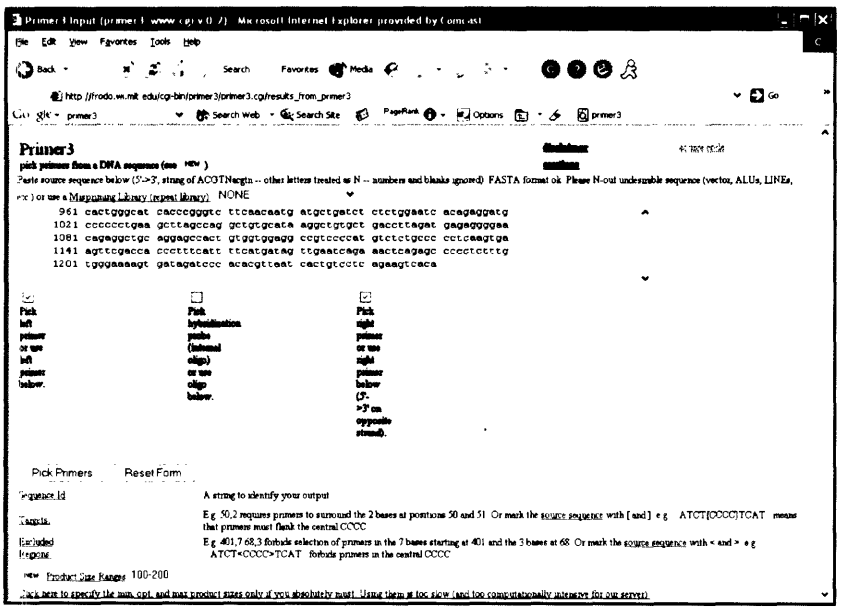

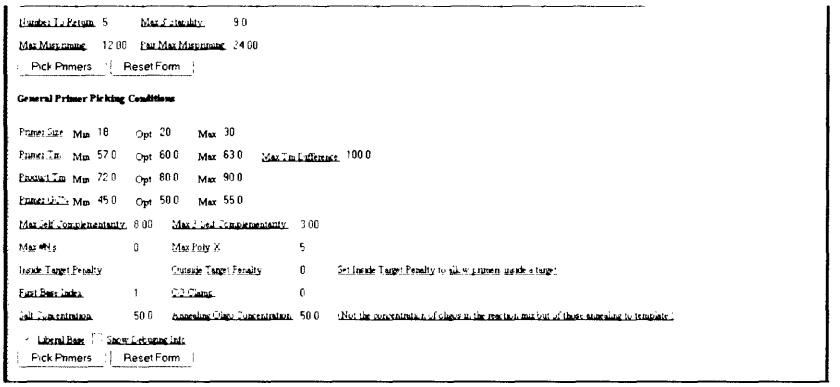

- Software will give a list of candidate primers in ranked order as determined by their algorithm

Select primers from the generated options that:

- Avoid runs of 3 or more G/C at the 3' end
- Avoid complementarities within the primer sequences and between the primer
- Avoid complementarities and mismatches of 2 or more bases at the 3' ends of the primer and the target-template sequence
- Avoid a 3' end T pair
- Use an annealing temperature 5C° above T_m

Step 4: *Verify Targets of Primer Design*

- Go NCBI Blast and input the determined primer sequence. This software will determine where on the genome that primer will amplify.
- The primer sequence should yield the target gene with considerably greater significance than the next closest match.

(Similarities between the gene specificity of different species is not important)

Appendix 6: Real-Time Reverse Transcription-PCR Protocol

Material Needed: Deoxyribonuclease I (Invitrogen #18068-015), Omniscript Reverse Transcriptase Kit (Qiagen #205111), QuantiTect SYBR Green PCR Kit (Qiagen #204143), T7-Oligo(dT)$_{24}$ primer (Affymetrix #900375), RNase inhibitor (Ambion #2684) designed primers for genes of interest, RT-PCR grade water, DNA Engine Opticon, RNase-free tips, tubes, and plates

Step 1: *Quantification of RNA concentration*

1) Add 2 µL of RNA sample to 98 µL of DEPC-water (1:50 dilution) (Witrup UV requires 200µL of sample or 4 RNA:196 H_2O
2) Blank UV Spec with DEPC water (or whatever the dilutant is)
3) Spec samples at 260 nm and 280 nm

(note- The UV spec in the Witrup Lab has much more precision and accuracy than Leona's)

4) Determine quality (Q_{RNA}) and quantity (W_{RNA}) of sample:

$$W_{RNA} = \frac{A_{260} * \alpha_{RNA}[\frac{\mu g}{mL}] * D_{factor} * V_{sample}[\mu L]}{1000[\frac{\mu L}{mL}]}, \quad where\ \alpha_{RNA} = 40$$

$$Q_{RNA} = \frac{A_{260}}{A_{280}}, \quad 1.7 \geq Q_{RNA} \geq 2.1$$

5) If the quality of the RNA sample falls outside of the defined range it should be thrown out.

Step 2: *DNase Treatment of RNA*

1) Prepare duplicate tubes for positive and negative reverse transcriptase (RNA) sample to be used in the PCR reaction.(RNA) samples are to be used in the amplification reaction.
2) Add the following to an RNAse-free, 0.5 mL Eppendorf, on ice
   - 1 µg RNA sample or desired amount
   - 1 µL 10X DNAse I reaction buffer
   - 1 µL DNAse I, amplification grade, 1 [U/µL]
   - DEPC treated water to 10 µL

(Note: reaction is optimized from 50ng-2µg of RNA. Regardless, of the initial amount of RNA be sure to perform the RT reaction at the same RNA concentration to standardize experimental error)

3) Incubate tubes for 15 min at room temperature.
4) Inactivate the DNAse by adding 1 µL of 25 mM EDTA solution to the mixture.
5) Heat for 10 min. at 65°C. After, keep the mixture on ice for use in the reverse transcription, or store at -20°C.

Step 3: *Reverse Transcription*

1) Make fresh dilution of T7 primer and RNase inhibitor
   - RT buffer from 10x to 1x in RT-PCR H_20 (1:10 dilution).
   - RNase Inhibitor (40 U/µL stock) to 10 U/µL in RT buffer (1:4 dilution)
   - T7 primer (50µM stock) to 10µM in RT-PCR H_20 (1:5 dilution)
2) Prepare the master mix on ICE

Component	Volume/reaction	Final concentration
Master mix		
[illegible]	[illegible]	[illegible]
dNTP Mix (5 mM each dNTP)	[illegible]	[illegible]
Oligo-dT primer (100 µM)*	[illegible]	[illegible]
RNase inhibitor (40 units/µl)	[illegible]	[illegible]
50 mM MgCl2	[illegible]	[illegible]
RNase-free water	Variable	
Template RNA		
Template RNA, added at step 5	Variable	Up to 2 µg (per 20 µL reaction)
Total volume	**20.0 µl**	-

3) Add the appropriate amount of master mix to the template RNA tube
4) Incubate @ 37°C for 60min and store @ -80°C (or –20°C) until PCR

(note: cDNA is much more stable to heat and proteases than RNA)

Step 4: *Quantification of cDNA concentration*

1) Add 2 µL of RNA sample to 98 µL of DEPC-water (1:50 dilution) (Witrup UV requires 200µL of sample or 4 RNA:196 H_2O
2) Blank UV Spec with DEPC water (or whatever the dilutant is)
3) Spec samples at 260 nm and 280 nm

(note- The UV spec in the Witrup Lab has much more precision and accuracy than Leona's)

4) Determine quality (Q_{cDNA}) and quantity (W_{cDNA}) of sample:

$$W_{cDNA} = \frac{A_{260} * \alpha_{cDNA}[\frac{\mu g}{mL}] * D_{factor} * V_{sample}[\mu L]}{1000[\frac{\mu L}{mL}]}, \quad where\ \alpha_{ssDNA} = 33$$

$$Q_{cDNA} = \frac{A_{260}}{A_{280}}, \quad 1.8 \geq Q_{cDNA} \geq 2.0$$

5) If the quality of the cDNA sample falls outside of the defined range it should be thrown out.

Step 5: *Real-Time PCR*

1) Prepare master mix according to the following table

Component	Volume/reaction	Final concentration
2x QuantiTect SYBR Green PCR Master Mix*	25 µl	1x
Primer A forward	10pmol: 1.0ul of 10uM	0.3 µM
Primer B reverse	10pmol: 1.0ul of 10uM	0.3 µM
RNAse-free water	21ul	-
Template DNA (added at step 4)	1ul	<500 ng/reaction
Total volume	50 µl	

2) Aliquot master mix into PCR tubes or plates
3) Program DNA Engine Opticon as follows:

Protocol

1. Incubate at 95.0 C for 00:15:00
2. Incubate at 94.0 C for 00:00:15
3. Incubate at 57.0 C for 00:01:00
4. Incubate at 72.0 C for 00:00:30
5. Plate Read
6. Goto line 2 for 45 more times
7. Incubate at 72.0 C for 00:02:00
8. Melting Curve from 50.0 C to 98.0 C, read every 1.0 C, hold 00:00:01

END

Appendix 7: ED-2 Immunostaining Protocol

Contributors: Albert Hwa and Megan Whitmore

1) Fix cells in 4% paraformaldehyde in Krebs buffer (145mM NaCl, 5mM KCl, 1.2mM $CaCl_2$, 1.3mM $MgCl_2 \bullet 6H_20$, 1.2mM NaH_2PO_4, 10mM Glucose, 20mM HEPES, 0.4M Sucrose) for 20-30 minutes. Rinse 3x with PBS.
2) Wash fixed cells with PBG (1x PBS + 0.5% Bovine Serum Albumin (MP BioMedicals) and 0.15% Glycine (Sigma)) 3x.
3) Block with 5% Goat serum (Sigma) in PBG for 30min at RT.
4) Wash with PBG 4x.
5) Add ED-2 (Mouse anti-rat CD163, Serotec) primary antibody at a dilution of 1:250 (2µg/mL). Incubate overnight at 4°C.
6) Wash with PBG 4x 2min. each.
7) Add Goat anti-mouse secondary antibody (Jackson ImmunoResearch Lab). Incubate 1h at RT (fluorophor color in 2° antibody is user).
8) Wash with PBG 4x 2min each.
9) Wash with PBS 4x 2min each.
10) Add Hoechst stain (Molecular Probes) at 1:1000 dilution (10µg/mL) in PBS. Incubate 1min at RT.
11) Wash with PBS 3x.
12) Store at 4°C in the dark.